# Asymptotic Models for Acoustic, Elastic and Electromagnetic Media. Corner and Edge Asymptotics for Elliptic Systems

Victor Péron

|--|--|--|--|--|--|--|--|--|--|--|

Mémoire d'Habilitation à Diriger des Recherches

Présenté par


Victor PÉRON

UNIVERSITÉ DE PAU ET DES PAYS DE L'ADOUR
LABORATOIRE DE MATHÉMATIQUES ET DE LEURS APPLICATIONS UMR CNRS 5142
ÉQUIPE-PROJET MAGIQUE-3D INRIA-UPPA-CNRS


# ASYMPTOTIC MODELS FOR ACOUSTIC, ELASTIC AND ELECTROMAGNETIC MEDIA. CORNER AND EDGE ASYMPTOTICS FOR ELLIPTIC SYSTEMS

December 6, 2017

## Defense committee

| | | |
|---|---|---|
| Ralf HIPTMAIR | Professor, ETH Zürich | Reviewer |
| Patrick JOLY | Senior Researcher INRIA, ENSTA Paris Tech | Reviewer |
| Olivier LAFITTE | Professor, Université de Paris 13 | Reviewer |
| Xavier ANTOINE | Professor, Université de Lorraine | Examiner |
| Hélène BARUCQ | Senior Researcher, INRIA Bordeaux Sud-Ouest | Examiner |
| Christophe GEUZAINE | Professor, Université de Liège | Examiner |
| Luis VEGA | Professor, BCAM - UPV / EHU, Bilbao | Examiner |
| Grégory VIAL | Professor, École Centrale de Lyon | Examiner |

# Contents

# Introduction générale

L'objet de ce manuscrit est de présenter une synthèse de mes travaux de recherche effectués au cours de la période qui a suivi ma thèse consacrée à la modélisation mathématique de phénomènes électromagnétiques dans des matériaux à fort contraste et qui a été soutenue en septembre 2009 à l'Université de Rennes 1 [121]. Au cours de ma thèse, je me suis intéressé principalement au phénomène de l'*effet de peau*, qui a été analysé finement à l'aide d'une méthode asymptotique et de la simulation numérique [23, 22, 41]. Lors de cette période et lors de mon post-doctorat effectué au sein de l'équipe MC2 (INRIA Bordeaux Sud-Ouest), je me suis aussi intéressé à des problèmes de couches minces. Il s'agissait notamment de déterminer des modèles asymptotiques pour la propagation du champ électromagnétique à travers une membrane de cellule biologique [55]. Depuis la fin de ma thèse, mes travaux de recherche s'inscrivent essentiellement dans trois thématiques de recherche : la modélisation de phénomènes de propagation d'ondes dans des milieux très contrastés ; l'analyse et le traitement numérique de singularités de coins et d'arêtes dans des problèmes elliptiques, pour des applications en électromagnétisme et en élasticité ; le développement de méthodes numériques pour des équations aux dérivées partielles et des équations intégrales.

Depuis mon recrutement à l'Université de Pau et des Pays de l'Adour en septembre 2010, je travaille au sein de l'équipe-projet Magique-3D (INRIA Bordeaux Sud-Ouest) sur des problèmes de perturbations singulières (problèmes de couche limite, de couche mince, avec petit défaut) dans le but de modéliser des phénomènes de propagation d'ondes acoustiques, élastiques ou électromagnétiques dans des milieux complexes. Dans la plupart des problèmes qui ont été abordés, il s'agissait de décrire un phénomène au moyen d'un développement asymptotique multi-échelle puis de développer et d'implémenter des modèles numériques réduits dans des codes d'éléments finis (tels que, par exemple, ceux basés sur des méthodes de Galerkin discontinues pour les applications géophysiques) afin de pouvoir étudier leurs propriétés. Ces travaux sont présentés dans une première partie qui s'articule autour de deux chapitres. Le premier chapitre porte sur des problèmes de couches minces qui ont été traités dans le cadre du projet HPC-GA (High Performance Computing for Geophysical Applications). Il s'agit principalement de problèmes de couplages d'ondes acoustiques et élastiques. Le second chapitre porte sur des problèmes de transmission en électromagnétisme à travers des interfaces minces dont la conductivité est très élevée. De tels problèmes ont été abordés dans le cadre de la thèse d'A. Erdozain [60] que j'ai co-dirigée avec Hélène Barucq et David Pardo (UPV-EHU, Bilbao) ainsi que dans le cadre du projet PHC Procope INRIA - TU Berlin. Ce chapitre est complété par une annexe (Annexe A) qui présente comparativement toute une famille de modèles de couches minces pour des problèmes de transmission en électromagnétisme. Il s'agit d'une étude qui a été initiée au cours de mon post-doctorat et qui a été motivée notamment par des applications bio-médicales (projet ANR-10-IDEX-03-02). Les travaux présentés dans cette première partie ont fait l'objet de plusieurs publications [123, 48, 27, 56, 125] et de rapports de recherche [28, 11]. Enfin, je me suis intéressé à un problème de couche limite pour un écoulement fluide dans un milieu poreux en présence d'un fort contraste de viscosités [7]. Ce travail, qui est le fruit d'une collaboration

ponctuelle avec Philippe Angot et Gilles Carbou, est présenté de façon synthétique en annexe (Annexe B).

La présence de singularités géométriques aux interfaces, en particulier dans les problèmes mentionnés précédemment, peut complexifier largement l'analyse des phénomènes physiques sous-jacents comparativement au cas d'une interface régulière, notamment lorsqu'il s'agit de les décrire au moyen de développements asymptotiques. Au cours de ces dernières années, je me suis intéressé à l'analyse de problèmes elliptiques en présence de singularités de coins et d'arêtes, principalement pour des applications en électromagnétisme et en élasticité. Nous avons ainsi soulevé des problèmes de courant de Foucault, notamment avec Laurent Krähenbühl (Laboratoire Ampère, EC Lyon), ainsi que des problèmes de fissures en élasticité avec Zohar Yosibash (Université de Beer-Sheva) et qui ont été traités dans le cadre de la thèse de S. Shannon. D'une façon générale, l'analyse de ce type de problème repose sur la détermination d'un développement asymptotique (de type Kondrat'ev) de la solution au voisinage d'une singularité géométrique. Ce type de développement qui généralise le développement de Taylor dans le cas régulier, peut s'effectuer au moyen de l'analyse de Mellin qui permet de déterminer les exposants de singularités ainsi que la nature des fonctions singulières associées (aussi appelées les *singularités*). Les coefficients de singularités associés à ces singularités ne peuvent être déterminés bien souvent que d'une façon approchée. Leur extraction peut s'effectuer parfois au moyen de méthodes numériques obtenues en adaptant des méthodes "exactes" valables dans le cas d'une géométrie régulière. C'est ainsi qu'est née par exemple la méthode de la fonction quasi-duale. Dans ce cadre, plusieurs travaux sont présentés de façon synthétique dans une seconde partie qui s'articule autour de deux chapitres, chacun concernant une des applications mentionnées précédemment. Le chapitre 3 porte principalement sur la détermination des asymptotiques de coins de la solution d'un problème de courant de Foucault bi-dimensionnel (construction des fonctions singulières et extraction des coefficients de singularités) ainsi que sur la question d'un développement asymptotique de la solution de ce problème par rapport au petit paramètre d'épaisseur de peau. Ce travail permet notamment d'en déduire une modification locale de la condition de Leontovich près d'un coin. Dans le chapitre 4, on s'intéresse à la détermination des singularités et des coefficients de singularités au voisinage d'une arête (et en particulier près d'une fissure), droite ou courbe, pour le problème modèle du Laplacien en 3D. Les travaux présentés dans cette seconde partie ont fait l'objet de plusieurs publications [40, 141, 21, 140, 90].

La plupart des problèmes que j'ai pu aborder au cours de ces dernières années ont suscité le développement de méthodes numériques. C'est le cas notamment des problèmes mentionnés au paragraphe précédent avec la méthode de la fonction singulière quasi-duale. Je me suis également intéressé à des méthodes spectrales et polynomiales pour des équations intégrales singulières, dans le cadre d'une collaboration spontanée [65] avec Leandro Farina et Paul Martin ainsi que dans le cadre du stage (Master Thesis) de M. Rondiney (UFRGS, Porto Alegre) [63]. Ces travaux sont présentés de façon synthétique en Annexe C. Enfin, je me suis intéressé au développement de méthodes d'éléments finis, en particulier à une méthode de type Galerkin discontinue combinée avec une méthode d'upscaling, dans le cadre du Projet de Fin d'Etude de T. Chaumont-Frélet (INSA Rouen) [12]. Dans un cadre un peu plus applicatif, nous nous sommes intéressés avec Patrick Dular à des méthodes éléments finis par sous-problèmes. Ces méthodes permettent notamment de corriger successivement des erreurs dues à des modèles (par exemple, en magnétodynamique) de conducteur parfait ou d'impédance, en particulier près de coins ou d'arêtes, pour une gamme large de fréquences et de conductivités [52, 50, 51].

# General introduction

The aim of this manuscript is to summarise my research activities during the period after my PhD thesis that I have defended in September 2009 and which was devoted to the mathematical modeling of electromagnetic phenomena in high-contrast media [121]. The main problem of my thesis concerned the *skin effect* which has been analyzed with an asymptotic method and the numerical simulation [23, 22, 41]. During my PhD thesis, and then during my postdoctoral year at INRIA Bordeaux Sud-Ouest in the team MC2, I have been working also on thin-layer transmission problems in order to determine approximate models for the propagation of electromagnetic waves across the membrane of a biological cell [55]. Since my PhD thesis, I mainly work around three research area : the mathematical modeling of wave propagation phenomena in complex media ; the analysis and the numerical treatment of corner and edge singularities in elliptic systems, with several applications in electromagnetism and in elasticity ; the development of numerical methods for PDEs and integral equations.

Since I have been recruited at the University of Pau (September 2010) as Maître de Conférences, I have been working in the team Magique 3D (INRIA Bordeaux Sud-Ouest) on singular perturbation problems (boundary layer or thin-layer problems; problem with small defects) arising in the context of acoustic, elastic or electromagnetic wave propagation phenomena [123, 56, 48, 27, 125, 28, 11]. In general, we aim at describing a phenomenon with an asymptotic method based on a multi-scale expansion, and at implementing reduced models in Finite Element codes (for example, those based on Discontinuous Galerkin Methods, for geophysical applications) in order to study their properties. These works are presented in a first part which is divided into two chapters. The first chapter is devoted to thin-layer transmission problems in acoustic and elastic media. These problems have been addressed in the frame of the HPC GA project (High Performance Computing for Geophysical Applications) [123, 48, 27]. The second chapter concerns transmission problems of electromagnetic waves across thin layers with high conductivities. These problems have been addressed in the frame of the PhD thesis of A. Erdozain [60] that I co-advised with Hélène Barucq and David Pardo (UPV-EHU, Bilbao), and in the frame of the Procope project (TU Berlin - INRIA) [125]. The first part is complemented with an appendix (Appendix A) which presents a review on the accuracy of different approximations of the electromagnetic field for thin-layer transmission problems. This study has been carried out in the frame of the Investments for the future Programme IdEx Bordeaux CPU (ANR-10-IDEX-03-02) [56]. I have been working also on a boundary layer problem arising in a context of fluid flow modeling in porous media, in collaboration with Philippe Angot and Gilles Carbou [7]. This work is summarised in Appendix B.

Corner and edge singularities on interfaces may increase the level of complexity in the analysis of elliptic problems (such as those presented for example in the previous paragraph) in comparison with smooth interfaces. Since a few years I have been working on the analysis and on the numerical treatment of corner and edge singularities in elliptic systems for several applications in electromagnetism [40, 21, 90] and in elasticity [141, 140]. In electromagnetism, eddy current problems with a corner singularity on an interface (dielectric/conductor) have been ad-

dressed with Laurent Krähenbühl (Laboratoire Ampère, EC Lyon). In elasticity, crack problems have been addressed with Zohar Yosibash (Beer-Sheva University) in the frame of the PhD thesis of S. Shannon. Roughly speaking, the analysis of such a problem relies on the determination of a Kondrat'ev expansion which is a series of asymptotics defined in a vicinity of a (corner/edge) singularity. This expansion generalizes the Taylor one which holds in smooth domains. The notion of asymptotics involve two ingredients which are the singular coefficients and the singular functions (also called the *singularities*). The singularities are associated with singular exponents and may be determined with the Mellin analysis. The singular coefficients may be extracted with numerical methods, for example with the quasi dual function method (QDFM) which requires the knowledge of dual singularities. Several works related to these problems are presented in a second part which is divided into two chapters. Chapter 3 is mainly devoted to the determination of corner asymptotics of the magnetic potential in the eddy-current model. The first terms of a multi-scale expansion of the magnetic potential are also introduced to tackle the magneto-harmonic problem as the skin depth goes to zero. As an application, a modified (Leontovich) impedance boundary condition close to a corner singularity has been proposed. Chapter 4 is devoted to the notion of edge asymptotics for the Laplace operator. We mainly focus on the extraction of edge flux intensity factors (EFIFs) associated with the integer eigenvalues for the Laplace operator over a 3-D domain with a straight crack. The dual singularities are determined and the QDFM has been extended for the extraction of these EFIFs.

I have been working also on the development of numerical methods for PDEs and integral equations. In [12], a method which combines operator-based upscaling with a discontinuous Galerkin method for the Laplace problem has been developed in the frame of an internship (T. Chaumont-Frélet, INSA Rouen). In [65, 63], spectral methods and polynomial solutions have been developed for singular integral equations (SIEs). Two-dimensional hypersingular integral equations have been considered with Leandro Farina and Paul Martin [65] and Cauchy type SIEs have been considered in the frame of a Master thesis (M. Rondiney, UFRGS Porto Alegre) [63]. These works are presented briefly in Appendix C. Finally, finite element subproblem methods (FE-SPM) have been developed with Patrick Dular, to correct the inaccuracies proper to impedance boundary condition models, in particular near edges and corners of conductors, for a large range of conductivities and frequencies. FE-SPMs allow to split for example eddy current analysis into subproblems of lower complexity regarding computational aspects and meshing. Local corrections, supported by fine local meshes, can be obtained from each approximate model to the other, allowing efficient extensions of their domains of validity [52, 50, 51].

# Part I

# Asymptotic models for acoustic, elastic and electromagnetic media

The numerical simulation is extensively used in many domains : geophysical applications, biomedical applications, electronic devices, non-destructive testing... However many difficulties are inherent to complex media featuring high contrast of physical parameters (e.g. electrical conductivities, magnetic permeabilities, viscosities) and thin inclusions. This is why the numerical simulation may represent a main challenge, for example for large-scale geophysics phenomena such as an earthquake as well as for small-scale electromagnetic phenomena in biological cells and in electronic devices.

To reproduce real physical phenomena with the simulation, the coupling of elastic and acoustic waves equations is essential. The propagation of seismic waves in the Earth's subsurface can thus be taken into account together with the propagation of acoustic waves in a part of an ocean. However, when the medium consists of land areas surrounded by fluid zones whose thickness is much smaller than the characteristic wavelength, this raises the difficulty of applying a finite element method (FEM) on a mesh that combines fine cells in the fluid zone and much larger cells outside this zone. The numerical modeling is simplified if the model in the fluid region is replaced by an approximate boundary condition. This idea has motived several works [123, 48, 27] that we have carried out in the frame of the HPC GA project (High Performance Computing for Geophysical Applications).

The electromagnetic modeling of biological cells has become extremely important since several years in the biomedical research area. When the cell is exposed to an electric field, the local field near the membrane may overcome physiological values. Then, complex phenomenon may occur in the cell membrane and some outer molecules might be internalized inside the cell [146]. These process hold great promises in oncology and gene therapy. This is the reason why several works deal with numerical modeling of the cell and with numerical computations of the membrane voltage (e.g. [111, 137]). The main difficulties of the calculation of the local electric field lie in the thinness of the membrane and in the high contrast between the electromagnetic properties of the cytoplasm and the membrane. More precisely, the membrane conductivity is much lower than the cytoplasm conductivity, which provides particular behavior of the electromagnetic field at low frequencies, for which the conduction currents predominate.

The numerical simulation of electronic devices with highly conductive thin sheets is also challenging, especially if standard methods like the FEM shall be applied. As the sheets have to be solved by the mesh in thickness direction, the number of cells in the mesh increases with decreasing sheet thickness. In addition for higher frequencies, the fields decay rapidly inside the sheets and can be only resolved by increasing the number of cells even more. The numerical modeling is much simplified if the thin conducting sheets are replaced by transmission conditions on an interface, which is usually its mid-surface. Using the so called *impedance transmission conditions*, which relate the electric and magnetic fields on both sides of the interface, meshes with much larger cells can be used.

The concept of impedance boundary conditions (also called approximate, effective or equivalent conditions) is rather classical in the modeling of wave propagation phenomena. These conditions are usually introduced to reduce the computational domain. The main idea consists in replacing a reference model inside a part of the domain (for instance a thin layer of dielectric or a highly absorbing material [131, 97, 94, 139, 8]) by an approximate boundary condition. This idea is pertinent when the effective condition can be readily handled for numerical computations, for instance when this condition is local. In the 1990's Engquist–Nédélec [59], Abboud–Ammari [1], Bendali–Lemrabet [14], Ammari–Nédélec [4], and Lafitte [93] derived equivalent conditions for acoustic and electromagnetic scattering problems to approximate an obstacle coated by a thin layer of dielectric (absorbing) material inside the domain of propagation.

In these last few years I have been working on singular perturbation problems arising in the context of wave propagation phenomena [123, 48, 27, 55, 56, 125, 28]. In these problems we

aimed at designing reduced models. All these works are concerned essentially with numerical and theoretical objectives. Our approach is commonly based on multi-scale expansions. Stability and convergence results have been proved and numerical models have been developed in order to be easily implemented in Finite Element codes (Garc6more, Hou10ni, Montjoie) [48, 27, 55, 56, 125, 28].

In [123, 48] asymptotic models have been derived for the propagation of elastic and acoustic waves in a region which contains a thin layer of fluid. Due to the thinness of the layer with respect to the wavelength, this problem is well suited for the design of equivalent conditions. This approach leads to solve only elastic equations. Equivalent conditions are derived rigorously up to the fourth order for the elastic displacement. The construction of equivalent conditions is based on a multi-scale expansion in power series of the thickness of the layer for the solution of the transmission problem. In [27] equivalent absorbing boundary conditions EABCs have been proposed to model the propagation of waves in semi-infinite bi-layered acoustic media. Our motivation was to restrict the computational domain in the simulation of seismic waves that propagate from the earth and are transmitted to the stratified heterogeneous media composed by ocean and atmosphere. These EABCs are adapted to Hagstrom-Warburton ABCs and appear as first and second order of approximation with respect to a small parameter which corresponds to the thinness of a layer. Computational tests illustrate the accuracy of the first approximate model with respect to the small parameter. Finally, approximate models have been derived for the solution of the Helmholtz equation set in a domain which represents the Sun and its atmosphere [28]. This problem involves a large parameter $\alpha$ which corresponds to the exponential decay rate of a radial density. Equivalent conditions are obtained up to the fourth order of approximation with respect to the parameter $\alpha^{-1}$. It leads to solve only equations set in a domain representing the Sun. These conditions have been implemented and numerical results illustrate the good accuracy of the asymptotic models for realistic values close to those observed for the Sun.

In [55, 56, 125], impedance transmission conditions for thin-layer and boundary-layer problems are proposed for the time-harmonic Maxwell equations. The main motivation of the works in Refs. [55, 56] concerns the computation of electromagnetic field in biological cells. A review on the accuracy of asymptotic models for the scattering problem of electromagnetic waves in domains with thin layer has been presented in [56]. These models appear as first order approximations of the electromagnetic field. The main difficulty to compute the local electric field lies in the thinness of the membrane and in the high contrast between the electrical conductivities of the cytoplasm and of the membrane, which provides a specific behavior of the electromagnetic field at low frequencies. The advantages and the drawbacks of several approximations together with numerical validations and simulations are presented in [56]. In [125], impedance conditions of order 1 and 2 for thin and highly conducting sheets for the time-harmonic Maxwell's equation are proposed. These conditions are derived asymptotically for vanishing sheet thickness $\varepsilon$ where the skin depth is kept proportional to $\varepsilon$. The condition of order 1 turns out to be the perfect electric conductor boundary condition. The conditions of order 2 appear as generalised Poincaré-Steklov maps between tangential components of the magnetic field and the electric field, and they are of Wentzell type involving second order surface differential operators. Numerical results with finite elements of higher order validate the asymptotic convergence for $\varepsilon \to 0$ and the robustness of the equivalent transmission condition of order 2. These studies have been carried out in the frame of the Investments for the future Programme IdEx Bordeaux CPU (ANR-10-IDEX-03-02) [56] and in the frame of the Procope project [125].

The outline of this part proceeds as follows. In Chapter 1, an asymptotic method is developed for the propagation of acoustic and elastic and waves in complex media with thin inclusions. In Chapter 2, this method is developed for the propagation of electromagnetic waves in complex media featuring high contrasts and thin layers. This chapter is complemented with an appendix

which concerns a review on the accuracy of different approximations of the electromagnetic field for thin-layer transmission problems, Appendix A.

# Chapter 1

# Asymptotic models for thin-layer problems in acoustic and elastic media

## 1.1 Introduction

Elasto-acoustic coupling problems are rather classical in the mathematical modeling of wave propagation phenomena, in particular in harmonic domain. The well-posedness and the theoretical analysis of the direct problem has been studied in [83, 99, 10, 53] and in the monography [36, §5.4.e]. Various other works have been devoted to the numerical solution of the problem, using for instance BEM/FEM type method, where Boundary Element Method (BEM) are used to discretize the fluid and Finite Element Method (FEM) to discretize the solid [30, 68, 67, 114, 101, 136]; plane waves based methods, as in [58, 80] or Discontinuous Galerkin Methods [9]. The transient problem is mostly studied for geophysical applications such as numerical simulation of earthquakes and many works have been devoted to the numerical discretization of fluid-structure problems using Finite Difference methods [129], Spectral Element Methods [86] or Discontinuous Galerkin Methods allowing for non-conforming meshes [84]. Finally, we refer to [109, 2, 62] for the study of inverse problems of shape reconstruction of solid body immersed in a fluid and we refer to the monography [3] for mathematical methods in elasticity imaging.

In [123, 48] one considers that the medium consists of land areas surrounded by fluid zones whose thickness is much smaller than the characteristic wavelength. To avoid numerical instabilities, an asymptotic method has been developed in order to approximate the fluid portion by an equivalent condition (EC). This boundary condition is then coupled with the elastic wave equation and a FEM can be applied to solve the resulting boundary value problem. We present elements of derivation together with mathematical justifications for ECs up to the fourth order approximations with respect to the small parameter $\varepsilon$ (the thickness of the fluid layer). These ECs are satisfied by the elastic displacement $\mathbf{u}$ and are of "$\mathbf{u}\cdot\mathbf{n}$–to–$\mathbf{T}(\mathbf{u})$" nature for elasto-acoustics since a local operator links the normal traces of $\mathbf{u}$ and the stress vector $\mathbf{T}(\mathbf{u})$. Stability and convergence results for these ECs have been proven by removing a discret set of resonant frequencies. The numerical pertinence of these ECs have been shown for the two-dimensional problem [47]. Second order ECs have also been developed when the thickness of the layer depends on the tangential variables [48].

In [27] equivalent boundary conditions have also been proposed in order to model the propagation of waves in acoustic media. Our motivation was to restrict the computational domain in the simulation of seismic waves that are propagated from the earth and transmitted to the stratified heterogeneous media composed by ocean and atmosphere. These new conditions approximate Hagstrom-Warburton conditions [75, 74] and appear as first and second order of approximation with respect to a small parameter $\varepsilon$ which corresponds to the thinness of a layer. Computational

tests illustrate the accuracy of the first approximate model with respect to this parameter.

In this chapter we restrict ourselves to present the conditions that have been developed in [123, 48]. The outline of this chapter proceeds as follows. The mathematical model and equivalent conditions are presented in Section 1.2. Then numerical results are presented in Section 1.3 to illustrate the convergence results.

## 1.2 The mathematical model. Main results

In this section, the elasto-acoustic problem is introduced. A formal derivation of the equivalent conditions (ECs) is presented. Then ECs are proposed and stability and convergence results are stated.

### 1.2.1 The model problem

Our interest lies in an elasto-acoustic wave propagation problem in time-harmonic regime set in a domain with a thin layer. We consider the fluid-solid transmission problem

$$\begin{cases} \Delta \mathsf{p}_\varepsilon + \kappa^2 \mathsf{p}_\varepsilon = 0 & \text{in} \quad \Omega_\mathsf{f}^\varepsilon \\ \nabla \cdot \underline{\underline{\sigma}}(\mathbf{u}_\varepsilon) + \omega^2 \rho \mathbf{u}_\varepsilon = \mathbf{f} & \text{in} \quad \Omega_\mathsf{s} \\ \partial_\mathbf{n} \mathsf{p}_\varepsilon = \rho_\mathsf{f} \omega^2 \mathbf{u}_\varepsilon \cdot \mathbf{n} & \text{on} \quad \Gamma \\ \mathbf{T}(\mathbf{u}_\varepsilon) = -\mathsf{p}_\varepsilon \mathbf{n} & \text{on} \quad \Gamma\,. \end{cases} \tag{1.1}$$

These equations are complemented with a Dirichlet or a Robin boundary condition on $\Gamma^\varepsilon$

$$\text{Either} \quad \mathsf{p}_\varepsilon = 0 \quad \text{(Dirichlet case)}, \quad \text{or} \quad \partial_\mathbf{n} \mathsf{p}_\varepsilon - i\kappa \mathsf{p}_\varepsilon = 0 \quad \text{(Robin case)},$$

where $\mathbf{n}$ denotes the outer normal vector. Problem (1.1) is set in a smooth bounded simply connected domain $\Omega^\varepsilon$ in $\mathbb{R}^3$ made of a solid, elastic object occupying a smooth connected subdomain $\Omega_\mathsf{s}$ entirely immersed in a fluid region occupying the subdomain $\Omega_\mathsf{f}^\varepsilon$. The domain $\Omega_\mathsf{f}^\varepsilon$ is a thin layer of uniform thickness $\varepsilon$, see Figure 1.1.

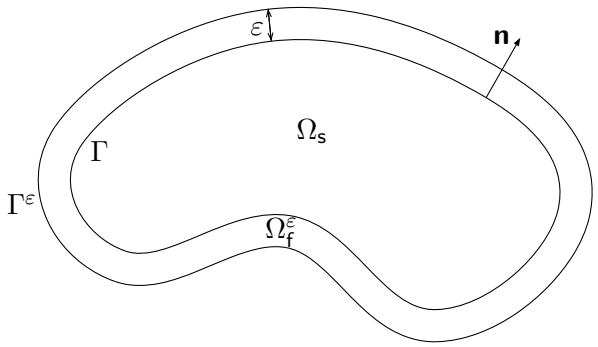


Figure 1.1: A cross-section of the domain $\Omega^\varepsilon$ and its subdomains $\Omega_\mathsf{s}$ and $\Omega_\mathsf{f}^\varepsilon$

In (1.1), we denote by $\mathbf{u}_\varepsilon$ the elastic displacement and by $\mathsf{p}_\varepsilon$ the acoustic pressure. The time-harmonic wave field with angular frequency $\omega \neq 0$ is characterized by using the Helmholtz equation for the pressure $\mathsf{p}_\varepsilon$, and by using an anisotropic linear elasticity system for the displacement $\mathbf{u}_\varepsilon$. These equations contain several physical constants: $\kappa = \omega/c$ is the acoustic wave number,

$c$ is the speed of the sound, $\rho$ is the density of the solid, and $\rho_{\mathsf{f}}$ is the density of the fluid. In the linear elastic equation, $\nabla\cdot$ denotes the divergence operator for tensors, $\underline{\underline{\sigma}}(\mathbf{u})$ is the stress tensor given by Hooke's law

$$\underline{\underline{\sigma}}(\mathbf{u}) = \underline{\underline{C}}\,\underline{\underline{\epsilon}}(\mathbf{u})\ .$$

Here $\underline{\underline{\epsilon}}(\mathbf{u}) = \frac{1}{2}(\underline{\underline{\nabla}}\mathbf{u} + \underline{\underline{\nabla}}\mathbf{u}^T)$ is the strain tensor where $\underline{\underline{\nabla}}$ denotes the gradient operator for tensors, and $\underline{\underline{C}} = \underline{\underline{C}}(\mathbf{x})$ is the elasticity tensor. The *traction operator* $\mathbf{T}$ is a surface differential operator defined on $\Gamma$ as

$$\mathbf{T}(\mathbf{u}) = \underline{\underline{\sigma}}(\mathbf{u})\mathbf{n}\ .$$

In this work the issue of Equivalent Conditions (ECs) is addressed for the elastic displacement $\mathbf{u}_\varepsilon$ as $\varepsilon \to 0$. This question is linked with the issue of uniform estimates for the couple $(\mathbf{u}_\varepsilon, \mathsf{p}_\varepsilon)$ which solves Problem (1.1) as $\varepsilon \to 0$ since it is a main ingredient in the validation of ECs. To answer these questions, we make several assumptions on the data and on the regularity of the surface $\Gamma$.

### 1.2.2 Framework

We work under usual assumptions (regularity, symmetry and positiveness) on the elasticity tensor $\underline{\underline{C}}$. Some resonant frequencies may appear in the solid domain. However we can prove uniform estimates for the field $(\mathbf{u}_\varepsilon, \mathsf{p}_\varepsilon)$ as $\varepsilon \to 0$ and we can validate ECs for $\mathbf{u}_\varepsilon$ under the following spectral assumptions on limit problems set in the solid part $\Omega_{\mathsf{s}}$

**Assumption 1.1 (Dirichlet case)** *The angular frequency $\omega$ is not an eigenfrequency of the problem*

$$\left\{\begin{array}{ll} \nabla\cdot\underline{\underline{\sigma}}(\mathbf{u}) + \omega^2\rho\mathbf{u} = 0 & \textit{in}\quad \Omega_{\mathsf{s}} \\ \mathbf{T}(\mathbf{u}) = 0 & \textit{on}\quad \Gamma\ . \end{array}\right.$$

**Assumption 1.2 (Robin case)** *The angular frequency $\omega$ is not an eigenfrequency of the problem*

$$\left\{\begin{array}{ll} \nabla\cdot\underline{\underline{\sigma}}(\mathbf{u}) + \omega^2\rho\mathbf{u} = 0 & \textit{in}\quad \Omega_{\mathsf{s}} \\ \mathbf{T}(\mathbf{u}) = 0 \quad \textit{and} \quad \mathbf{u}\cdot\mathbf{n} = 0 & \textit{on}\quad \Gamma\ . \end{array}\right. \tag{1.2}$$

Jones eigenmodes (1.2) exist for axisymmetric bodies $\Omega_{\mathsf{s}}$ and for a discrete set of frequencies $\omega$ [83, 99] but do not exist for generic domains, [76]. Our whole analysis is valid under the assumption that the surfaces $\Gamma$ and $\Gamma^\varepsilon$ are smooth, and $\mathbf{f}$ is a smooth $\varepsilon$-independent data. In this framework, we prove in [123, 48] that it is possible to replace the domain $\Omega_{\mathsf{f}}^\varepsilon$ by ECs and set on $\Gamma$.

### 1.2.3 Formal derivation of equivalent conditions

In this section, a formal derivation of equivalent conditions (ECs) is presented in two steps. All the details and formal calculi are presented in [123, Sec. 4] (Dirichlet case) and in [48, Sec. 5] (Fourier case).

**First step : a multiscale expansion**

A multiscale expansion in power series of the small parameter $\varepsilon$ is derived for the solution $(\mathbf{u}_\varepsilon, \mathsf{p}_\varepsilon)$ of Problem (1.1) :

$$\begin{aligned}\mathbf{u}_\varepsilon(\mathbf{x}) &= \mathbf{u}_0(\mathbf{x}) + \varepsilon\mathbf{u}_1(\mathbf{x}) + \varepsilon^2\mathbf{u}_2(\mathbf{x}) + \cdots \quad \text{in} \quad \Omega_\mathsf{s}\,,\\ \mathsf{p}_\varepsilon(\mathbf{x}) &= \mathsf{p}_0(\mathbf{x};\varepsilon) + \varepsilon\mathsf{p}_1(\mathbf{x};\varepsilon) + \varepsilon^2\mathsf{p}_2(\mathbf{x};\varepsilon) + \cdots \quad \text{in} \quad \Omega_\mathsf{f}^\varepsilon\,,\\ &\text{with} \quad \mathsf{p}_j(\mathbf{x};\varepsilon) = \mathfrak{p}_j(y_\alpha, \frac{y_3}{\varepsilon})\,.\end{aligned}$$

Here $\mathbf{x} \in \mathbb{R}^3$ are the cartesian coordinates and $(y_\alpha, y_3)$ is a "*normal coordinate system*" [22, 122] to the surface $\Gamma = \partial\Omega_\mathsf{s}$ on the manifold $\Omega_\mathsf{f}^\varepsilon$ : $y_\alpha$ ($\alpha \in \{1,2\}$) is a tangential coordinate on $\Gamma$ and $y_3 \in (0,\varepsilon)$ is the distance to the surface $\Gamma$. The term $\mathfrak{p}_j$ is a "*profile*" defined on $\Gamma \times (0,1)$. The first terms $(\mathfrak{p}_j, \mathbf{u}_j)$ are obtained for $j = 0,1,2,3$ in [123, Sec. 4.2] (Dirichlet case) and for $j = 0,1,2$ in [48, Sec. 5.2] (Robin case).

**Second step : construction of equivalent conditions**

The second step consists to identify a simpler problem satisfied by the truncated expansion

$$\mathbf{u}_{k,\varepsilon} := \mathbf{u}_0 + \varepsilon\mathbf{u}_1 + \varepsilon^2\mathbf{u}_2 + \cdots + \varepsilon^k\mathbf{u}_k$$

up to a residual term in $\mathcal{O}(\varepsilon^{k+1})$. The simpler problem which satisfies an EC on $\Gamma$ writes

$$\left\{\begin{array}{ll}\nabla\cdot\underline{\underline{\sigma}}(\mathbf{u}_\varepsilon^k) + \omega^2\rho\mathbf{u}_\varepsilon^k = \mathbf{f} & \text{in} \quad \Omega_\mathsf{s}\\ \mathbf{T}(\mathbf{u}_\varepsilon^k) + \mathsf{B}_{k,\varepsilon}(\mathbf{u}_\varepsilon^k\cdot\mathbf{n})\,\mathbf{n} = 0 & \text{on} \quad \Gamma\,.\end{array}\right. \tag{1.3}$$

Here $\mathsf{B}_{k,\varepsilon}$ is a differential operator acting on functions defined on $\Gamma$ which depends on $\varepsilon$. The boundary condition in (1.3) is called an equivalent condition of *order* $k+1$. Hence we obtain a hierarchy of boundary conditions in (1.3), each one gives a model with a different order of accuracy in $\varepsilon$.

### 1.2.4 Statement of equivalent conditions (Dirichlet case)

When the set of equations (1.1) is complemented with a Dirichlet boundary condition on $\Gamma^\varepsilon$, the first order equivalent conditions are

**Order 1**

$$\mathbf{T}(\mathbf{u}_0) = 0 \quad \text{on} \quad \Gamma$$

**Order 2**

$$\mathbf{T}(\mathbf{u}_\varepsilon^1) - \varepsilon\omega^2\rho_\mathsf{f}\mathbf{u}_\varepsilon^1\cdot\mathbf{n}\,\mathbf{n} = 0 \quad \text{on} \quad \Gamma$$

**Order 3**

$$\mathbf{T}(\mathbf{u}_\varepsilon^2) - \varepsilon\omega^2\rho_\mathsf{f}\,(1-\varepsilon\mathcal{H}(y_\alpha))\,\mathbf{u}_\varepsilon^2\cdot\mathbf{n}\,\mathbf{n} = 0 \quad \text{on} \quad \Gamma$$

**Order 4**

$$\mathbf{T}(\mathbf{u}_\varepsilon^3) - \varepsilon\omega^2\rho_{\mathsf{f}}\left(1 - \varepsilon\mathcal{H}(y_\alpha) + \frac{\varepsilon^2}{3}\left[\Delta_\Gamma + \kappa^2\mathbb{I} + 4\mathcal{H}^2(y_\alpha) - \mathcal{K}(y_\alpha)\right]\right)(\mathbf{u}_\varepsilon^3\cdot\mathbf{n})\,\mathbf{n} = 0 \quad \text{on} \quad \Gamma$$

Here $\mathcal{H}$ and $\mathcal{K}$ denote the *mean curvature* and the *Gaussian curvature* of the surface $\Gamma$ and $\Delta_\Gamma$ is the Laplace-Beltrami operator along $\Gamma$. We refer to [123, Sec. 4.3] for the construction of these ECs.

### 1.2.5 Statement of equivalent conditions (Robin case)

When the set of equations (1.1) is complemented with a Robin boundary condition on $\Gamma^\varepsilon$, the first order equivalent conditions are

**Order 1**

$$\mathbf{T}(\mathbf{u}_0) - i\omega c\rho_{\mathsf{f}}\mathbf{u}_0\cdot\mathbf{n}\,\mathbf{n} = 0 \quad \text{on} \quad \Gamma$$

**Order 2**

$$\mathbf{T}(\mathbf{u}_\varepsilon^1) - i\omega c\rho_{\mathsf{f}}\left(\mathbb{I} + \varepsilon P_1(D)\right)(\mathbf{u}_\varepsilon^1\cdot\mathbf{n})\,\mathbf{n} = 0 \quad \text{on} \quad \Gamma$$

**Order 3**

$$\mathbf{T}(\mathbf{u}_\varepsilon^2) - i\omega c\rho_{\mathsf{f}}\left(\mathbb{I} + \varepsilon P_1(D) + \varepsilon^2 P_2(D)\right)(\mathbf{u}_\varepsilon^2\cdot\mathbf{n})\,\mathbf{n} = 0 \quad \text{on} \quad \Gamma$$

Here $P_1(D)$ and $P_2(D)$ are surface differential operators which are defined respectively as

$$P_1(D) = -2\mathcal{H}\,\mathbb{I} + i\kappa^{-1}\Delta_\Gamma$$

$$P_2(D) = -2i\kappa\mathcal{H}\,\mathbb{I} + \left((4\mathcal{H}^2 - \mathcal{K})\,\mathbb{I} - \Delta_\Gamma\right) + (i\kappa)^{-1}\left[2\mathcal{H}\Delta_\Gamma - \mathrm{div}_\Gamma(\mathcal{H}\mathbb{I} - \mathcal{R})\nabla_\Gamma) + \Delta_\Gamma(2\mathcal{H})\right] + (i\kappa)^{-2}\Delta_\Gamma^2\,,$$

where $\mathcal{R}$ is an intrinsic symmetric linear operator defined on the tangent plane $\mathbf{T}_{\mathbf{x}_\Gamma}(\Gamma)$ to $\Gamma$ at the point $\mathbf{x}_\Gamma \in \Gamma$ which characterizes the curvature of $\Gamma$ at the point $\mathbf{x}_\Gamma$. The construction of these conditions is detailed in [48, Sec. 5.3].

### 1.2.6 Stability and convergence results for equivalent conditions

The validation of equivalent conditions (ECs) consist in proving uniform estimates for $\mathbf{u}_\varepsilon - \mathbf{u}_\varepsilon^k$, where $\mathbf{u}_\varepsilon^k$ is the solution of the approximate model (1.3), and $\mathbf{u}_\varepsilon$ satisfies the problem (1.1). In the Dirichlet case, the functional setting for $\mathbf{u}_\varepsilon^k$ is described by the Hilbert space $\mathbf{V}^k = \mathbf{H}^1(\Omega_{\mathsf{s}})$ when $k \in \{0,1,2\}$, and $\mathbf{V}^k = \{\mathbf{u} \in \mathbf{H}^1(\Omega_{\mathsf{s}}) \,|\quad \mathbf{u}\cdot\mathbf{n}|_\Gamma \in \mathrm{H}^1(\Gamma)\}$ when $k = 3$. We refer the reader to [48, Sec. 2.5] for the Robin case.

**Theorem 1.3** *Under Assumption 1.1, for all $k \in \{0,1,2,3\}$ there exists constants $\varepsilon_k, C_k > 0$ such that for all $\varepsilon \in (0,\varepsilon_k)$, the problem (1.3) with data $\mathbf{f} \in \mathbf{L}^2(\Omega_{\mathsf{s}})$ has a unique solution $\mathbf{u}_\varepsilon^k \in \mathbf{V}^k$ which satisfies uniform estimates*

$$\|\mathbf{u}_\varepsilon - \mathbf{u}_\varepsilon^k\|_{1,\Omega_{\mathsf{s}}} \leqslant C_k\varepsilon^{k+1}\,. \tag{1.4}$$

Since it is nontrivial to work straightforwardly with the difference $\mathbf{u}_\varepsilon - \mathbf{u}_\varepsilon^k$, we use the truncated series $\mathbf{u}_{k,\varepsilon}$ introduced in Sec. 1.2.3 as intermediate quantities. Hence, the error analysis is split into two steps which are detailed in [123] :

1. We prove uniform estimates for the difference $\mathbf{u}_\varepsilon - \mathbf{u}_{k,\varepsilon}$ [123, Th. 4.2],
2. We prove uniform estimates for the difference $\mathbf{u}_{k,\varepsilon} - \mathbf{u}_\varepsilon^k$ [123, Sec. 5.2].

The first step relies on uniform estimates for the solution $\mathbf{u}_\varepsilon$ to Problem (1.1) which are stated in Sec. 1.2.7. We prove that Problem (1.3) is well-posed and its solution satisfies uniform estimates in $\mathbf{H}^1$ norm, see [123, Th. 4.3]. Then we can deduce the second step stated above.

### 1.2.7 Uniform estimates

In the framework above $\varepsilon$-uniform a priori estimates have been proven for the solution to Problem (1.1).

**Theorem 1.4** *Under Assumption 1.1, there exists constants $\varepsilon_0, C > 0$ such that for all $\varepsilon \in (0, \varepsilon_0)$, the problem (1.1) has a unique solution $(\mathbf{u}_\varepsilon, \mathsf{p}_\varepsilon) \in \{(\mathbf{u}, \mathsf{p}) \in \mathbf{H}^1(\Omega_\mathsf{s}) \times \mathrm{H}^1(\Omega_\mathsf{f}^\varepsilon) \,|\, \gamma_0 \mathsf{p} = 0 \quad on \quad \Gamma^\varepsilon\}$ which satisfies*

$$\|\mathsf{p}_\varepsilon\|_{1,\Omega_\mathsf{f}^\varepsilon} + \|\mathbf{u}_\varepsilon\|_{1,\Omega_\mathsf{s}} \leqslant C \|\mathbf{f}\|_{0,\Omega_\mathsf{s}} \,. \tag{1.5}$$

This result has been proven in [123, Sec. 3] (for more general right-hand sides). The proof is based on a compactness argument and a formulation of the problem set in a fixed domain. This formulation is obtained through a scaling along the thickness of the layer. As an application of uniform estimates (1.5), we can prove estimates for the remainders $\mathbf{u}_\varepsilon - \mathbf{u}_{k,\varepsilon}$.

## 1.3 Numerical simulations

In the numerical experiments, the scattering problem of an acoustic plane wave from an aluminum disk embedded in water has been considered. The computational domain for the domain $\Omega_\mathsf{s}$ is a disk with a radius $R = 0.01$ m. The source term is an incident wave with support on $\Gamma$ defined as $\mathsf{p}_i(\mathbf{x}) = \exp(i\omega \mathbf{x} \cdot \mathbf{d})$ with $\mathbf{d} = (1, 0)$. The angular frequency is $\omega = 1.5 \times 10^6$ Hz. The Navier equation is solved in the domain $\Omega_\mathsf{s}$ :

$$\mu \Delta \mathbf{u} + (\lambda + \mu) \nabla \operatorname{div} \mathbf{u} + \omega^2 \rho \mathbf{u} = 0 \,,$$

where $\lambda$ and $\mu$ are the Lamé coefficients : $\mu \simeq 26.32 \times 10^9$ and $\lambda \simeq 51.08 \times 10^9$. The speed of the sound is $c = 1500$ m.s$^{-1}$ and the density of water is $\rho_f = 1000$ kg.m$^{-3}$, while the density of the solid is $\rho_f = 2700$ kg.m$^{-3}$, [80].

The ECs have been implemented in several codes. For the FE computations, we use an Interior Penalty Discontinuous Galerkin Method (IPDGM) and $\mathbb{P}_3$-finite elements (Lagrange) which are available in the Finite Element code Hou10ni. The mesh of the computational domain contains 140000 triangles.

### 1.3.1 Dirichlet case

We compute the $\mathrm{L}^2$-errors $\mathrm{Err}_k(\varepsilon) := \|\mathbf{u}_\varepsilon - \mathbf{u}_\varepsilon^k\|_{0,\Omega_\mathsf{s}}$ between the analytical solution $\mathbf{u}_\varepsilon$ to Problem (1.1) and FE solutions $\mathbf{u}_\varepsilon^k$ with curved elements which is associated with an EC of order $1, 2$, or $3$ in the Dirichlet case. We also compute the $\mathrm{L}^2$-errors between the analytical solution to Problem

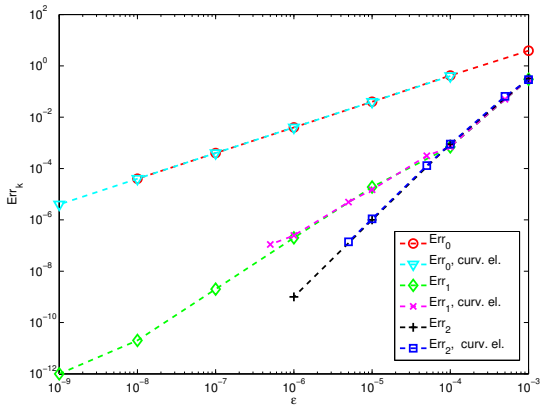


Figure 1.2: $\mathrm{L}^2$-errors $\mathrm{Err}_k$ with respect to $\varepsilon$ for $k = 0, 1, 2$ (Dirichlet external b.c.). Comparison between analytical solutions and numerical (DG Finite Elements) solutions with curved elements

(1.1) and the analytical solution associated with an EC. These errors are plotted on Figure 1.2. We observe that the numerical convergence rate coincides with the theory since the $\mathrm{L}^2$ error is of order $\varepsilon^{k+1}$ : $\mathrm{Err}_k(\varepsilon) = \mathcal{O}(\varepsilon^{k+1})$ for $k = 0, 1, 2$.

### 1.3.2 Robin case

We compute the $\mathrm{L}^2$-errors between the analytical solution to Problem (1.1) and FE solutions (with straight or curved elements) $\mathbf{u}_\varepsilon^0$ (which is associated with an EC of order 1) in the Robin case. We also compute the $\mathrm{L}^2$-errors between the analytical solution of the exact problem (1.1) and each analytical solution associated with an EC of order 1, or 2. We observe that the numerical convergence rate coincides with the theory since the $\mathrm{L}^2$ error satisfies $\mathrm{Err}_k(\varepsilon) = \mathcal{O}(\varepsilon^{k+1})$ for $k = 0, 1$, See Figure 1.3.

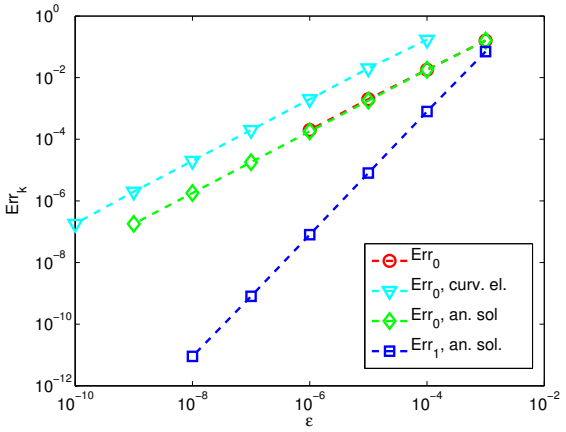


Figure 1.3: $\mathrm{L}^2$-errors $\mathrm{Err}_k$ with respect to $\varepsilon$, $k = 0, 1$ (Robin external b.c.). Comparison between numerical solutions and analytical solutions

## 1.4 Conclusion and perspectives

New boundary conditions have been proposed to approximate a thin layer of water with a Dirichlet or Robin boundary condition on top of it. The new asymptotic model has been derived up to the fourth order thanks to a two scale asymptotic expansion. The stability of the new condition and the convergence of the asymptotic model have been proven. The equivalent condition has been designed in order to be easily implemented in Finite Element codes, in particular in those based on Discontinuous Galerkin methods. Thus, the next of this work will be the performance analysis of the equivalent condition on numerical simulations. The next issue to tackle is the case where the layer of fluid, which usually models the ocean, is coupled with the atmosphere. In such a case, a first solution consists in replacing the ocean by an equivalent boundary condition (EC). However, since the atmosphere can be considered as infinite, it is usually modeled thanks to a high order absorbing boundary condition (ABC). Hence, a very promising perspective of this work is the construction of EC in the case where a high order ABC is imposed on top of the water. A simpler problem has been investigated in [27] for the propagation of acoustic waves in semi-infinite bi-layered media and equivalent ABCs have been derived. Finally, the extension of the proposed EC to transient problems is far from trivial (See e.g. [16] for thin-layer problems in elastodynamics) and should be the object of a future work.

# Chapter 2

# Impedance conditions for highly conductive thin sheet for the time-harmonic Maxwell equations

## 2.1 Introduction

Already in 1902 Levi-Civita introduced impedance transmission conditions [98] (see also [13, 138]) for Maxwell's equations. He postulated that the electric field is continuous over the interface whereas the magnetic field has a discontinuity, which is proportional to the sheet thickness and conductivity. As variation of the conditions by Levi-Civita the so called *shielding element* [113] has been introduced. In an alternative way the so called *thin layer boundary condition* [147, 91, 105, 81, 69] are derived taking into account the boundary layer behaviour of the solution. In this way, the thin layer boundary conditions exhibit jumps in both the electric and magnetic field and involve sheet thickness and conductivity as arguments of hyperbolic functions.

Impedance transmission conditions (ITCs) fit naturally with finite element methods [127, 130, 15, 82] as well as boundary integral formulations [85, 107, 134], where for the latter only the interface has to be discretized. ITCs with drastically reduced error levels can systematically been derived by an *asymptotic analysis* of the Maxwell's equations with thin conducting sheets where the sheet thickness $\varepsilon$ tends to zero. For example, for the eddy current model in 2D the family ITC-2-N [133], in which the conductivity is scaled like $1/\varepsilon^2$ and $N$ corresponds to the order, where the convergence of the modelling error outside the sheet is like $\varepsilon^{N+1}$ in their respective asymptotic regime. This convergence is not always robust in terms of the conductivity [132]. However, it turns out that the ITC-2-0 and ITC-2-1 conditions are robust and can be used from very low to very high frequencies.

Since most electromagnetic devices necessitate the modeling in three dimensions, ITCs have been derived for the full time-harmonic Maxwell's equations in 3D and their numerical properties have been investigated in [125]. To obtain robust transmission conditions as the ITC-2-1 in two dimensions we choose the asymptotic regime in which the conductivity is scaled like $1/\varepsilon^2$. We consider the general case of curved thin sheets where all the material constants may take different values inside and on the two sides of the sheet. With this investigation we provide transmission conditions which apply for high frequencies where electromagnetic wave propagation cannot be neglected as well as for the magneto-quasistatic eddy current model.

In this chapter we restrict ourselves to presenting ITCs for highly conductive sheets [125]. A brief review on the accuracy of different approximations of the electromagnetic field for time-harmonic thin-layer transmission problems is also presented in Appendix A [56, 55]. Section 2.2

presents the model with a formulation in terms of the electric field and a formal derivation of impedance conditions based on an asymptotic expansion in the thickness parameter $\varepsilon$. Then, in Section 2.3 as main results the equivalent model of order 1, which satisfies perfect electric conductor boundary conditions, and the equivalent model of order 2 are given. The equivalent model of order 2 involves as a transmission condition a generalized Poincaré-Steklov map with a second order surface differential operator. A mixed variational formulation including as additional unknowns the mean and jump of the tangential magnetic field components on the interface is introduced. The properties of the equivalent models have been investigated numerically for two examples. These studies include the convergence of the modeling error and the robustness with respect to the sheet conductivity, Section 2.4.

## 2.2 The mathematical model and equivalent models with transmission conditions

In this section we aim at giving a guideline on the derivation of impedance conditions. Let us first present the mathematical model.

### 2.2.1 Time-harmonic Maxwell equations

We denote by $\Omega \subset \mathbb{R}^3$ the domain of interest, which is composed of three subdomains (see Figure 2.1) as

$$\Omega = \Omega_-^\varepsilon \cup \overline{\Omega_o^\varepsilon} \cup \Omega_+^\varepsilon$$

corresponding to different linear materials. The subdomain $\Omega_o^\varepsilon$ is a thin layer of constant thickness $\varepsilon$ surrounding the subdomain $\Omega_-^\varepsilon$. The boundary of the subdomain $\Omega_-^\varepsilon$ is the smooth surface denoted by $\Gamma_-^\varepsilon$ while $\Gamma_+^\varepsilon$ is the boundary of the subdomain $\overline{\Omega_-^\varepsilon} \cup \Omega_o^\varepsilon$. The mid-surface of the thin layer $\Omega_o^\varepsilon$ is denoted by $\Gamma$. In all that follows, unless specified, all the considered domains are smooth domains in $\mathbb{R}^3$.

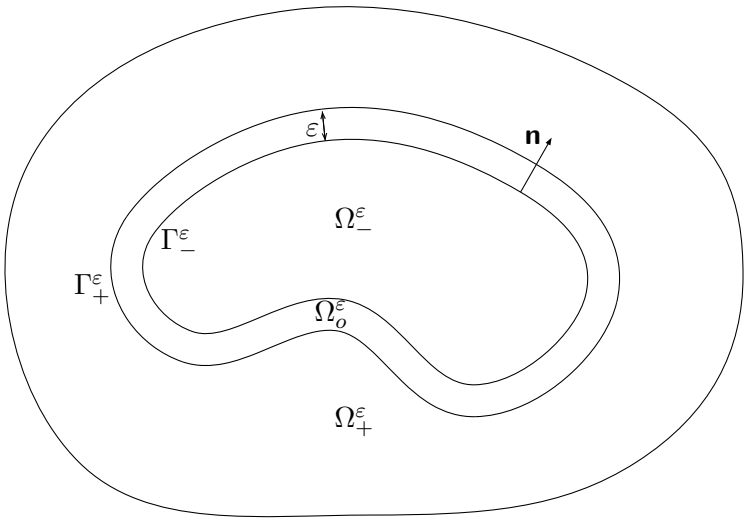


Figure 2.1: A cross-section of the domain $\Omega$ and the subdomains $\Omega_-^\varepsilon$, $\Omega_o^\varepsilon$, $\Omega_+^\varepsilon$.

The electromagnetic properties in $\Omega$ are given by the piecewise-constant and strictly positive functions $\underline{\mu}^\varepsilon$, $\underline{\epsilon}^\varepsilon$, and $\underline{\sigma}^\varepsilon$ corresponding to the respective magnetic permeability, electric permittivity, and conductivity of the possibly different materials in the three subdomains :

$$\underline{\mu}^\varepsilon = \begin{cases} \mu_-, & \text{in } \Omega_-^\varepsilon, \\ \mu_o, & \text{in } \Omega_o^\varepsilon, \\ \mu_+, & \text{in } \Omega_+^\varepsilon, \end{cases} \quad \underline{\epsilon}^\varepsilon = \begin{cases} \epsilon_-, & \text{in } \Omega_-^\varepsilon, \\ \epsilon_o, & \text{in } \Omega_o^\varepsilon, \\ \epsilon_+, & \text{in } \Omega_+^\varepsilon, \end{cases} \quad \underline{\sigma}^\varepsilon = \begin{cases} \sigma_-, & \text{in } \Omega_-^\varepsilon, \\ \sigma_o^\varepsilon = \varepsilon^{-2}\tilde{\sigma}, & \text{in } \Omega_o^\varepsilon, \\ \sigma_+, & \text{in } \Omega_+^\varepsilon. \end{cases}$$

We consider $\varepsilon$ as a parameter, on which $\underline{\mu}^\varepsilon$ and $\underline{\epsilon}^\varepsilon$ depend through the definition of the subdomains, where in $\underline{\sigma}^\varepsilon$ in addition we assume an explicit dependence of the layer conductivity $\sigma_o^\varepsilon$ on $\varepsilon$. With this correlation the thinner is the layer, the larger is the conductivity in the layer. The dependence like $\varepsilon^{-2}$ corresponds for $\varepsilon \to 0$ to asymptotically constant ratio of skin depth $d_{\text{skin}} = \sqrt{2/(\omega\mu_o\sigma_o^\varepsilon)}$ and thickness $\varepsilon$, *i.e.* , they behave the same for $\varepsilon \to 0$.

Let $\omega > 0$ be the angular frequency. Let us denote by $\mathbf{j}$ a smooth time-harmonic current source which support does not meet the layer $\Omega_o^\varepsilon$. Maxwell's equations link the electric field $\mathbf{E}^\varepsilon$ and the magnetic field $\mathbf{H}^\varepsilon$, through Faraday's and Ampère's laws in $\Omega$ :

$$\operatorname{curl} \mathbf{E}^\varepsilon - i\omega\underline{\mu}^\varepsilon \mathbf{H}^\varepsilon = 0 \quad \text{and} \quad \operatorname{curl} \mathbf{H}^\varepsilon + (i\omega\underline{\epsilon}^\varepsilon - \underline{\sigma}^\varepsilon)\, \mathbf{E}^\varepsilon = \mathbf{j} \quad \text{in} \quad \Omega\,.$$

This problem is complemented with a Silver-Müller boundary condition set on $\partial\Omega$.

### 2.2.2 Electric field formulation for the time-harmonic Maxwell equations

Maxwell's system of first order partial differential equations can be reduced to the following second-order equation for the electric field

$$\operatorname{curl}\operatorname{curl} \mathbf{E}^\varepsilon - (\underline{\kappa}^\varepsilon)^2 \mathbf{E}^\varepsilon = i\omega\underline{\mu}\mathbf{j}, \qquad \text{in} \quad \Omega_-^\varepsilon \cup \Omega_o^\varepsilon \cup \Omega_+^\varepsilon\,, \tag{2.1a}$$

with the continuity conditions for the Dirichlet and Neumann traces (*cf.* [79, Sec. 3]) across $\Gamma_\pm^\varepsilon$

$$\mathbf{E}_\pm^\varepsilon \times \mathbf{n} = \mathbf{E}_o^\varepsilon \times \mathbf{n}, \qquad \text{on} \quad \Gamma_\pm^\varepsilon\,, \tag{2.1b}$$

$$\frac{1}{\mu_\pm} \operatorname{curl} \mathbf{E}_\pm^\varepsilon \times \mathbf{n} = \frac{1}{\mu_o} \operatorname{curl} \mathbf{E}_o^\varepsilon \times \mathbf{n}, \quad \text{on} \quad \Gamma_\pm^\varepsilon\,, \tag{2.1c}$$

and with the boundary conditions

$$\operatorname{curl} \mathbf{E}_+^\varepsilon \times \mathbf{n} - i\kappa_+\, \mathbf{n} \times \mathbf{E}_+^\varepsilon \times \mathbf{n} = 0 \qquad \text{on} \quad \partial\Omega\,. \tag{2.1d}$$

Here we denote by $\underline{\kappa}^\varepsilon$ the piecewise-constant function (complex wave number) given by

$$(\underline{\kappa}^\varepsilon)^2(x) = \omega^2 \underline{\mu}^\varepsilon(x) \left( \underline{\epsilon}^\varepsilon(x) + \mathrm{i}\frac{\underline{\sigma}^\varepsilon(x)}{\omega} \right)\,, \quad \operatorname{Im}(\underline{\kappa}^\varepsilon(x)) \geq 0\,,$$

and $\mathbf{E}_\dagger^\varepsilon$, $\dagger = -, o, +$ are the restrictions of $\mathbf{E}^\varepsilon$ to the respective subdomain $\Omega_\dagger^\varepsilon$.

### 2.2.3 Guideline on the derivation of impedance conditions

We give a guideline on the derivation of generalized impedance transmission conditions for the electric field, which is based on an asymptotic expansion in the thickness parameter $\varepsilon$ [125, Sec. 5]. We will then propose two equivalent models $\mathbf{E}_0$ in Sec. 2.3.1 and $\mathbf{E}_\varepsilon^1$ in Sec. 2.3.2, both for the electric field. The first model $\mathbf{E}_0$ is of order 1 , *i.e.* , it satisfies at least formally $\mathbf{E}^\varepsilon - \mathbf{E}_0 = \mathcal{O}(\varepsilon)$

and the second model $\mathbf{E}_\varepsilon^1$ is of order 2, i.e. it satisfies at least formally $\mathbf{E}^\varepsilon - \mathbf{E}_\varepsilon^1 = \mathcal{O}(\varepsilon^2)$. These models are defined in $\varepsilon$-independent domains $\Omega_-$, $\Omega_+$, where $\Omega_-$ denotes the domain $\Omega_-^\varepsilon$ in the limit $\varepsilon \to 0$ and $\Omega_+$ the domain $\Omega_+^\varepsilon$ for $\varepsilon \to 0$, *i.e.* $\Omega_+ = \Omega \setminus \overline{\Omega}_-$ (see Figure 2.2).

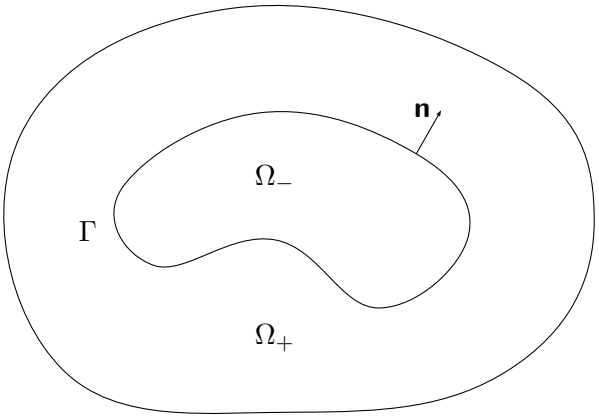


Figure 2.2: A cross-section of the domain $\Omega$ and the subdomains $\Omega_-$, $\Omega_+$.

To define asymptotic models it is convenient to introduce the electromagnetic properties of the "background" problem by simple extension of the values of $\underline{\mu}^\varepsilon$, $\underline{\epsilon}^\varepsilon$ and $\underline{\sigma}^\varepsilon$ outside the sheet in the extended domains $\Omega_-$ and $\Omega_+$:

$$\mu = \begin{cases} \mu_-, & \text{in } \Omega_-, \\ \mu_+, & \text{in } \Omega_+, \end{cases} \qquad \epsilon = \begin{cases} \epsilon_-, & \text{in } \Omega_-, \\ \epsilon_+, & \text{in } \Omega_+, \end{cases} \qquad \sigma = \begin{cases} \sigma_-, & \text{in } \Omega_-, \\ \sigma_+, & \text{in } \Omega_+. \end{cases}$$

Similarly, we define a complex wave number $\kappa$ as $\kappa = \kappa_\pm$ in $\Omega_\pm$. In the following we present a formal derivation of impedance conditions in two steps.

**First step : a multiscale expansion.** The first step consists in deriving a multiscale expansion for the solution $\mathbf{E}^\varepsilon$ to Problem (2.1) : it possesses an asymptotic expansion in power series of the small parameter $\varepsilon$

$$\mathbf{E}^\varepsilon(\mathbf{x}) \approx \mathbf{E}_0(\mathbf{x}) + \varepsilon \mathbf{E}_1(\mathbf{x}) + \varepsilon^2 \mathbf{E}_2(\mathbf{x}) + \cdots \qquad \text{for a.e.} \quad \mathbf{x} \in \Omega_-^\varepsilon \cup \Omega_+^\varepsilon \,, \tag{2.2a}$$

$$\mathbf{E}^\varepsilon(\mathbf{x}) \approx \mathfrak{E}_0\left(y_\alpha, \frac{h}{\varepsilon}\right) + \varepsilon \mathfrak{E}_1\left(y_\alpha, \frac{h}{\varepsilon}\right) + \cdots \qquad \text{for a.e.} \quad \mathbf{x} \in \Omega_o^\varepsilon \,. \tag{2.2b}$$

Here, $\mathbf{x} \in \mathbb{R}^3$ are the cartesian coordinates, $(y_\alpha, h)$ is a local *normal coordinate system* to the surface $\Gamma$ in the thin layer $\Omega_o^\varepsilon$ : $y_\alpha$, $\alpha = 1, 2$ are tangential coordinates on $\Gamma$ and $h \in (-\frac{\varepsilon}{2}, \frac{\varepsilon}{2})$ is the distance to $\Gamma$. The term $\mathfrak{E}_j$ is a "*profile*" defined on $\Gamma \times (-\frac{1}{2}, \frac{1}{2})$. Note, that the intrinsic domain of the "far field terms" $\mathbf{E}_j$ is $\Omega_- \cup \Omega_+$. The first asymptotics $(\mathfrak{E}_j, \mathbf{E}_j)$ are derived step by step in [125, Sec. 5].

The derivation is based on an expansion of the differential operators inside the thin layer $\Omega_o^\varepsilon$ in terms of $\varepsilon$, a Taylor expansion of $\mathbf{E}_j|_{\Gamma_\pm^\varepsilon}$ around the mid-surface $\Gamma$ and a collection of terms of same powers of $\varepsilon$ in the governing PDE inside and outside the sheet, the continuity conditions for the Dirichlet and Neumann traces on $\Gamma_\pm^\varepsilon$ and the boundary conditions. Since, moreover, the terms $\mathfrak{E}_j$ of the expansion inside the sheet can be explicitly expressed in terms of $\mathbf{E}_i$, $i = 0, \ldots, j-1$

we obtain formally

$$\operatorname{curl}\operatorname{curl}\mathbf{E}_j^{\pm} - \kappa^2\mathbf{E}_j^{\pm} = i\omega\mu\mathbf{j}\,\delta_{0j}\,, \quad \text{in } \Omega_{\pm}\,, \tag{2.3a}$$

$$\operatorname{curl}\mathbf{E}_j^{+}\times\mathbf{n} - i\kappa_+\,\mathbf{n}\times\mathbf{E}_j^{+}\times\mathbf{n} = 0\,, \quad \text{on } \partial\Omega\,, \tag{2.3b}$$

for the restrictions $\mathbf{E}_j^{\pm}$ of $\mathbf{E}_j$ to $\Omega_{\pm}$, with Dirichlet boundary conditions on $\Gamma$:

$$\mathbf{E}_j^{\pm}\times\mathbf{n} = \sum_{i=0}^{j}\mathcal{G}_i^{\pm}\begin{pmatrix}\left\{\frac{1}{\mu}(\operatorname{curl}\mathbf{E}_{j-i})_{\mathbf{T}}\right\}_{\Gamma}\\ \left[\frac{1}{\mu}(\operatorname{curl}\mathbf{E}_{j-i})_{\mathbf{T}}\right]_{\Gamma}\end{pmatrix}. \tag{2.3c}$$

Here $\mathcal{G}_i^{\pm}$ are differential operators on $\Gamma$ where $\mathcal{G}_0^{\pm}=0$. For any vector field $\mathbf{v}$ on $\Gamma$ we denote by $\mathbf{v}_{\mathbf{T}} = \mathbf{n}\times(\mathbf{v}\times\mathbf{n})$ the vector field of its tangent components and $[\mathbf{v}_{\mathbf{T}}]_{\Gamma}$ (resp. $\{\mathbf{v}_{\mathbf{T}}\}_{\Gamma}$) denote the jump (resp. the mean value) of $\mathbf{v}_{\mathbf{T}}$ across $\Gamma$ ($[\mathbf{v}_{\mathbf{T}}]_{\Gamma} = \mathbf{v}_{\mathbf{T}}|_{\Gamma^+} - \mathbf{v}_{\mathbf{T}}|_{\Gamma^-}$).

**Second step : impedance transmission conditions and equivalent models.** The second step consists in identifying a simpler problem satisfied by an approximation $\mathbf{E}_{\varepsilon}^k$ of the truncated expansion $\mathbf{E}_0(\mathbf{x}) + \varepsilon\mathbf{E}_1(\mathbf{x}) + \varepsilon^2\mathbf{E}_2(\mathbf{x}) + \cdots + \varepsilon^k\mathbf{E}_k(\mathbf{x})$ up to a residual term in $\mathcal{O}(\varepsilon^{k+1})$. For this the equations in (2.3) for $i=0,\dots,k$ are multiplied with $\varepsilon^i$ and added up, and terms in $\mathcal{O}(\varepsilon^{k+1})$ are neglected. In this way we obtain the simpler problem as

$$\operatorname{curl}\operatorname{curl}\mathbf{E}_{\varepsilon}^k - \kappa^2\mathbf{E}_{\varepsilon}^k = i\omega\mu\mathbf{j}\,, \quad \text{in } \Omega_-\cup\Omega_+\,, \tag{2.4a}$$

$$\operatorname{curl}\mathbf{E}_{\varepsilon}^k\times\mathbf{n} - i\kappa_+\,\mathbf{n}\times\mathbf{E}_{\varepsilon}^k\times\mathbf{n} = 0\,, \quad \text{on } \partial\Omega\,, \tag{2.4b}$$

with the following transmission conditions on $\Gamma$:

$$\begin{pmatrix}\left[\mathbf{E}_{\varepsilon}^k\times\mathbf{n}\right]_{\Gamma}\\ \left\{\mathbf{E}_{\varepsilon}^k\times\mathbf{n}\right\}_{\Gamma}\end{pmatrix} = \mathcal{G}_{k,\varepsilon}\begin{pmatrix}\left\{\frac{1}{\mu}(\operatorname{curl}\mathbf{E}_{\varepsilon}^k)_{\mathbf{T}}\right\}_{\Gamma}\\ [(\frac{1}{\mu}\operatorname{curl}\mathbf{E}_{\varepsilon}^k)_{\mathbf{T}}]_{\Gamma}\end{pmatrix}, \tag{2.4c}$$

where $\mathcal{G}_{k,\varepsilon} = \sum_{i=0}^{k}\varepsilon^i([\mathcal{G}_i]_{\Gamma},\{\mathcal{G}_i\}_{\Gamma})^{\top}$ is the truncation of the weigthed sum of operators $\mathcal{G}_i^{\pm}$ where the jump or mean value is taken respectively. With this derivation it holds at least formally $\mathbf{E}^{\varepsilon} - \mathbf{E}_{\varepsilon}^k = \mathcal{O}(\varepsilon^{k+1})$. Hence, we say that $\mathbf{E}_{\varepsilon}^k$ is an equivalent (or approximate) model of order $k+1$.

## 2.3 Equivalent models up to order 2

In this section we present the approximate models of order 1 (Sec. 2.3.1) and 2 (Sec. 2.3.2). Then we introduce a mixed variational formulation for the second order model (Sec. 2.3.3).

### 2.3.1 Equivalent model of order 1

The equivalent model of order 1 is given by the limit solution $\mathbf{E}_0$ of (2.1) when $\varepsilon\to 0$. The limit solution satisfies the perfect electric conductor (PEC) boundary condition on $\Gamma$ and can be defined independently in the two subdomains $\Omega_-,\Omega_+$. Hence, $\mathbf{E}_0^- = \mathbf{E}_0|_{\Omega_-}$ satisfies

$$\operatorname{curl}\operatorname{curl}\mathbf{E}_0^- - \kappa_-^2\,\mathbf{E}_0^- = i\omega\mu_-\mathbf{j}_-\,, \quad \text{in } \Omega_-, \tag{2.5a}$$

$$\mathbf{E}_0^-\times\mathbf{n} = 0\,, \quad \text{on } \Gamma, \tag{2.5b}$$

whereas $\mathbf{E}_0^+ = \mathbf{E}_0|_{\Omega_+}$ is given by

$$\begin{aligned} \operatorname{curl}\operatorname{curl}\mathbf{E}_0^+ - \kappa_+^2\mathbf{E}_0^+ &= i\omega\mu_+\mathbf{j}_+\,, && \text{in } \Omega_+, && (2.6a)\\ \mathbf{E}_0^+\times\mathbf{n} &= 0\,, && \text{on } \Gamma, && (2.6b)\\ \operatorname{curl}\mathbf{E}_0^+\times\mathbf{n} - i\kappa_+\,\mathbf{n}\times\mathbf{E}_0^+\times\mathbf{n} &= 0\,, && \text{on } \partial\Omega. && (2.6c) \end{aligned}$$

### 2.3.2 Equivalent model of order 2

We define a second order approximate solution $\mathbf{E}_\varepsilon^1$, which shall be much more accurate approximation of $\mathbf{E}^\varepsilon$ than the limit solution $\mathbf{E}_0$ when $\varepsilon \to 0$. The equations defining $\mathbf{E}_\varepsilon^1$ outside the mid-surface $\Gamma$ remain the same, *i.e.* , it solves

$$\begin{aligned} \operatorname{curl}\operatorname{curl}\mathbf{E}_\varepsilon^1 - \kappa^2\mathbf{E}_\varepsilon^1 &= \mathrm{i}\omega\mu\mathbf{j}\,, && \text{in } \Omega_-\cup\Omega_+\,, && (2.7a)\\ \operatorname{curl}\mathbf{E}_\varepsilon^1\times\mathbf{n} - \mathrm{i}\kappa_+\,\mathbf{n}\times\mathbf{E}_\varepsilon^1\times\mathbf{n} &= 0\,, && \text{on } \partial\Omega, && (2.7b) \end{aligned}$$

and at the mid-surface $\Gamma$ the transmission conditions

$$\begin{pmatrix} \left[\mathbf{E}_\varepsilon^1\times\mathbf{n}\right]_\Gamma \\ \left\{\mathbf{E}_\varepsilon^1\times\mathbf{n}\right\}_\Gamma \end{pmatrix} = \varepsilon \begin{pmatrix} \mathrm{L}_1 & \mathrm{L}_3 \\ \mathrm{L}_3 & \mathrm{L}_2 \end{pmatrix} \begin{pmatrix} \left\{\frac{1}{\mu}(\operatorname{curl}\mathbf{E}_\varepsilon^1)_\mathbf{T}\right\}_\Gamma \\ \left[(\frac{1}{\mu}\operatorname{curl}\mathbf{E}_\varepsilon^1)_\mathbf{T}\right]_\Gamma \end{pmatrix} \qquad (2.7c)$$

are posed. Here, $\mathrm{L}_i$ are differential operators given by

$$\mathrm{L}_i = A_i\ \mathbf{curl}_\Gamma\operatorname{curl}_\Gamma - B_i\mathbb{I}\,, \qquad i=1,2,3,$$

in which $A_i, B_i$ are constants defined by

$$\begin{aligned} A_1 &= -\omega^{-2}\left\{(\epsilon+\mathrm{i}\frac{\sigma}{\omega})^{-1}\right\}_\Gamma, & B_1 &= 2\frac{\mu_o}{\gamma}\tanh(\frac{\gamma}{2}) - \{\mu\}_\Gamma\,,\\ A_2 &= \frac{A_1}{4}, & B_2 &= \frac{\mu_o}{2\gamma}\coth(\frac{\gamma}{2}) - \frac{\{\mu\}_\Gamma}{4}, \qquad (2.8)\\ A_3 &= -\frac{1}{4}\omega^{-2}\left[(\epsilon+\mathrm{i}\frac{\sigma}{\omega})^{-1}\right]_\Gamma, & B_3 &= -\frac{1}{4}\left[\mu\right]_\Gamma\,, \end{aligned}$$

and $\gamma = \exp(\frac{3\mathrm{i}\pi}{4})\sqrt{\omega\mu_o\tilde{\sigma}}$.

### 2.3.3 Mixed variational formulation

The transmission condition (2.7c) is in its general form of Wentzel type when regarded as a Poincaré-Steklov map $\mathbf{H}_\mathbf{T}$–to–$\mathbf{E}\times\mathbf{n}$ and tends to the PEC boundary condition for $\varepsilon\to 0$. Therefore, we use the mixed variational formulation with additional unknowns $\boldsymbol{\lambda}_\varepsilon$ and $\boldsymbol{\mu}_\varepsilon$ defined as

$$\boldsymbol{\lambda}_\varepsilon = \left\{\frac{1}{\mu}(\operatorname{curl}\mathbf{E}_\varepsilon^1)_\mathbf{T}\right\}_\Gamma \quad \text{and} \quad \boldsymbol{\mu}_\varepsilon = \left[\frac{1}{\mu}(\operatorname{curl}\mathbf{E}_\varepsilon^1)_\mathbf{T}\right]_\Gamma\,,$$

in which the Poincaré-Steklov map (2.7c) is incorporated in weak sense. This formulation is also known as saddle point problem with penalty term [18, § 4, pp. 138ff]. In this formulation we search for $\mathbf{E}_\varepsilon^1$ in the Hilbert space

$$\mathbf{V} = \left\{\mathbf{E}\in\mathbf{H}(\operatorname{curl},\Omega_\pm),\ \mathbf{E}\times\mathbf{n}\in\mathbf{L}_t^2(\partial\Omega)\right\}, \qquad (2.9)$$

and for $\boldsymbol{\lambda}_\varepsilon$ and $\boldsymbol{\mu}_\varepsilon$ in the Hilbert space $\mathbf{W} = \mathrm{TH}(\mathrm{curl}_\Gamma, \Gamma)$. Hence, we obtain the mixed variational formulation : Find $(\mathbf{E}^1_\varepsilon, \boldsymbol{\lambda}_\varepsilon, \boldsymbol{\mu}_\varepsilon) \in \mathbf{V} \times \mathbf{W} \times \mathbf{W}$ such that for all $(\mathbf{U}, \boldsymbol{\xi}_1, \boldsymbol{\xi}_2) \in \mathbf{V} \times \mathbf{W} \times \mathbf{W}$

$$\begin{aligned} &\int_{\Omega_+ \cup \Omega_-} \frac{1}{\mu} \operatorname{curl} \mathbf{E}^1_\varepsilon \cdot \operatorname{curl} \overline{\mathbf{U}} - \frac{\kappa^2}{\mu} \mathbf{E}^1_\varepsilon \cdot \overline{\mathbf{U}} \, \mathrm{d}\mathbf{x} - \mathrm{i}\frac{\kappa_+}{\mu_+} \int_{\partial\Omega} \mathbf{E}^1_\varepsilon \times \mathbf{n} \cdot \overline{\mathbf{U}} \times \mathbf{n} \, \mathrm{d}S \\ &- \int_\Gamma \begin{pmatrix} \mathbf{n} \times \boldsymbol{\lambda}_\varepsilon \\ \mathbf{n} \times \boldsymbol{\mu}_\varepsilon \end{pmatrix} \cdot \begin{pmatrix} \left[ \overline{\mathbf{U}}_\mathbf{T} \right] \\ \left\{ \overline{\mathbf{U}}_\mathbf{T} \right\} \end{pmatrix} \mathrm{d}S \;=\; \mathrm{i}\omega \int_\Omega \mathbf{j} \cdot \overline{\mathbf{U}} \, \mathrm{d}\mathbf{x} \,, \end{aligned} \tag{2.10a}$$

and

$$\int_\Gamma \begin{pmatrix} \left[ \mathbf{n} \times \mathbf{E}^1_\varepsilon \right] \\ \left\{ \mathbf{n} \times \mathbf{E}^1_\varepsilon \right\} \end{pmatrix} \cdot \begin{pmatrix} \overline{\boldsymbol{\xi}}_1 \\ \overline{\boldsymbol{\xi}}_2 \end{pmatrix} + \varepsilon \, \mathsf{A} \begin{pmatrix} \mathrm{curl}_\Gamma \boldsymbol{\lambda}_\varepsilon \\ \mathrm{curl}_\Gamma \boldsymbol{\mu}_\varepsilon \end{pmatrix} \cdot \begin{pmatrix} \mathrm{curl}_\Gamma \overline{\boldsymbol{\xi}}_1 \\ \mathrm{curl}_\Gamma \overline{\boldsymbol{\xi}}_2 \end{pmatrix} - \varepsilon \, \mathsf{B} \begin{pmatrix} \boldsymbol{\lambda}_\varepsilon \\ \boldsymbol{\mu}_\varepsilon \end{pmatrix} \cdot \begin{pmatrix} \overline{\boldsymbol{\xi}}_1 \\ \overline{\boldsymbol{\xi}}_2 \end{pmatrix} \mathrm{d}S \;=\; 0 \,. \tag{2.10b}$$

Here, $\mathsf{A}$ and $\mathsf{B}$ are matrices given by

$$\mathsf{A} = \begin{pmatrix} A_1 & A_3 \\ A_3 & A_2 \end{pmatrix} \quad \text{and} \quad \mathsf{B} = \begin{pmatrix} B_1 & B_3 \\ B_3 & B_2 \end{pmatrix}$$

where the constants $A_i, B_i$ are defined in (2.8).

## 2.4 Numerical investigation of the equivalent model properties

This section illustrates the different equivalent models for both the diffraction and shielding problem of an incoming plane wave by a spherical thin conducting layer (Sec. 2.4.1) and the shielding problem of a Gaussian current source by a flat layer (Sec. 2.4.2). Numerical convergence rates show the order of accuracy for each equivalent model. Section 2.4.3 presents numerical results for the robustness of each equivalent model with respect to the parameter $\tilde{\sigma}$.

### 2.4.1 Configuration of a spherical layer

The reference model has been tested for a spherical layer whose mid-surface has radius 1, the computational domain is the ball of radius 1.5. The following parameters are chosen

$$\epsilon_+ = 1, \qquad \mu_+ = 1, \qquad \sigma_+ = 0, \tag{2.11a}$$
$$\epsilon_- = 2, \qquad \mu_- = 1.5, \qquad \sigma_- = 0.5, \tag{2.11b}$$
$$\epsilon_o = 3.5, \qquad \mu_o = 2.0, \qquad \tilde{\sigma} = 0.5. \tag{2.11c}$$

They are chosen such that all the coefficients $A_i$ and $B_i$ are different from 0. The source is here an incident plane wave, $\mathbf{E}^{\mathrm{inc}} = \exp(-\mathrm{i}\omega\, x_3)\, \mathbf{e}_1$, *i.e.*, there is no current source, and Silver-Müller radiation condition applies to the scattered field $\mathbf{E}^{k,\mathrm{sc}}_\varepsilon = \mathbf{E}^k_\varepsilon - \mathbf{E}^{\mathrm{inc}}$.

Nédélec's elements of the first kind on hexahedral curved elements are used to compute the approximate solution. We have used sixth order elements on a fine enough mesh such that the discretisation error is negligible over the modelling errors. On the mid-surface of the sheet the impedance conditions of order 1 (which are the PEC boundary conditions (2.5b) and (2.6b)) or order 2 (see (2.7c)) are applied, where we use edge elements for the auxiliary variables $\boldsymbol{\lambda}_\varepsilon$ and $\boldsymbol{\mu}_\varepsilon$ on the interface $\Gamma$ (the finite element space for auxiliary variables is the tangential trace of the 3-D finite element space used for the electrical field).

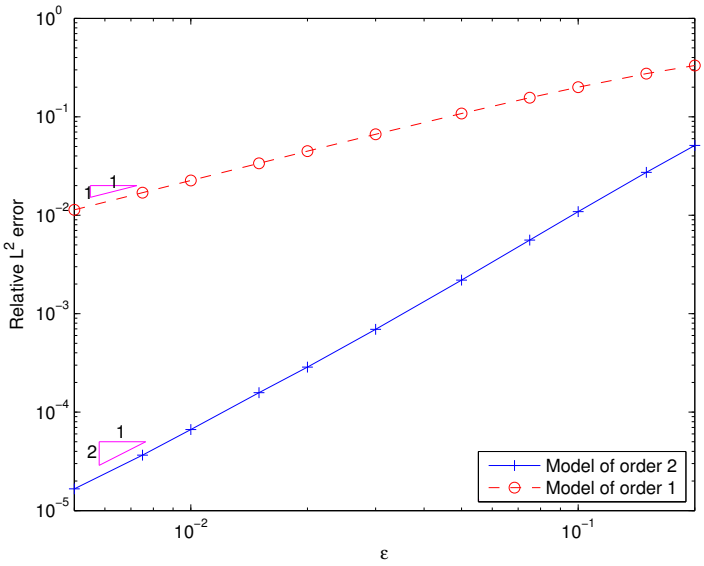


Figure 2.3: Relative $\mathbf{L}^2$ errors of the solutions $\mathbf{E}_0$, $\mathbf{E}_\varepsilon^1$ of the equivalent models of order 1 and 2 versus the thickness $\varepsilon$ (lower frequency $\omega = \frac{\pi}{5}$).

We have performed the numerical experiments for two frequencies, a lower frequency $\omega = \frac{\pi}{5}$ and a higher frequency $\omega = \pi$. The relative $\mathbf{L}^2$ errors (computed in $\Omega_{\text{ext}}$, the domain $\Omega$ excluding the spherical crown $0.9 < r < 1.1$) of the equivalent models of order 1 and order 2 are shown in Fig. 2.3 for the lower frequency as a function of the thickness parameter $\varepsilon$. The model of order 1 with PEC boundary condition, see (2.5)-(2.6), shows in the numerical experiments only a convergence as $O(\varepsilon)$ (see dashed line in Fig. 2.3) as expected by the asymptotic expansion. When the model of order 2, see (2.7), is used for the lower frequency we observe the expected second-order convergence (see solid line in Fig. 2.3). For the larger frequency $\omega = \pi$ we have observed for the investigated thicknesses $\varepsilon$ a local convergence approximately as $O(\varepsilon^{2.5})$ for the model of order 2 (pre-asymptotic behaviour) [125].

### 2.4.2 Configuration of a flat layer

In this simulation, the computational domain is the cube $[-5, 5]^3$, and the conducting sheet is centered at $z = 0$. The material parameters are the same as for the spherical layer, see (2.11), where $\epsilon_+$, $\mu_+$, $\sigma_+$ apply for $z > 0$ and $\epsilon_-$, $\mu_-$, $\sigma_-$ for $z < 0$. The pulsation is given as $\omega = \frac{2\pi}{5}$. Here, we use a current source $\mathbf{j}$ which is a Gaussian centered at $(0, 0, 2.5)$ and truncated at a distance of 1.5 from the center, and which is, hence, null in the thin layer. Periodic boundary conditions are applied on lateral surfaces and the Silver-Müller condition is applied on surfaces $z = \pm 5$. In [125] we observe that the equivalent model $\mathbf{E}_\varepsilon^1$ converges towards the exact solution even as $O(\varepsilon^3)$ as observed for flat sheets in 2-D (see [132]).

### 2.4.3 Robustness of the equivalent models versus the parameter $\tilde{\sigma}$

Since $d_{\text{skin}} = \varepsilon\sqrt{2/(\omega\mu_o\widetilde{\sigma})}$, the parameter $\tilde{\sigma}$ corresponds to the skin-depth-to-thickness ratio of the sheet $d_{\text{skin}}/\varepsilon$ for fixed frequency. In Fig. 2.4, we observe numerically that the model of order 2 is robust in $\tilde{\sigma}$ (since an error reduction for any small or large value of $\tilde{\sigma}$ can be observed) whereas the model of order 1 is not robust in $\tilde{\sigma}$.

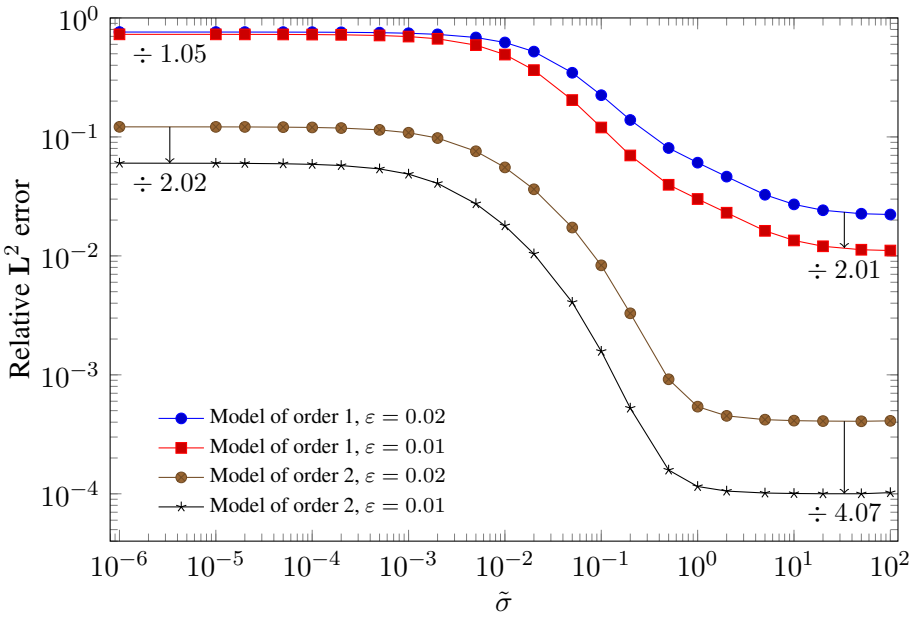


Figure 2.4: Relative $\mathbf{L}^2$ error of the solutions $\mathbf{E}_0$ and $\mathbf{E}^1_\varepsilon$ of the equivalent models of order 1 and order 2 versus the parameter $\tilde{\sigma}$ (in abscissa) for $\varepsilon = 0.01$ and $\varepsilon = 0.02$.

## 2.5 Perspectives

Impedance transmission conditions (ITCs) have been developed for thin and highly conductive sheets for the time-harmonic Maxwell equations. These ITCs have been derived up to the second order. It is worth noting that we can not apply the second order transmission conditions when neglecting the displacement currents and when the conductivities vanish outside the sheet. Hence, a next of this work is to extend these conditions to the 3D eddy current problem [124]. A very promising perspective of this work is to integrate all these conditions in boundary element methods.

All these models are available for "non-magnetic" materials when the relative permeability $\mu_r = \mu_-/\mu_+$ (between two media) is soft. The next issues to tackle are the Maxwell equations and the eddy current problem in magnetic media where the contrast of permeabilities $\mu_r$ is high. As a preliminary work the problem for the magnetic potential in the bi-dimensional eddy current model is currently investigated [126].

In the framework of the PhD thesis of Justine Labat, which is advised by S. Tordeux, we consider a three dimensional scattering problem of electromagnetic waves by small obstacles in the time-harmonic regime. When the size of an obstacle is significantly small with respect to the incident wavelength, we propose to replace the reference model with a reduced model using the method of *matched asymptotic expansions*. This method consists in deriving a multi-scale expansion for the *far*-field and for the *near*-field.

# Part II

# Numerical treatment of corner and edge singularities for elliptic systems

The numerical treatment of corner and edge singularities in elliptic systems is of great interest in the electrical engineering and mechanical engineering fields. The knowledge of asymptotics (which involve singularity functions and their corresponding singular coefficients) is important from the engineering point of view as they may affect for example the path stability of slightly curved or kinked cracks [38, 96], and play an important role in determining the size and shape of a crack tip plastic zone [95, 128].

Accurate knowledge of eddy currents is of great interest for the design of many electromagnetic devices such as used in electrothermics. Taking advantage of the fast decrease of the electromagnetic field inside a conductor, impedance conditions are usually considered to reduce the computational domain. Impedance boundary conditions were first proposed by Leontovich [97] and by Rytov [131] in the 1940's and then extended by Senior and Volakis [139]. These conditions can be derived up to the required precision for any conductor with a smooth surface : we refer to Haddar *et al.* [73] for the mathematical justification of conditions of order 1, 2 and 3. However such conditions are not valid near corners. Few authors have proposed heuristic impedance modifications close to the corners [45, 155], but these modifications are neither satisfactory nor proved. In particular in [155], the modified impedance appears to blow up near the corner, which does not seem valid for non-magnetic materials with a finite conductivity as presented in [21].

I have been working for the last years on elliptic problems with corner and edge singularities [90, 21, 40, 140, 141]. In several works we aimed at determining an asymptotic expansion of the solution in the vicinity of a singularity [40, 140, 141]. When a small parameter is also involved in such a problem, multi-scale analysis has been used to derive asymptotic expansions with *corner profiles* as this parameter tends to zero [21, 90].

In [40, 21], eddy current problems are addressed in a bidimensional setting where the conducting medium embedded in a dielectric medium is non-magnetic and has a corner singularity. For any fixed skin depth we show that the flux density is bounded near the corner, unlike the perfect conducting case. Then as the skin depth goes to zero, the first terms of a multiscale expansion of the magnetic potential have been introduced to tackle the magneto-harmonic problem [21]. The heuristics of the method are given and the derivation of the impedance condition is considered. Numerical computations illustrate the obtained accuracy. In [40], we aim at describing the magnetic potential in the vicinity of the corner singularity, considering the conductivity $\sigma$, as well as the angular frequency $\kappa$, as given parameters. We emphasize that these considerations will be helpful in understanding the behavior of the impedance condition near corner singularities. The asymptotic expansion of the magnetic potential as the distance to the corner goes to zero has been provided [40]. Such asymptotics involve two main ingredients : the singular functions, also called *singularities*, which belong to the kernel of the considered operator ; the singular coefficients, whose calculation requires the knowledge of dual singular functions. A method for the calculation of the singular functions near the corner is introduced and two methods to extract the singular coefficients are provided : the method of moments and the quasi-dual function method (QDFM).

The precise description of an object containing *rounded corners* leads to consider meshes with a large number of nodes in the corner neighborhood when the finite element method (FEM) is straightforwardly applied. Dealing with such meshes makes the computation time- and resource-consuming. Moreover, these computations have to be repeated if the curvature radius of the rounded corner is modified. In order to avoid this computational cost, the rounded corners are usually replaced by *sharp corners*. The obtained computational results are then globally accurate but locally inaccurate in the neighborhood of the corners. In order to remedy this drawback, we have developed numerical techniques to compute electrostatic fields in devices with rounded corners in 2D situations [90]. An asymptotic expansion leads to solve two problems : one on the device where rounded corners are replaced by sharp corners and the other on an unbounded

domain representing the shape of the rounded corner after an appropriate rescaling. A generic self-similar solution enables to estimate the electric field close to the corner by post-processing for several values of the curvature radius. Some numerical tests have assessed the relevance of the proposed approach. It has been also shown that forgotten techniques, as conformal maps, enable, in some cases, to build exactly the generic solution and in every case, to approximate it. They can be coupled with more computationally intensive numerical methods as the FEM, by providing speed and accuracy.

The computation of the elliptical edge (e.g. as a sharp V-notch or a crack front) asymptotics to the elasticity system is of major engineering importance because most surface cracks are semi-elliptical. However an explicit asymptotic solution to this system in a three-dimensional domain close to an elliptical edge is still unavailable. Towards its derivation we have first derived an asymptotic solution of the Laplace equation in the vicinity of an elliptical singular edge in a three-dimensional domain [140]. We have shown that the solution in the vicinity of an elliptical edge is composed of three series (as for the circular edge case), but the specific feature with eigenfunctions being functions of two coordinates. The dual singular solution is also provided to be used in a future study to extract the edge flux intensity functions (EFIFs) by the quasi-dual function method (QDFM).

The singular solution to the linear elasticity system in the vicinity of a straight or curved edge can be represented by a series of eigenpairs, shadows and their associated singular coefficients, the edge stress intensity functions (ESIFs) [37, 153]. The QDFM has been successfully applied for the extraction of ESIFs associated with the non-integer eigenvalues from finite element (FE) solutions, but it does not apply to ESIFs associated with the integer eigenvalues [37]. This is why we have addressed the issue of computing the EFIFs associated with the integer eigenvalues by the QDFM [141]. The specific non-standard feature of this problem lies in the structure of the dual singularities associated with the integer eigenvalues : contrary to the non-integer eigenvalues these dual singularities involve logarithmic terms. These singularities have been used with the QDFM to extract EFIFs from p-version finite element solutions and numerical examples are provided.

The outline of this part proceeds as follows. In Chapter 3, corner asymptotics of the magnetic potential in the eddy-current model are presented. As the skin depth goes to zero, the first terms of a multi-scale expansion of the magnetic potential are introduced to tackle the magneto-harmonic problem. As an application, a modified impedance boundary condition close to a corner singularity is proposed. In Chapter 4, we concentrate on the extraction of EFIFs associated with the integer eigenvalues for the Laplace operator over a 3-D domain with a straight crack. The dual singularities are determined and the QDFM is applied to extract EFIFs.

# Chapter 3

# Corner asymptotics of the magnetic potential in the eddy-current model

## 3.1 Introduction

In [40, 21], the magnetic potential has been considered in a non-magnetic domain composed of a conducting material $\Omega_-$ with one corner surrounded by a dielectric material $\Omega_+$. The operator acting on the magnetic potential is not homogeneous and has a discontinuous piecewise constant coefficient in front of its zeroth order part:

$$-\Delta + \mathrm{i}\kappa\mu_0\sigma\mathbb{1}_{\Omega_-}.$$

Though pertaining to the wide class of elliptic boundary value problems or transmission problems in conical domains, see for instance the papers [87, 88] and the monographs [72, 39, 115, 89], this problem has specific features which make the derivation of the asymptotics not obvious—namely the fact that singularities are generated by a non-principal term. Despite its great interest for the applications, this problem has not yet been explicitly analyzed.

Another disturbing factor is the nature of the limit problem when the product $\kappa\mu_0\sigma$ tends to infinity (large frequency/high conductivity limit). This limit is simply the homogeneous Dirichlet problem for the Laplace operator set in the dielectric medium $\Omega_+$, whose corner singularities are well known [87, 72]. In particular, when the conductor $\Omega_-$ has a convex corner, its surrounding domain $\Omega_+$ has a non-convex corner, thus the Dirichlet problem has non $\mathcal{C}^1$ singularities, in opposition to the problem for any finite $\kappa\mu_0\sigma$. This apparent paradox can be solved by a delicate multi-scale analysis, whose heuristics are exposed in [21]. Roughly speaking, there exists *profiles* in $\mathbb{R}^2$ which have the singular behavior of the operator $-\Delta + 2\mathrm{i}\mathbb{1}_{\Omega_-}$ near the corner, and which connect at infinity with the singular functions of the Dirichlet problem in $\Omega_+$, as described by equation (13) in [21]. This is why the knowledge of the singularities of $-\Delta + \mathrm{i}\kappa\mu_0\sigma\mathbb{1}_{\Omega_-}$ at given $\kappa$ and $\sigma$ is a milestone in the full multi-scale analysis.

Besides the mere description of singular functions, the computation of singular coefficients is considered in [40]. Various works concern the extraction of singular coefficients associated with the solution to an elliptic problem set in a domain with a corner singularity, see [106, 42] for theoretical formulas, and [110, 144, 37] for more practical methods. In [40], we choose to extend the quasi-dual function method initiated in [37] to the case of resonances, which was discarded in the latter reference.

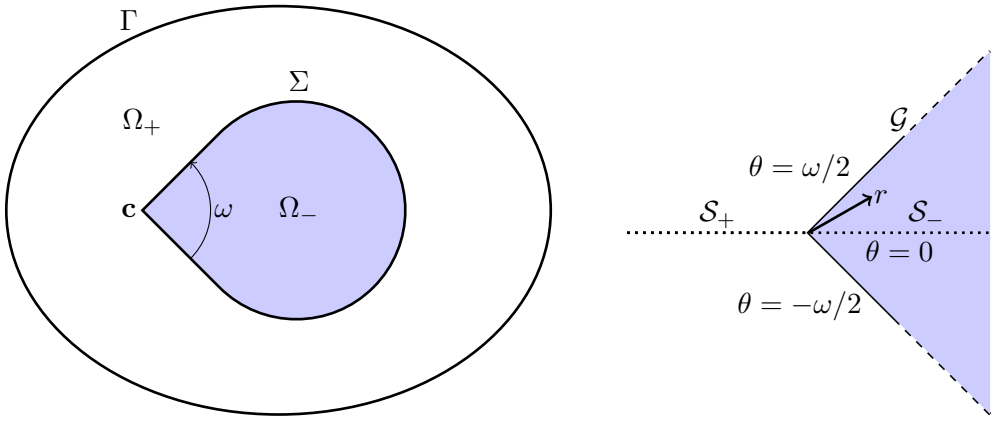


(a) Domain for the eddy-current problem. (b) Infinite sectors $\mathcal{S}_+$ and $\mathcal{S}_-$ in $\mathbb{R}^2$.

Figure 3.1: Geometries of the considered problems.

## Corner asymptotics

The magnetic vector potential $\mathcal{A}$ satisfies the following problem (see Fig. 3.1) :

$$\left\{\begin{array}{rl} -\Delta\mathcal{A}^+ = \mu_0 J \text{ in } \Omega_+, & \\ -\Delta\mathcal{A}^- + \dfrac{2\mathrm{i}}{\delta^2}\mathcal{A}^- = 0 \text{ in } \Omega_-, & [\mathcal{A}]_\Sigma = 0, \text{ on } \Sigma, \\ \mathcal{A}^+ = 0 \text{ on } \Gamma, & [\partial_n \mathcal{A}]_\Sigma = 0, \text{ on } \Sigma. \end{array}\right. \tag{3.1}$$

Here, $\delta = \sqrt{2/(\kappa\mu_0\sigma)}$. There exists a unique solution $\mathcal{A}$ in $H_0^1(\Omega)$ to problem (3.1) and $\mathcal{A}$ belongs to $H^{\frac{5}{2}-\varepsilon}(\Omega)$ for any $\varepsilon > 0$. In particular, the magnetic potential $\mathcal{A}$ belongs to $\mathcal{C}^1(\overline{\Omega})$. However, in general, $\mathcal{A}$ does not belong to $\mathcal{C}^2(\overline{\Omega})$, but $\mathcal{A}$ possesses a corner asymptotic expansion as the distance $r$ to $\mathbf{c}$ goes to zero.

In contrast with problems involving only *homogeneous* operators, problem (3.1) involves the lower order term $2\mathrm{i}/\delta^2$ in $\Omega_-$. As a consequence the singularities are not homogeneous functions, but infinite sums of quasi-homogeneous terms of the general form [87]

$$r^{\lambda+\ell}\log^n r\,\Phi(\theta), \quad \lambda \in \mathbb{C},\ \ell \in \mathbb{N},\ n \in \mathbb{N}$$

in polar coordinates $(r,\theta)$ centered at $\mathbf{c}$. In the present situation, the *leading exponents* $\lambda$ can be made precise: they are determined by the principal part of the operator at $\mathbf{c}$, which is nothing but the Laplacian $-\Delta$ at the interior point $\mathbf{c}$. Thus, the leading exponents are *integers* $k \in \mathbb{N}$ corresponding to leading singularities in the form of *harmonic polynomials*, written in polar coordinates as

$$1 \qquad \text{and} \qquad r^k\cos(k\theta - p\pi/2), \quad k \in \mathbb{N}\setminus\{0\},\ p \in \{0,1\}\ . \tag{3.2}$$

This is why $\mathcal{A}$ can be expanded close to the corner as

$$\mathcal{A}(r,\theta) \underset{r\to 0}{\sim} \Lambda^{0,0}\mathfrak{S}^{0,0}(r,\theta) + \sum_{k\geq 1}\sum_{p\in\{0,1\}} \Lambda^{k,p}\mathfrak{S}^{k,p}(r,\theta), \tag{3.3}$$

where the terms $\mathfrak{S}^{k,p}$ are the so-called *primal singular functions*, which belong to the formal kernel of the considered operator in $\mathbb{R}^2$, and the numbers $\Lambda^{k,p}$ are the *singular coefficients*.

Therefore, the derivation of the singular functions $\mathfrak{S}^{k,p}$ and the determination of the singular coefficients $\Lambda^{k,p}$ are key points in understanding the behavior of the magnetic potential in the vicinity of the corner. This was the double aim of the work in Ref. [40], where a constructive procedure is provided to determine the singular functions $\mathfrak{S}^{k,p}$ as well as two different methods to compute the singular coefficients $\Lambda^{k,p}$. Generally speaking, the singular functions are sums of the *kernel functions* of the Laplacian plus *shadow terms*. Since the leading part of the operator is the Laplacian in the whole plane $\mathbb{R}^2$, its singular functions are the harmonic polynomials (3.2) and we show that for any $(k,p) \in \mathbb{N} \times \{0,1\}$, the singular function $\mathfrak{S}^{k,p}$ writes as formal series

$$\mathfrak{S}^{k,p}(r,\theta) = r^k \sum_{j\geq 0} (\mathrm{i}\zeta^2)^j \, r^{2j} \sum_{n=0}^{j} \log^n r \, \Phi_{j,n}^{k,p}(\theta), \tag{3.4}$$

where the angular functions $\Phi_{j,n}^{k,p}$ are $\mathcal{C}^1$ functions of $\theta$ globally in $\mathbb{R}/(2\pi\mathbb{Z})$ (and piecewise analytic) and for the sake of normalization the positive parameter $\zeta$ is introduced as $\zeta^2 = 1/(2\delta^2)$.

In Section 3.2, the problem satisfied by the singular functions $\mathfrak{S}^{k,p}$ in the whole plane $\mathbb{R}^2$ split into two infinite sectors $\mathcal{S}_\pm$ (cf. Figure 3.1(b)) is provided. In order to determine the coefficients $\Lambda^{k,p}$, the method of moments and the method of quasi-dual singular functions have been generalized, after [37, 142]. Contrary to the case when $\zeta = 0$, these methods are approximate methods. Estimates for their convergence are presented. In Section 3.3, numerical simulations by finite elements methods illustrate the method of quasi-dual functions and the local expansion (3.3). In the concluding Section 3.4, heuristics of a multi-scale expansion as $\kappa\mu_0\sigma$ tends to infinity and a modified impedance boundary condition close to a corner are exposed [21].

## 3.2 Construction of singularities. Extraction of singular coefficients

Let $\omega \in (0, 2\pi)$ be the opening of the conductor part $\Omega_-$ near its corner. We define the origin of the angular variable, so that $\theta = 0$ cuts the conductor part by half (see Figure 3.1(b)). Let $\mathcal{S}_+$ and $\mathcal{S}_-$ be the two infinite sectors of $\mathbb{R}^2$ defined as

$$\mathcal{S}_- = \big\{(x,y) = (r\cos\theta, r\sin\theta) \in \mathbb{R}^2 : \ r > 0,\, \theta \in (-\omega/2,\, \omega/2)\big\}, \quad \mathcal{S}_+ := \mathbb{R}^2 \setminus \overline{\mathcal{S}_-}\,.$$

We denote by $\mathcal{G}$ the common boundary of $\mathcal{S}_-$ and $\mathcal{S}_+$. Finally, introduce the unit circle $\mathbb{T} = \mathbb{R}/(2\pi\mathbb{Z})$ and set

$$\mathbb{T}_- = (-\omega/2,\, \omega/2) \quad \text{and} \quad \mathbb{T}_+ = \mathbb{T} \setminus \overline{\mathbb{T}_-}\,.$$

Thus, the configuration $(\Omega_-, \Omega_+)$ coincides with the configuration $(\mathcal{S}_-, \mathcal{S}_+)$ inside a ball $\mathcal{B}(\mathbf{c}, R)$ for a sufficiently small $R$.

The positive parameter $\zeta$ being chosen, we denote by $\mathscr{L}_\zeta$ the operator defined on $\mathbb{R}^2$ by

$$\mathscr{L}_\zeta(u) = \begin{cases} -\Delta u, & \text{in } \mathcal{S}_+, \\ -\Delta u + 4\mathrm{i}\zeta^2 u, & \text{in } \mathcal{S}_-, \end{cases} \tag{3.5}$$

acting on functions $u$ such that $\partial_\theta^q u_-|_{\mathcal{G}} = \partial_\theta^q u_+|_{\mathcal{G}}$ for $q = 0,\, 1$. The singularities of problem (3.1) are these of the model operator $\mathscr{L}_\zeta$, with continuous Dirichlet and Neumann traces across $\mathcal{G}$.

As described above, the asymptotics of $\mathcal{A}$ near the corner involve the *singularities* of $\mathscr{L}_\zeta$ which, by convention, are formal solutions $\mathfrak{U}$ to the equation $\mathscr{L}_\zeta(\mathfrak{U}) = 0$. It is therefore crucial to make explicit these singularities.

Note that the operator $\mathscr{L}_\zeta$ is the sum of its leading part $\mathscr{L}_0$ which is the Laplacian $-\Delta$ in $\mathbb{R}^2$, and of its secondary part $4\mathrm{i}\zeta^2\mathscr{L}_1$ where $\mathscr{L}_1$ is the restriction to $\mathcal{S}_-$. According to the general

principles of Kondratev's paper [87], the singularities $\mathfrak{U}$ of $\mathscr{L}_\zeta = \mathscr{L}_0 + 4\mathrm{i}\zeta^2\mathscr{L}_1$ can be described as formal sums

$$\mathfrak{U} = \sum_j (\mathrm{i}\zeta^2)^j \mathfrak{u}_j, \tag{3.6}$$

where each term $\mathfrak{u}_j$ is derived through an inductive process by solving recursively

$$\mathscr{L}_0\mathfrak{u}_0 = 0, \quad \mathscr{L}_0\mathfrak{u}_1 = -4\mathscr{L}_1\mathfrak{u}_0, \quad \dots, \quad \mathscr{L}_0\mathfrak{u}_j = -4\mathscr{L}_1\mathfrak{u}_{j-1}, \tag{3.7}$$

in spaces of quasi-homogeneous functions $\mathsf{S}^\lambda$ defined for $\lambda \in \mathbb{C}$ by

$$\mathsf{S}^\lambda = \mathsf{Span}\left\{ r^\lambda \log^q r\, \Phi(\theta), \quad q \in \mathbb{N}, \ \ \Phi \in \mathcal{C}^1(\mathbb{T}), \ \Phi^\pm \in \mathcal{C}^\infty(\overline{\mathbb{T}_\pm}) \right\}. \tag{3.8}$$

The numbers $\lambda$ are essentially determined by the leading equation $\mathscr{L}_0\mathfrak{u}_0 = 0$, whose solutions are harmonic functions in $\mathbb{R}^2 \setminus \{\mathbf{c}\}$. The first term $\mathfrak{u}_0$ is the *leading part* of the singularity while the next terms $\mathfrak{u}_j$, for $j \geq 1$, are called the *shadows*.

The existence of the terms $\mathfrak{u}_j$ relies on the following result [40].

**Lemma 3.1** *For $\lambda \in \mathbb{C}$, let $\mathsf{S}^\lambda$ be defined by (3.8) and let $\mathsf{T}^\lambda$ be defined as*

$$\mathsf{T}^\lambda = \mathsf{Span}\left\{ r^\lambda \log^q r\, \Psi(\theta), \quad q \in \mathbb{N}, \ \ \Psi \in L^2(\mathbb{T}), \ \Psi^\pm \in \mathcal{C}^\infty(\overline{\mathbb{T}_\pm}) \right\}. \tag{3.9}$$

*For an element $\mathfrak{g}$ of $\mathsf{S}^\lambda$ or $\mathsf{T}^\lambda$, the degree $\deg \mathfrak{g}$ of $\mathfrak{g}$ is its degree as polynomial of $\log r$.*

*Let $\lambda \in \mathbb{C}$ and $\mathfrak{f} \in \mathsf{T}^{\lambda-2}$. Then, there exists $\mathfrak{u} \in \mathsf{S}^\lambda$ such that $\mathscr{L}_0\mathfrak{u} = \mathfrak{f}$. Moreover*

(i) *If $\lambda \notin \mathbb{Z}$, $\deg \mathfrak{u} = \deg \mathfrak{f}$,*

(ii) *If $\lambda \in \mathbb{Z} \setminus \{0\}$, $\deg \mathfrak{u} \leq \deg \mathfrak{f} + 1$,*

(iii) *If $\lambda = 0$, $\deg \mathfrak{u} \leq \deg \mathfrak{f} + 2$.*

At this point, we distinguish the *primal singular functions*, which belong to $H^1$ in any bounded neighborhood $\mathcal{B}$ of $\mathbf{c}$, from the *dual singular functions*, which do not belong to $H^1$ in such a neighborhood. The primal singular functions $\mathfrak{S}$ appear in the expansion as $r \to 0$ of the solutions to problem (3.1), while the dual singular functions $\mathfrak{K}$ are needed for the determination of the coefficients $\Lambda$ involved in the asymptotics.

### 3.2.1 Principles of the construction of the primal singularities

The primal singular functions start with (quasi-homogeneous) terms $\mathfrak{u}_0 \in H^1(\mathcal{B})$ satisfying $\Delta\mathfrak{u}_0 = 0$. Therefore, $\mathfrak{u}_0$ is a homogeneous harmonic polynomial. We are looking for a basis for primal singular functions, so we choose $\mathfrak{u}_0 = \mathfrak{s}_0^{k,p}$ where

$$\mathfrak{s}_0^{k,p}(r,\theta) = \begin{cases} 1, & \text{if } \ k = 0 \ \text{ and } \ p = 0, \\ r^k \cos(k\theta - p\pi/2), & \text{if } \ k \geq 1 \ \text{ and } \ p = 0, 1. \end{cases} \tag{3.10}$$

Each $\mathfrak{s}_0^{k,p}$ belongs to $\mathsf{S}^k$ and is the leading part of the singular function $\mathfrak{S}^{k,p}$ defined by

$$\mathfrak{S}^{k,p}(r,\theta) = \sum_{j\geq 0} (\mathrm{i}\zeta^2)^j \mathfrak{s}_j^{k,p}(r,\theta). \tag{3.11}$$

For $j \geq 1$, the terms $\mathfrak{s}_j^{k,p}$ in the previous series are the *shadow terms of order* $j$. According to the sequence of problems (3.7), the function $\mathfrak{s}_j^{k,p}$ is searched in $\mathsf{S}^{k+2j}$ as a particular solution to the following problem:

$$\begin{cases} \Delta \mathfrak{s}_j^{k,p\,+} = 0, & \text{in } \mathcal{S}_+ \,, \\ \Delta \mathfrak{s}_j^{k,p\,-} = 4\mathfrak{s}_{j-1}^{k,p\,-}, & \text{in } \mathcal{S}_- \,. \end{cases} \tag{3.12}$$

We deduce from Lemma 3.1 that, for any $j \geq 1$, there exists $\mathfrak{s}_j^{k,p} \in \mathsf{S}^{k+2j}$ satisfying (3.12). Moreover $\deg \mathfrak{s}_j^{k,p} \leq j$. This is why $\mathcal{A}$ can be expanded close to the corner as (3.3) and the singular functions $\mathfrak{S}^{k,p}$ writes as formal series (3.4).

### 3.2.2 Principles of the construction of the dual singularities

We start with the dual singularities of the Laplace operator

$$\mathfrak{k}^{k,p}(r,\theta) = \begin{cases} -\dfrac{1}{2\pi}\,\log r, & \text{if } \ k=0,\ p=0, \\ \dfrac{1}{2k\pi}\,r^{-k}\cos(k\theta - p\pi/2), & \text{if } \ k\geq 1,\ p=0,1. \end{cases} \tag{3.13}$$

Setting $\mathfrak{k}_0^{k,p} = \mathfrak{k}^{k,p}$, the dual singularities of $\mathscr{L}_\zeta$ are given by series

$$\mathfrak{K}^{k,p}(r,\theta) = \sum_{j\geq 0} (\mathrm{i}\zeta^2)^j \mathfrak{k}_j^{k,p}(r,\theta), \tag{3.14}$$

where, for $j \geq 1$, the shadow terms $\mathfrak{k}_j^{k,p}$ are solutions in $\mathsf{S}^{-k+2j}$ to

$$\begin{cases} \Delta \mathfrak{k}_j^{k,p\,+} = 0, & \text{in } \mathcal{S}_+ \,, \\ \Delta \mathfrak{k}_j^{k,p\,-} = 4\mathfrak{k}_{j-1}^{k,p\,-}, & \text{in } \mathcal{S}_- \,. \end{cases} \tag{3.15}$$

We deduce from Lemma 3.1 that, for any $j \geq 1$, there exists $\mathfrak{k}_j^{k,p} \in \mathsf{S}^{-k+2j}$ satisfying (3.15). Moreover, if $j$ is odd, or if $j$ is even and $2j < k$, then $\deg \mathfrak{k}_j^{k,p} \leq j$. Otherwise (*i.e.* if $j$ is even and $2j \geq k$) then $\deg \mathfrak{k}_j^{k,p} \leq j+1$. This is why the singular function $\mathfrak{K}^{k,p}$ writes as formal series

$$\mathfrak{K}^{k,p}(r,\theta) = \begin{cases} r^{-k} \displaystyle\sum_{j\geq 0} (\mathrm{i}\zeta^2)^j\, r^{2j} \sum_{n=0}^{j} \log^n r\, \Psi_{j,n}^{k,p}(\theta) \\ r^{-k} \Bigg( \displaystyle\sum_{0\leq j<k/2} (\mathrm{i}\zeta^2)^j\, r^{2j} \sum_{n=0}^{j} \log^n r\, \Psi_{j,n}^{k,p}(\theta) + \sum_{j\geq k/2} (\mathrm{i}\zeta^2)^j\, r^{2j} \sum_{n=0}^{j+1} \log^n r\, \Psi_{j,n}^{k,p}(\theta) \Bigg) \end{cases}$$

when $k$ is odd or even, respectively.

### 3.2.3 The method of moments

To extract the singular coefficients with the method of moments, we introduce the symmetric bilinear form $\mathcal{M}_R$ defined for $R > 0$ by

$$\mathcal{M}_R(K,A) := R^{-1} \int_{r=R} K\, A\, R\, \mathrm{d}\theta. \tag{3.16}$$

When $\zeta = 0$ we can extract the scalar product of $\mathcal{A}$ versus 1 to compute $\Lambda^{0,0}$ and versus $\mathfrak{k}^{k,p}$ to compute $\Lambda^{k,p}$ when $k \geq 1$ [40].

**Proposition 3.2** *Let $\mathcal{A}$ be the solution to the Laplace equation with a smooth right-hand side $F$ with support outside the ball $\mathcal{B}(\mathbf{c}, R)$. Then*

$$\mathcal{M}_R(1, \mathcal{A}) = 2\pi\Lambda^{0,0}, \quad \textit{and} \quad \mathcal{M}_R(\mathfrak{k}^{k,p}, \mathcal{A}) = \frac{1}{2k}\,\Lambda^{k,p}, \qquad \textit{for } k \geq 1,\ p = 0, 1. \tag{3.17}$$

A naive approach to extract the coefficients consists in following the heuristics of the case when $\zeta = 0$, cf. (3.16)-(3.17): compute $\mathcal{M}_R(1/(2\pi), \mathcal{A})$ in order to extract the coefficient $\Lambda^{0,0}$ and $\mathcal{M}_R(2k\mathfrak{k}^{k,p}, \mathcal{A})$ for the coefficient $\Lambda^{k,p}$ of expansion (3.3). This method makes possible a quite rough approximation of the first coefficients only, as described in [40]. This method can be useful if a low order of accuracy of the first 3 coefficients is sufficient. For a systematic computation of all the coefficients, the method of quasi-dual functions is more accurate.

### 3.2.4 The method of quasi-dual functions

When $\zeta \neq 0$, and in contrast to the case $\zeta = 0$, we do not use exact dual functions satisfying $\mathscr{L}_\zeta \mathfrak{K} = 0$ inside the anti-symmetric bilinear form $\mathcal{J}_R$ defined over a circle of radius $R > 0$ by

$$\mathcal{J}_R(K, A) := \int_{r=R} (K\partial_r A - A\partial_r K)\ R\mathrm{d}\theta. \tag{3.18}$$

Instead we use the *quasi-dual* functions $\mathfrak{K}_m^{k,p}$, which are the truncated series of (3.14):

$$\mathfrak{K}_m^{k,p}(r, \theta) := \sum_{j=0}^{m} (\mathrm{i}\zeta^2)^j \mathfrak{k}_j^{k,p}(r, \theta). \tag{3.19}$$

Here, $m$ is a nonnegative integer, which is the order of the quasi-dual function. By construction

$$\mathscr{L}_\zeta \mathfrak{K}_m^{k,p} = 4\mathrm{i}\zeta^2 (\mathrm{i}\zeta^2)^m \mathfrak{k}_m^{k,p}\, \mathbb{1}_{\mathcal{S}_-}, \tag{3.20}$$

which is not zero, but smaller and smaller as $r \to 0$ when $m$ is increased. The extraction of coefficients $\Lambda^{k,p}$ in expansion (3.3) is performed through the evaluation of quantities

$$\mathcal{J}_R(\mathfrak{K}_m^{k,p}, \mathcal{A}), \quad k = 0, 1, 2, \ldots$$

and corresponding $p \in \{0, 1\}$, for suitable values of $m \in \{0, 1, \ldots\}$. The quasi-dual function method (QDFM) was introduced in [37] for straight edges and developed in [142] for circular edges and homogeneous operators with constant coefficients. The expansions considered there do not contain any logarithmic terms. This theory was revisited in our framework where, on the contrary, we have an accumulation of logarithmic terms. The main result follows.

**Theorem 3.3** *Let $\mathcal{A}$ be the solution to problem (3.1), under the assumptions of the introduction. Let $k \in \mathbb{N}$ and $p \in \{0, 1\}$ ($p = 0$ if $k = 0$). Let $m$ such that $2m + 2 > k$. For the extraction quantity $\mathcal{J}_R(\mathfrak{K}_m^{k,p}, \mathcal{A})$ defined through (3.18) and (3.19), there exist coefficients $\mathcal{J}^{k,p;k',p'}$ independent of $R$ and $\mathcal{A}$ such that*

$$\mathcal{J}_R(\mathfrak{K}_m^{k,p}, \mathcal{A}) \underset{R\to 0}{=} \Lambda^{k,p} + \sum_{\ell=1}^{[k/2]} \mathcal{J}^{k,p\,;\,k-2\ell,p} \Lambda^{k-2\ell,p} + \mathcal{O}(R^{-k} R_0^{2m+2} \log R)\,, \tag{3.21}$$

*where $R_0 = \zeta R\,(1 + \sqrt{|\log R|})$. If $p = 1$, the remainder is improved to $\mathcal{O}(R^{1-k} R_0^{2m+2} \log R)$. The extra term $\log R$ disappears if $k$ is odd.*

Finally, a formalism using complex variables $z_\pm$ along the lines of [34] has been introduced in [40] to simplify the analytic calculations of the primal singular functions $\mathfrak{S}^{k,p}$ and the dual singular functions $\mathfrak{K}^{k,p}$, required by the quasi-dual function method.

## 3.3 Numerical simulations

In order to illustrate the QDFM to compute the coefficients of expansion (3.3), we consider problem (3.1) (with $J = 0$ and $\mathcal{A} = \frac{|\theta|}{2\pi}$ on $\Gamma$). Since the source term is even with respect to $\theta$, the solution $\mathcal{A}$ is $\theta$-even. As a consequence, only the terms with indices $p = 0$ are involved in the Kondratev-type expansion (3.3). The computational domain $\Omega$ is a disk of radius $50\mathrm{mm}$. We consider a conducting sector for $\omega = \pi/4$ (other values have been tested and the conclusions are similar). We particularly focus on the behavior of the solution in the vicinity of the corner $\mathbf{c}$. Parameter $\zeta$ is equal to $1/(5\sqrt{2})\mathrm{mm}^{-1}$, which corresponds to a physical skin depth of $5\mathrm{mm}$. The solution is computed by the finite element method, using $P_2$ finite elements available in the library GetDP and a mesh with $64192$ triangles.

First, we consider the computation of $\Lambda^{0,0}$ by the use of formula (3.21) for the case $m = 0$ and $m = 1$. The value of $\mathcal{A}$ computed at the corner $\mathbf{c}$ is defined as the reference value for $\Lambda^{0,0}$; note that it is already a numerically approximated value. This reference value is compared to $\mathcal{J}_R(\mathfrak{K}_m^{0,0}, \mathcal{A})$ for $m = 0$ and $m = 1$, a quantity which provides an approximate value of $\Lambda^{0,0}$ by the method described in subsection 3.2.4. Note that the convergence rate as a function of $R$ is related to the first neglected terms. The results are shown in Figure 3.2 and are consistent with the theoretical convergence rate (remind $R_0 = \zeta R\,(1 + \sqrt{|\log R|})$). Note that concerning $m = 1$ and the smallest values of $R$, we can presume that the discretization accuracy is attained: This should explain the behavior for the smallest values of $R$ in Figure 3.2.

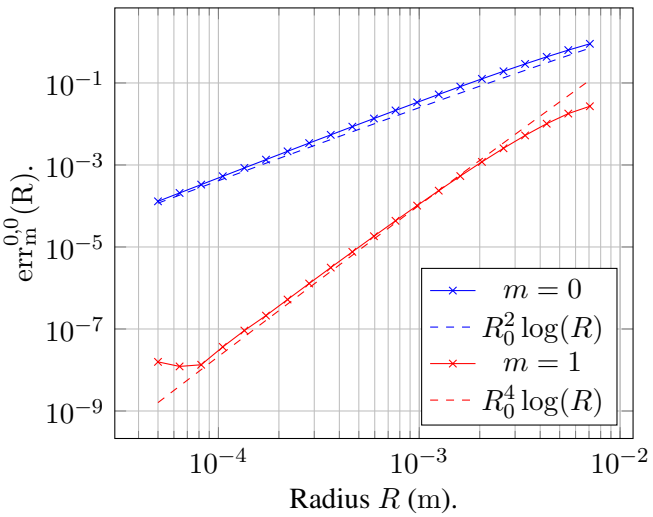


Figure 3.2: Accuracy for the computation of $\Lambda^{0,0}$ as a function of $R$.
Quantity $\mathrm{err}_{\mathrm{m}}^{0,0}(\mathrm{R})$ is the relative error $|\mathcal{J}_R(\mathfrak{K}_m^{0,0}, \mathcal{A}) - \mathcal{A}(\mathbf{c})|/|\mathcal{A}(\mathbf{c})|$.

Second, we consider the computation of the coefficients $\Lambda^{1,0}$. The reference values are taken from the computation of $\mathcal{J}_R$ for the small value $R_{\mathrm{s}} = 5 \cdot 10^{-5}\mathrm{m}$ of $R$. Results for $\mathcal{J}_R(\mathfrak{K}_m^{1,0}, \mathcal{A})$, $m = 0, 1$ are shown in Figure 3.3; they are also consistent with the expected theoretical behaviors. We also consider the computation of the coefficient $\Lambda^{2,0}$ in [40].

In Figure 3.4, we perform a qualitative description of the isovalues of $\mathcal{A}$ close to the corner comparing the finite element solution and expansion (3.3) restricted to the terms which behave as $r^k$ for $k = 0, 1, 2$ and $r^2 \log r$, *i.e.*

$$\mathcal{J}_{R_{\mathrm{s}}}(\mathfrak{K}_1^{0,0}, \mathcal{A})(1 + \mathrm{i}\zeta^2 \mathfrak{s}_1^{0,0}) + \mathcal{J}_{R_{\mathrm{s}}}(\mathfrak{K}_1^{1,0}, \mathcal{A})\mathfrak{s}_0^{1,0} + \left(\mathcal{J}_{R_{\mathrm{s}}}(\mathfrak{K}_1^{2,0}, \mathcal{A}) - \mathcal{J}^{2,0;0,0}\mathcal{J}_{R_{\mathrm{s}}}(\mathfrak{K}_1^{0,0}, \mathcal{A})\right)\mathfrak{s}_0^{2,0}\,.$$

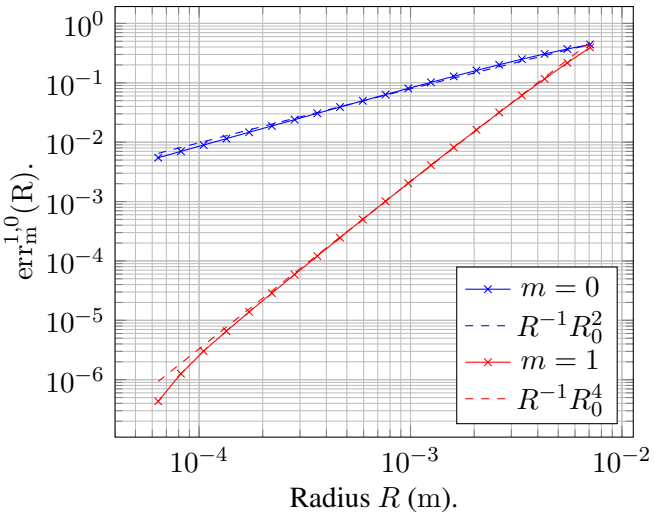


Figure 3.3: Accuracy for the computation of $\Lambda^{1,0}$ as a function of $R$.
Quantity $\mathrm{err}_{\mathrm{m}}^{1,0}(\mathrm{R})$ stands for the relative error $|\mathcal{J}_R(\mathfrak{K}_m^{1,0}, \mathcal{A}) - \mathcal{J}_{R_\mathrm{s}}(\mathfrak{K}_1^{1,0}, \mathcal{A})|/|\mathcal{J}_{R_\mathrm{s}}(\mathfrak{K}_1^{1,0}, \mathcal{A})|$.

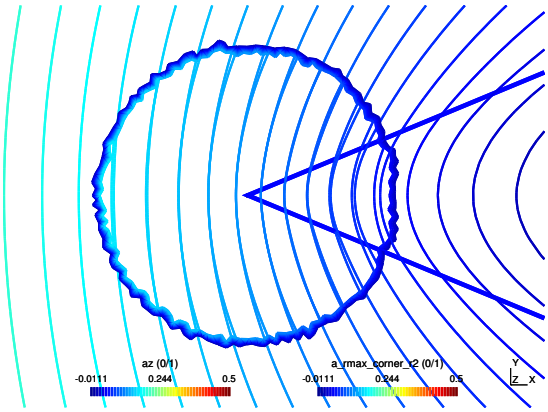


(a) Expansion restricted to composite order 2. Real part.

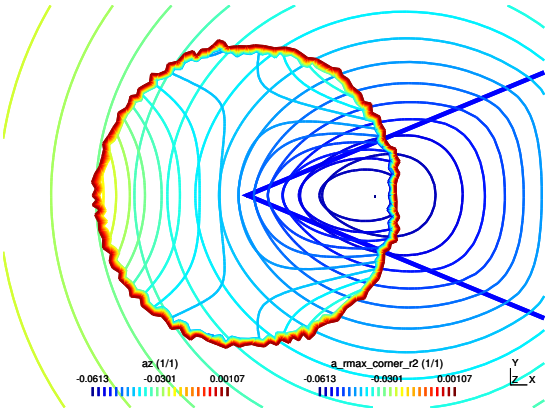


(b) Expansion restricted to composite order 2. Imaginary part.

Figure 3.4: Comparison of the finite element solution and of the local expansion.

## 3.4 Large frequency or high conductivity regimes

An asymptotic method has been developed in [21] to tackle the magneto-harmonic problem (3.1) as $\delta \to 0$. For a regular interface $\Sigma$ the potential $\mathcal{A}_0$ solution to

$$\begin{cases} -\Delta \mathcal{A}_0^+ = \mu_0 J \text{ in } \Omega_+, \\ \mathcal{A}_0^+ = 0 \text{ on } \Sigma, \qquad \mathcal{A}_0^- = 0, \text{ in } \Omega_-, \\ \mathcal{A}_0^+ = 0 \text{ on } \Gamma, \end{cases} \tag{3.22}$$

intuitively approximates $\mathcal{A}_\delta$ (3.1) in the dielectric medium and it can be proved that the "power norm" [135] of the error $\mathcal{A}_\delta - \mathcal{A}_0$ is of order $\delta$ [23]. Yet this accuracy is no more valid near a corner singularity since the $j^{th}$-order shadow function $\mathfrak{s}_j^{k,p}$ of $\mathfrak{s}_0^{k,p}$ in the Kondrat'ev expansion (3.3) behaves like $r^{k+2j}\log^j r$ as $r$ goes to zero, therefore $\nabla\mathcal{A}_\delta$ is bounded whereas $\nabla\mathcal{A}_0$ blows up at the corner. Hereafter the heuristics of a method to obtain the order $\delta$ by adding a correction in the neighborhood of the corner are presented with numerical experiments [21].

### Heuristics of a multi-scale expansion

Let first note that similarly to the regular case, $\mathcal{A}_0$ defined by (3.22) is the solution to the limit problem of (3.1) as $\delta$ goes to zero, at least far from the corner. Hence the first term of the expansion should start by $\mathcal{A}_0$. Since the respective behaviors of $\mathcal{A}_\delta$ and $\mathcal{A}_0$ are different at the corner for any non-zero $\delta$, it is natural to truncate $\mathcal{A}_0$ by a cut-off function $\varphi$ which is zero close to the corner and 1 far from it. We intuit that $\varphi(\,\cdot\,/\delta)\mathcal{A}_0$ is a good approximation and the following results show this. Let $r_0^\delta = \mathcal{A}_\delta - \varphi(\,\cdot\,/\delta)\mathcal{A}_0$, it satisfies:

$$-\Delta r_0^\delta = [\Delta;\varphi\,(./\delta)]\,\mathcal{A}_0^+, \text{ in } \Omega_+, \quad r_0^\delta|_\Gamma = 0, \text{ on } \Gamma, \tag{3.23a}$$

$$-\Delta r_0^\delta + \frac{2\mathrm{i}}{\delta^2} r_0^\delta = 0, \quad \text{in } \Omega_-, \tag{3.23b}$$

$$\left[r_0^\delta\right]_\Sigma = 0, \ \left[\partial_n r_0^\delta\right]_\Sigma = -\partial_n\left(\varphi(./\delta)\mathcal{A}_0^+\right), \quad \text{on } \Sigma, \tag{3.23c}$$

where for any pair of functions $(\nu, u)$, $[\Delta;\nu]u = \Delta(\nu u) - \nu\Delta u$. Solving exactly (3.23) provides no benefits compared with the computation of (3.1), but we will take advantage of the knowledge of $\mathcal{A}_0^+$ near the corner:

$$\mathcal{A}_0^+ \underset{r\to 0}{\simeq} a_1 r^\alpha \sin(\alpha(\theta-\omega)), \quad \text{where } \alpha = \frac{\pi}{2\pi-\omega}. \tag{3.24}$$

Insert (3.24) into such (3.23) and perform the rescaling $X = x/\delta$ ($R = r/\delta$). Let $\delta$ go to zero ($\Gamma$ is thus "sent" to the infinite) to make appear the "profile" term $V_\alpha$ that is *independent of* $\mathcal{A}_0$ *and* $\delta$ and satisfies in $\mathbb{R}^2$

$$-\Delta_X V_\alpha = [\Delta_X;\varphi]\,(R^\alpha \sin(\alpha(\theta-\omega))), \text{ in } S_+, \tag{3.25a}$$

$$-\Delta_X V_\alpha + 2\mathrm{i}V_\alpha = 0, \text{ in } S_-, \tag{3.25b}$$

$$[V_\alpha]_{\mathcal{G}} = 0, \quad \left[\frac{1}{R}\partial_\theta V_\alpha\right]_{\mathcal{G}} = \alpha\varphi R^{\alpha-1}, \tag{3.25c}$$

$$V_\alpha \to_{|X|\to+\infty} 0. \tag{3.25d}$$

Observe that near the corner, $a_1\delta^\alpha V_\alpha(./\delta)$ does not correct exactly (3.23c), however according to (3.24), it corrects its leading term, the other terms being neglected. Hence $\mathcal{A}_\delta$ writes

$$\mathcal{A}_\delta = \varphi\left(\frac{\cdot}{\delta}\right)\mathcal{A}_0 + (1-\varphi)a_1\delta^\alpha V_\alpha\left(\frac{\cdot}{\delta}\right) + r_\alpha^\delta. \tag{3.26}$$

### Numerical results and modified impedance conditions

The errors $|r_0^\delta|$ and $|r_\alpha^\delta|$ are plotted respectively in Fig. 3.5(a) and 3.5(b). The terms $\mathcal{A}_\delta$, $a_1$, $\mathcal{A}_0$ and $V_\alpha$ are computed by using the finite element method. On both figures, the same color scale is used except the white area around the corner in Fig. 3.5(a) where the error is higher (between 0.04 and 0.14). Fig. 3.5(b) shows the profile correction (3.25): the highest error lies now in the regular part of the interface $\Sigma$, for which the correction is known [23].

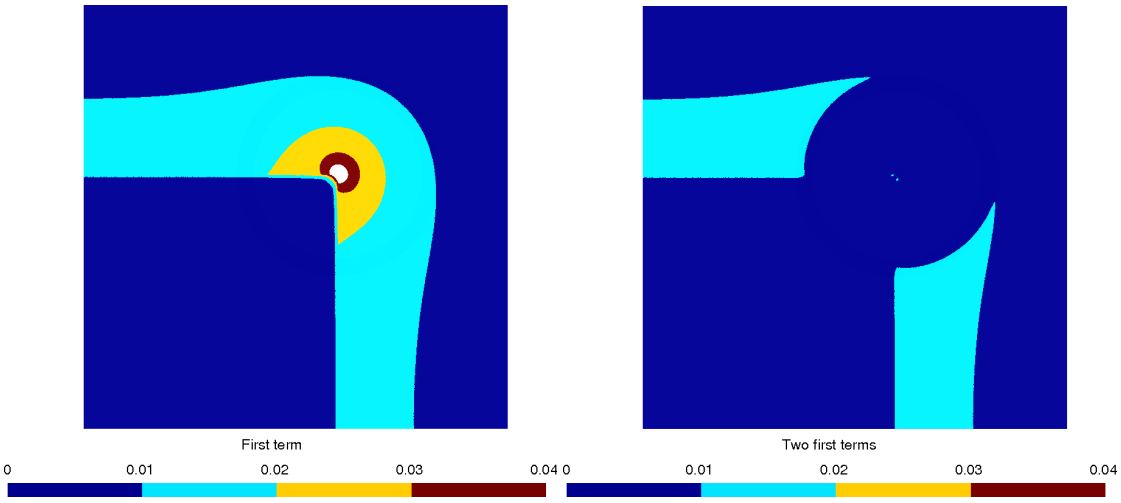


(a) $|r_0^\delta|$. (b) $|r_\alpha^\delta|$.

Figure 3.5: Modulus of the errors between the solution and the two first orders of (3.26) for $\delta = 0.025$.

Assume that $a_1 \neq 0$and denote by $Z_s = (1+\mathrm{i})/(\sigma\delta)$ the regular surface impedance. According to the expansion (3.26), the surface impedance $Z_\delta$ close to the corner can be approximated by:

$$Z_\delta = Z_s \frac{1+\mathrm{i}}{\delta} \frac{\mathcal{A}_\delta}{\partial_n \mathcal{A}_\delta} \underset{r\to 0}{\simeq} Z_s(1+\mathrm{i}) \frac{V_\alpha(\,\cdot\,/\delta)}{(\partial_n V_\alpha)(\,\cdot\,/\delta)}, \tag{3.27}$$

therefore for any $\sigma$ and $f$ such that $\delta$ is small enough, the function $Z_\delta(\delta\,\cdot\,)/|Z_s|$ behaves close to zero as $\sqrt{2}\mathrm{i}V_\alpha/(\partial_n V_\alpha)$. These similar behaviors are shown in Fig. 3.6 where the "impedance" from the profile function is compared to the real impedance for two values of $\delta$, where $f$ and $\sigma$ are different.

The modified impedance boundary condition (3.27) has been used in [52] where a finite element subproblem method (FE-SPM) has been developed to correct the inaccuracies proper to impedance condition models, in particular near edges and corners of conductors, for a large range of conductivities and frequencies. The FE-SPM allows to split eddy current analysis into subproblems of lower complexity regarding computational aspects and meshing. Local corrections, supported by fine local meshes, can be obtained from each approximate model to the other, allowing efficient extensions of their domains of validity.

## 3.5 Conclusion and perspectives

We have provided corner asymptotics of the magnetic potential for the eddy current problem in a bidimensional domain. Such expansions involve two ingredients: The calculation of both primal and dual singularities, and the computation of the singular coefficients. Primal and dual singularities of the non-homogeneous operator $-\Delta + \mathrm{i}\kappa\mu_0\sigma\mathbb{1}_{\Omega_-}$ in $\mathbb{R}^2$ are derived as infinite series,

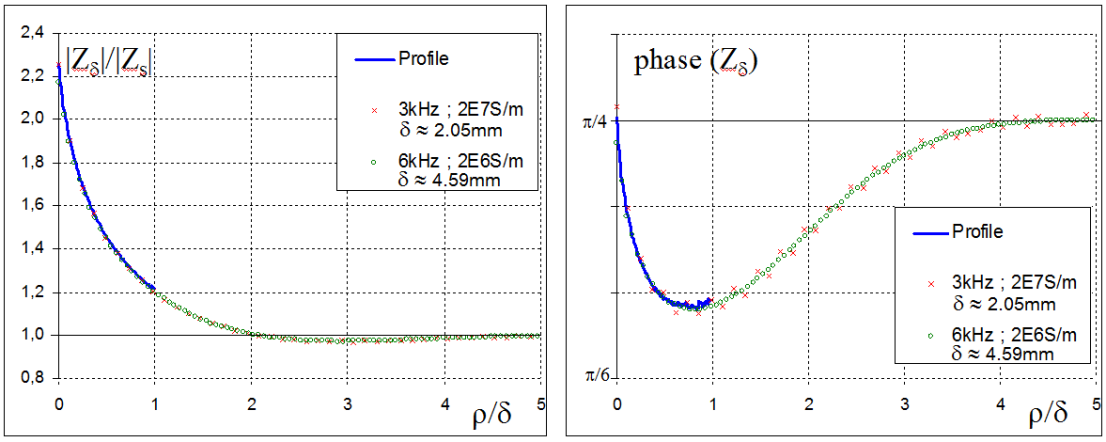


Figure 3.6: Behavior of $Z_\delta/|Z_s|$ vs $r/\delta$. The domain characteristic length $L$ is here 0.1m, then $\delta/L$ is between 2 and $4.6\%$ for the considered situations.

whose coefficients are obtained recursively. To compute the singular coefficients, we first tried to apply the method of moments, straightforwardly derived from the case of the Laplace operator. This method is limited since it makes possible to obtain only the first singular coefficients of the corner asymptotics and at a low order of accuracy, therefore we adapted the method of quasi-dual functions introduced in [37] to our specific problem. Numerical simulations of section 3.3 corroborate the theoretical order of accuracy obtained in the previous sections, illustrating the accuracy of the asymptotics.

Forthcoming work will deal with the high conducting case, (i.e. the case $\sigma$ goes to infinity), for which two small parameters appear: the distance to the corner and the skin depth $\sqrt{2/(\kappa\mu_0\sigma)}$. Preliminary results of the formal derivation of the magnetic potential have been obtained in [21], which have to be rigorously justified and extended. The theoretical proof of the existence and uniqueness of the profile $V_\alpha$ as well as the justification that the remainder $r_\alpha^\delta$ in (3.26) is of order $\delta$ will be presented in a future work.

# Chapter 4

# Edge asymptotics for the Laplace equation

## 4.1 Introduction

Asymptotic solutions of the elasticity system or the Laplace equation in the vicinity of singular points over two dimensional domains have been investigated for over half a century. For the Laplace equation these are described by an infinite series of the eigenpairs $(\alpha_k, \phi_k(\varphi))$ and their coefficients named flux intensity factors $A_k$ (FIFs) as follows:

$$\tau(\rho, \varphi) = \sum_k A_k \rho^{\alpha_k} \phi_k(\varphi). \tag{4.1}$$

In three-dimensional domains such as polyhedra, both vertex and edge singularities exist [39, 151]. For straight edges an explicit representation of the singular solutions along the edge was provided in [77, 37, 118, 153]. It is given by two infinite series containing the 2-D series and another series of the derivative of the FIFs $A_k$ which are functions along the straight singular edge (see Fig. 4.1) as follows:

$$\tau(\rho, \varphi, z) = \sum_k \sum_{\ell=0,2,4,6\cdots}^{\infty} \partial_z^\ell A_k(z) \rho^{\alpha_k+\ell} \phi_{k,\ell}(\varphi). \tag{4.2}$$

It was shown in [154] that for three-dimensional domains with a circular singular edges, the solution of the Laplace equation is given by three series:

$$\tau(\rho, \varphi, \theta) = \sum_k \sum_{\ell=0,2,4,6\cdots}^{\infty} \partial_\theta^\ell A_k(\theta) \rho^{\alpha_k} \left(\frac{\rho}{R}\right)^\ell \sum_{i=0}^{\infty} \left(\frac{\rho}{R}\right)^i \phi_{k,\ell,i}(\varphi), \tag{4.3}$$

where $\theta$ is the angle surround the circular edge, $\rho$ is the normal distance from the circular edge and $R$ is the radius of the circular edge, $A_k(\theta)$ are the Edge Flux Intensity Functions (EFIFs), $\alpha_k$ are the 2-D eigenvalues and $\phi_{k,\ell,i}(\varphi)$ are the 2-D eigenfunctions and their shadow functions. This expansion contains the 3-D straight edge series and another series associated to the curvature of the singular edge.

The computation of the elliptical edge asymptotics to the elasticity system is of major engineering importance because most surface cracks are semi-elliptical. Towards its derivation we have first considered the Laplace equation in [140] and we have shown that as for the circular

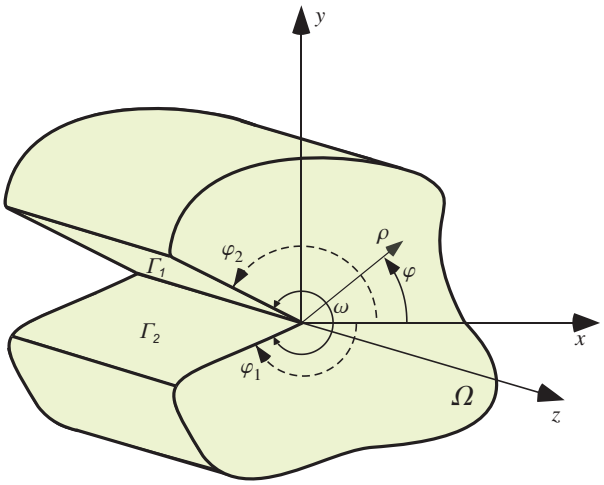


Figure 4.1: A 3-D domain containing a straight singular edge at $(x, y) = (0, 0)$.

edge case, the solution in the vicinity of an elliptical edge is composed of three series,

$$\tau = \sum_{k} \sum_{\ell=0}^{\infty} \partial_{\gamma}^{\ell} A_k(\gamma) \rho^{\alpha_k} \left( \frac{\rho \, q(\gamma)}{a \, g(\gamma)} \right)^{\ell} \sum_{i=0}^{\infty} \left( \frac{\rho \, \sinh(2\beta_0)}{a \, g(\gamma)} \right)^{i} \phi_{k,\ell,i}(\varphi, \gamma) \, . \tag{4.4}$$

Here the eigenfunctions $\phi_{k,\ell,i}$ are functions of the coordinate $\varphi$ *and of the coordinate* $\gamma$ *along the elliptical edge*; $a, \beta_0 > 0$ are given parameters for an ellipse, functions $q$ and $g$ are defined as $q(\gamma) = \cosh(2\beta_0) - \cos(2\gamma)$ and $g(\gamma) = \sqrt{q^3(\gamma)/2}$. Specific examples for an elliptical crack with homogeneous Dirichlet or Neumann BCs on the crack faces are provided in [140]. Since the dual singularities are required to extract the edge flux intensity function (EFIFs) using the QDFM, the first terms of the dual solution have also been derived.

The EFIFs and the edge stress intensity functions (ESIFs) may be computed using the dual eigenpairs by an extraction method named the quasi-dual function method (QDFM) (See [37, 118]). The QDFM has been successfully applied for the extraction of EFIFs and ESIFs associated with the non-integer eigenvalues from finite element (FE) solutions [37]. Other methods for extracting EFIFs are available (see e.g. [31, 117]), however these methods do not apply to integer eigenvalues either. Integer eigenvalues exist, for example for crack problems with homogeneous Dirichlet or Neumann boundary conditions on the crack faces [34]. In [141] the QDFM has been applied for the extraction of the EFIFs $A_k(z)$ in (4.2) which are associated with the integer eigenvalues for the Laplace operator over a 3-D domain with a straight crack. We have first determined dual singularities which are associated with the negative integer eigenvalues. Contrary to the primal singularities [35], these dual singularities involve logarithmic terms. We implement the presented methods and provide numerical examples using the p-version of the FE method.

In this chapter, we focus on the issue of EFIFs associated with the integer eigenvalues for the Laplace operator over a 3-D domain with a straight crack. The dual singularities are determined and the QDFM is adapted for the extraction of these EFIFs.

## 4.2 Dual singularities for a straight 3-D crack front

The solution to the Laplace equation in the vicinity of a straight singular edge with homogeneous Dirichlet or Neumann BCs on the crack faces is given by (4.2). The negative eigenvalues and the

corresponding eigenfunctions form the "dual solution" that we define by $K(\rho,\varphi,z)$ :

$$K(\rho,\varphi,z)=\sum_k \sum_{\ell=0,2,4,6\cdots}^{\infty} \partial_z^\ell B_k(z)\rho^{\alpha_k+\ell}\psi_{k,\ell}(\rho,\varphi) \tag{4.5}$$

Here the dual eigenvalues are **negative** for both Dirichlet BCs or Neumann BCs : $\alpha_k=-k/2$, $k=1,2,3,\cdots$ and $\alpha_0=0$ in the case of Neumann BCs.

The dual eigenfunctions $\psi_{k,\ell}$ associated with the negative non-integer eigenvalues (i.e. $\alpha_k=-k/2$, $k=1,3,\cdots$) and their shadows are independent of $\rho$. These functions can be computed by solving recursively the ODEs

$$\alpha_k^2\psi_{k,0}(\varphi)+\psi_{k,0}''(\varphi)=0, \qquad \varphi\in(-\pi,\pi), \tag{4.6}$$

$$(\alpha_k+\ell)^2\psi_{k,\ell}(\varphi)+\psi_{k,\ell}''(\varphi)+\psi_{k,\ell-2}(\varphi)=0, \qquad \varphi\in(-\pi,\pi), \quad \ell\in 2\mathbb{N}\setminus\{0\} \tag{4.7}$$

with Dirichlet or Neumann BCs.

In this section, we emphasize the problem of computing dual shadows associated with integer eigenvalues (i.e. $\alpha_k=-k/2$, $k=0,2,4,\cdots$). Let $K^{(\alpha_j)}$ be the part of the dual solution (4.5) associated with the eigenvalue $\alpha_j\in\mathbb{Z}_-$, so that

$$K=\sum_j K^{(\alpha_j)} \quad \text{and} \quad K^{(\alpha_j)}(\rho,\varphi,z)=\sum_{\ell=0,2,4,6\cdots}^{\infty}\partial_z^\ell B_j(z)\rho^{\alpha_j+\ell}\psi_{j,\ell}(\rho,\varphi) \tag{4.8}$$

Following the construction of dual singularities introduced in [40], the dual singularities $K^{(\alpha_j)}$ contain logarithmic terms in $\rho$

$$K^{(\alpha_j)}(\rho,\varphi,z)=\sum_{\ell=0,2,4,6\cdots}^{\infty}\partial_z^\ell B_j(z)\rho^{\alpha_j+\ell}\left(\psi_{j,\ell}(\varphi)+\log\rho\,\tilde\psi_{j,\ell}(\varphi)\right) \tag{4.9}$$

We provide recursive ODEs for the determination of the polar parts $\psi_{j,\ell}$ and $\tilde\psi_{j,\ell}$

$$(\alpha_j+\ell)^2\,\tilde\psi_{j,\ell}+\tilde\psi_{j,\ell}''+\tilde\psi_{j,\ell-2}=0 \tag{4.10}$$

$$(\alpha_j+\ell)^2\,\psi_{j,\ell}+\psi_{j,\ell}''+2\,(\alpha_j+\ell)\,\tilde\psi_{j,\ell}+\psi_{j,\ell-2}=0 \tag{4.11}$$

for all $\ell\geq 0$ (with the convention $\tilde\psi_{j,-2}=\psi_{j,-2}=0$). As an application the dual singularities $K^{(-1)}$ and $K^{(0)}$ have been derived [141] : for homogeneous Dirichlet BCs on the crack faces, we obtain

$$\begin{aligned} K^{(-1)} \;=\; \rho^{-1}\Big\{ & B_2(z)\sin\varphi-B_2''(z)\rho^2\log\rho\frac{\sin\varphi}{2} \\ & +B_2^{(4)}(z)\rho^4\left(-\frac{3}{64}+\log\rho\frac{1}{16}\right)\sin\varphi \\ & +B_2^{(6)}(z)\rho^6\left(\frac{7}{2304}-\log\rho\frac{1}{384}\right)\sin\varphi+\cdots\Big\} \end{aligned} \tag{4.12}$$

For homogeneous Neumann BCs on the crack faces, we obtain

$$\begin{aligned} K^{(0)} \;=\; -\Big\{ & B_0(z)\log\rho+B_0''(z)\rho^2\frac{1}{4}(1-\log\rho) \\ & +B_0^{(4)}(z)\rho^4\left(-\frac{3}{128}+\log\rho\frac{1}{64}\right)+B_0^{(6)}(z)\rho^6\left(\frac{11}{13824}-\log\rho\frac{1}{2304}\right)+\cdots\Big\} \end{aligned} \tag{4.13}$$

and

$$K^{(-1)} = \rho^{-1}\left\{B_2(z)\cos\varphi - B_2''(z)\rho^2\log\rho\frac{\cos\varphi}{2} + B_2^{(4)}(z)\rho^4\left(-\frac{3}{64}+\log\rho\frac{1}{16}\right)\cos\varphi \right.$$
$$\left. + B_2^{(6)}(z)\rho^6\left(\frac{7}{2304}-\log\rho\frac{1}{384}\right)\cos\varphi+\cdots\right\}$$

## 4.3 Extraction of EFIFs associated with integer eigenvalues

To compute the EFIFs we apply the QDFM [37]. A path integral $\mathcal{Q}_\rho\left[\tau, K_n^{(\alpha_j)}\right]$ over a cylindrical surface with a radius $\rho$ surrounding the straight singular edge is considered:

$$\mathcal{Q}_\rho\left[\tau, K_n^{(\alpha_j)}\right] = \int_z\int_{-\pi}^{\pi}\left(\partial_\rho\tau K_n^{(\alpha_j)} - \tau\partial_\rho K_n^{(\alpha_j)}\right)\rho d\varphi dz\ . \tag{4.14}$$

Here, $K_n^{(\alpha_j)}$ is composed of the dual eigenfunction and its first $n$ shadow functions.

Since the EFIFs $A_k(z)$ are unknown, we approximate it (and also $B_j(z)$) by a family of orthogonal polynomials in the range $[-1,1]$. For this purpose we use the Jacobi polynomials as follows (see [118]) :

$$A_k^{\{p,m\}}(z) = \sum_{i=0}^{p} a_{k_i} J^{\{i,m\}}(z) \tag{4.15}$$

$$B_j^{\{\ell,m\}}(z) = \frac{1}{2\pi}\frac{2\ell+2m+1}{2^{2m+1}}\frac{(2m+\ell)!\ell!}{((\ell+m)!)^2}\left(1-z^2\right)^m J^{\{\ell,m\}}(z) \tag{4.16}$$

where $J^{\{\ell,m\}}(z)$ is a Jacobi polynomial of order $m$ and a polynomial degree $\ell$. Since $n$ is finite, the integral $\mathcal{Q}_\rho\left[\tau, K_n^{(\alpha_j)}\right]$ is surface-dependent. For the computation of the coefficients $a_{j_\ell}$ in (4.15) we used the $\mathcal{Q}_{\rho_0}\left[\tau, K_n^{(\alpha_j)}\right]$ integral with a remainder of:

$$\mathcal{Q}_\rho\left[\tau, K_n^{(\alpha_j)}\left[B_j^{\{\ell,m\}}(z)\right]\right] = a_{j_\ell} + \mathcal{O}\left(\rho^{\alpha_s-\alpha_j+n+2}(1+|\log\rho|)\right) \tag{4.17}$$

where $\alpha_s$ is the smallest positive eigenvalue. For a crack with homogeneous Dirichlet BCs the smallest positive eigenvalues is $\alpha_1 = 1/2$, and for a crack with homogeneous Neumann BCs the smallest positive eigenvalues is $\alpha_0 = 0$.

### 4.3.1 Computation of integer EFIFs with the QDFM : analytical examples

In [141] we extract the integer EFIFs for a straight crack with homogeneous Dirichlet and Neumann BCs. We use Jacobi polynomials of order $m = 4$ and polynomial degree $p = 8$ to approximate the EFIF $A_k(z)$ with (4.15) and to approximate $B_j(z)$ with (4.16).

To extract $A_2(z)$ for Dirichlet BCs we compute $\mathcal{Q}_\rho\left[\tau, K_n^{(-1)}\left[B_2^{\{\ell,4\}}(z)\right]\right]$ by using (4.14) and (4.12) with an explicit representation of the solution $\tau$ in (4.2), chosen up to order $\rho^6$, for

$z \in [-1,1]$, $\ell = 0, 1$ and different values of $n$.

$$
\begin{aligned}
\mathcal{Q}_\rho\left[\tau, K_0^{(-1)}\left[B_2^{\{0,4\}}(z)\right]\right] &= a_{2_0} - \frac{33}{4}\rho^2 a_{2_2} - \frac{91}{11}\rho^2 a_{2_4} + \cdots \\
\mathcal{Q}_\rho\left[\tau, K_0^{(-1)}\left[B_2^{\{1,4\}}(z)\right]\right] &= a_{2_1} - \frac{273}{20}\rho^2 a_{2_3} - \frac{189}{13}\rho^2 a_{2_5} + \cdots \\
\mathcal{Q}_\rho\left[\tau, K_2^{(-1)}\left[B_2^{\{0,4\}}(z)\right]\right] &= a_{2_0} - \frac{1365}{32}\rho^4 a_{2_4} + \frac{1365}{8}\rho^4 \log\rho\, a_{2_4} + \cdots \\
\mathcal{Q}_\rho\left[\tau, K_2^{(-1)}\left[B_2^{\{1,4\}}(z)\right]\right] &= a_{2_1} - \frac{3213}{32}\rho^4 a_{2_5} + \frac{3213}{8}\rho^4 \log\rho\, a_{2_5} + \cdots \\
\mathcal{Q}_\rho\left[\tau, K_4^{(-1)}\left[B_2^{\{0,4\}}(z)\right]\right] &= a_{2_0} + \frac{266475}{128}\rho^6 a_{2_6} - \frac{72675}{32}\rho^6 \log\rho\, a_{2_6} + \cdots \\
\mathcal{Q}_\rho\left[\tau, K_4^{(-1)}\left[B_2^{\{1,4\}}(z)\right]\right] &= a_{2_1} + \frac{820743}{128}\rho^6 a_{2_7} - \frac{223839}{32}\rho^6 \log\rho\, a_{2_7} + \cdots
\end{aligned}
$$

To extract $A_0(z)$ (Neumann BCs) we use $K^{(0)}$ in (4.13) and we compute $\mathcal{Q}_\rho\left[\tau, K_n^{(0)}\left[B_2^{\{\ell,4\}}(z)\right]\right]$ by using (4.14) with an explicit representation of the solution $\tau$ in (4.2), for $z \in [-1,1]$, $\ell = 0, 1$ and for different values of $n = 0, 2, 4$.

$$
\begin{aligned}
\mathcal{Q}_\rho\left[\tau, K_0^{(0)}\left[B_0^{\{0,4\}}(z)\right]\right] &= a_{0_0} - \frac{33}{4}\rho^2 a_{0_2} + \frac{33}{2}\rho^2 \log\rho\, a_{0_2} + \cdots \\
\mathcal{Q}_\rho\left[\tau, K_0^{(0)}\left[B_0^{\{1,4\}}(z)\right]\right] &= a_{0_1} - \frac{273}{20}\rho^2 a_{0_3} + \frac{273}{10}\rho^2 \log\rho\, a_{0_3} + \cdots \\
\mathcal{Q}_\rho\left[\tau, K_2^{(0)}\left[B_0^{\{0,4\}}(z)\right]\right] &= a_{0_0} + \frac{6825}{32}\rho^4 a_{0_4} - \frac{1365}{8}\rho^4 \log\rho\, a_{0_4} + \cdots \\
\mathcal{Q}_\rho\left[\tau, K_2^{(0)}\left[B_0^{\{1,4\}}(z)\right]\right] &= a_{0_1} + \frac{16065}{32}\rho^4 a_{0_5} - \frac{3213}{8}\rho^4 \log\rho\, a_{0_5} + \cdots \\
\mathcal{Q}_\rho\left[\tau, K_4^{(0)}\left[B_0^{\{0,4\}}(z)\right]\right] &= a_{0_0} - \frac{121125}{64}\rho^6 a_{0_6} + \frac{72675}{64}\rho^6 \log\rho\, a_{0_6} + \cdots \\
\mathcal{Q}_\rho\left[\tau, K_4^{(0)}\left[B_0^{\{1,4\}}(z)\right]\right] &= a_{0_1} - \frac{373065}{64}\rho^6 a_{0_7} + \frac{223839}{64}\rho^6 \log\rho\, a_{0_7} + \cdots
\end{aligned}
$$

### 4.3.2 Extracting $A_0$ and $A_2$ from p-FE solutions by the QDFM

Consider a finite elements model of a cracked cylinder with a radius $0.5$ and a height $2$ ($z \in [-1,1]$), as shown in Fig 4.2. On the crack faces of the FE model we prescribe homogeneous Dirichlet BCs. On the cylindrical outer surface the following Dirichlet BC is prescribed:

$$
\tau = \frac{1}{2}\left[\left(1 + z + z^2 + z^3 + z^4\right)\sin\varphi - \frac{1}{8}\left(2 + 6z + 12z^2\right)\left(\frac{1}{2}\right)^2 \sin\varphi + \frac{1}{8}\left(\frac{1}{2}\right)^4 \sin\varphi\right]
$$

On the cylinder's basis $z = -1$ the Dirichlet BC is:

$$
\tau = \rho\left(\sin\varphi - \rho^2 \sin\varphi + \frac{1}{8}\rho^4 \sin\varphi\right)
$$

and on the cylinder's basis $z = 1$ the Dirichlet BC is:

$$
\tau = \rho\left(5\sin\varphi - \frac{5}{2}\rho^2 \sin\varphi + \frac{1}{8}\rho^4 \sin\varphi\right)
$$

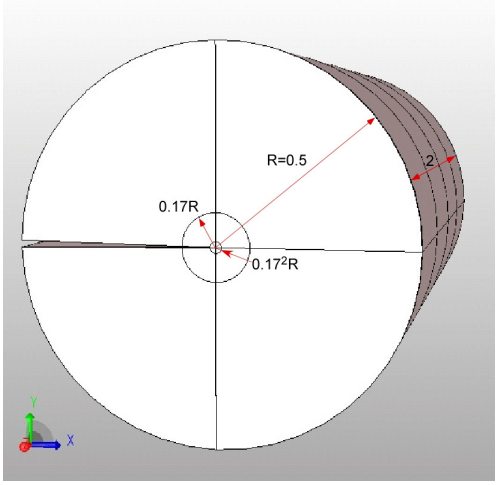


Figure 4.2: A cracked cylinder.

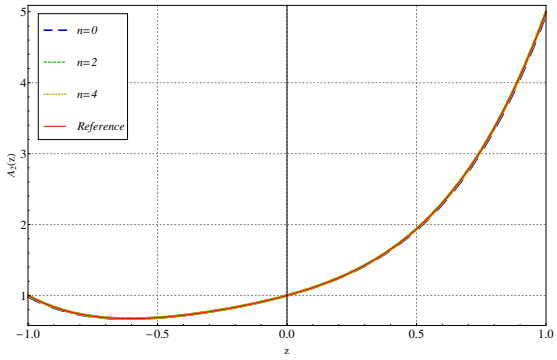


Figure 4.3: $A_2(z)$ for different values of $n$ and the exact function - homogeneous Dirichlet BCs.

These boundary conditions result in $A_2(z) = 1 + z + z^2 + z^3 + z^4$ and $A_k = 0$ for $k \neq 2$ so that the solution is:

$$\tau = \rho \left[ \left(1 + z + z^2 + z^3 + z^4\right) \sin\varphi - \frac{1}{8}\left(2 + 6z + 12z^2\right) \rho^2 \sin\varphi \, . + \frac{1}{8}\rho^4 \sin\varphi \right]$$

The integral $\mathcal{Q}_\rho \left[ \tau^{FE}, K_n^{\alpha_j} \left[ B_j^{\{m,\ell\}}(z) \right] \right]$ was computed at $\rho = 0.1$ with Jacobi polynomials of order $m = 6$ and $\ell = 0 \cdots 20$ for different values of $n$. The solution $\tau^{FE}$ was extracted from the p-FE solution with 4387 DOF at $p = 8$ having an relative error in energy norm of $0.1\%$. Figures 4.3-4.4 show the extracted $A_2^{FE}(z)$ for different values of $n$ and the relative error in the extracted $A_2^{FE}(z)$ in percentage. As expected, the error in the extracted EFIFs decreases as the number of the shadow functions $n$ that construct the quasi-dual function $K$ increases.

In [141] we extract also $A_0(z)$ and $A_2(z)$ from p-FE solutions by the QDFM when prescribing homogeneous Neumann BCs on the crack faces. We observed that the error in EFIFs decreases as the number of the shadow functions increases.

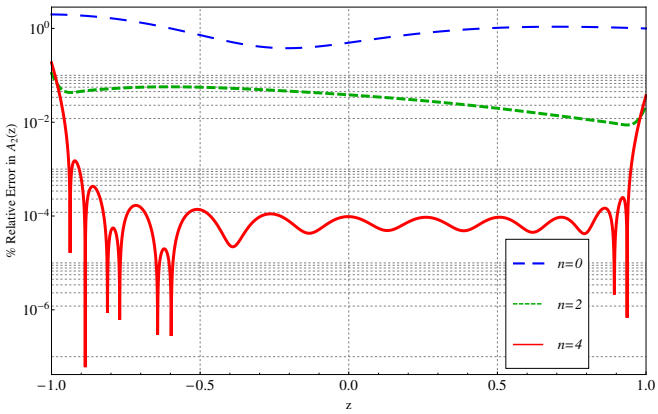


Figure 4.4: Relative error in the extracted $A_2(z)$ in percentage - homogeneous Dirichlet BCs.

## 4.4 Conclusion and perspectives

The dual singularities of the Laplace equation has been presented in the vicinity of a straight crack [141]. The dual integer eigenfunctions and their shadow functions contain logarithmic terms. The QDFM has been extended for extracting the EFIFs in the vicinity of a straight singular edge for the EFIFs that depend on the integer eigenvalues. The formulation and performance of the method is demonstrated on the simplified Laplace equation. Although the QDFM is a mildly-surface-dependent integral, we demonstrated that by using a proper quasi-dual function $K_n^{(\alpha_j)}$ and proper extraction functions $B_j(z)$, one may extract the functional representation of the EFIFs $A_k(z)$ accurately and efficiently.

Because, in general, only a FE approximation of the solution is available, the QDFM in conjunction with $p$-FE methods provide highly accurate EFIFs. These were obtained as a function along the straight edge. Another major advantage is the possibility to use the FE solution on a cylindrical surface at a distance from the singular edge, thus it is not necessary to have a refined mesh in the vicinity of the singularity (which is a complicated and tedious task in 3-D domains). The presented methods may be extended to the elasticity system and to circular singular edges following the same methodology presented herein.

We provided also the machinery to develop an asymptotic solution for the Laplace equation in the vicinity of an elliptical crack or a sharp V-notch in a three dimensional domain [140]. These machinery and solution for the Laplace equation serve as a cornerstone for the asymptotic solution for the elasticity system, and the next of this work is to obtain an asymptotic solution to the elasticity system in the vicinity of an elliptical and semi-elliptic crack.

# Part III

# Appendix

# Appendix A

# Thin-layer models for transmission problems in electromagnetism

## A.1 Introduction

In this appendix one presents a review on the accuracy of different approximations of the electromagnetic field for time-harmonic thin-layer transmission problems. The simplified configuration is mainly motivated by the computation of the electromagnetic field in biological cells. In [55] we derived a multi-scale expansion in power series of a small parameter $\varepsilon$ (which represents the relative size of a cell membrane) for the electromagnetic field at mid-frequency. We inferred appropriate transmission conditions "at first order" on the boundary of the cytoplasm satisfied by the first two terms of the expansion $\mathbf{E}^0 + \varepsilon\mathbf{E}^1$. We proved uniform estimates (in energy norm) with respect to $\varepsilon$ for the error between the exact solution $\mathbf{E}^\varepsilon$ and the approximate solution $\mathbf{E}^0+\varepsilon\mathbf{E}^1$ [55, Th. 2.9]. We validated the asymptotic expansion up to the first two terms, proving estimates for the remainder of the expansion defined as $\mathbf{E}^\varepsilon - (\mathbf{E}^0 + \varepsilon\mathbf{E}^1)$ [55, Th. 6.3]. We provided numerical simulations that validate approximate models.

Since the expansion [55, Eq. (5.1)] is no longer valid in the low-frequency regime, we derived a resistive model adapted to this frequency range, [54, 56]. We derived a GITC (Generalized Impedance Transmission Condition) model of order 2 (A.7). Delourme *et al.* derived a second order asymptotic model [46, Eqs. (1)-(5)] for the electrical field in a domain with a periodic oscillating thin (and straight) layer. We have made explicit the model of Delourme *et al.* in the case of an homogeneous thin layer. It corresponds to the GITC model (A.7) for a specific choice of parameters $\alpha = \beta = \frac{1}{2}$. A new unified formulation, which involves the coefficients $A_\beta$, $B_\beta$, $C_\beta$, and $D_\beta$ in (A.8) was introduced in order to write the different models in the same framework [56]. This simplifies the comparison between the models and we make the link with the work in Ref. [32]. We show the numerical accuracy of the different asymptotic models for the diffraction problem of a penetrable sphere surrounded by a conducting thin layer. Then, we apply the different models to the case of a spherical biological cell: the membrane is then very resistive. We observe a mid-frequency regime (for which GITCs provide a second order approximation) when the currents of displacement are prominent and we observe a low-frequency regime (for which only a first order approximation is observed for GITCs), when the ohmic currents are dominant. We discuss advantages and drawbacks for all these models.

## A.2 The mathematical model

We introduce the framework and the exact model that will be approximated in the next sections.

### A.2.1 Time-harmonic Maxwell equation in single cell

Biological cells consist of a cytoplasm surrounded by a thin resistive layer. We denote by $\mathcal{O}$ the domain of interest which is composed of the outer cell medium and the cell. Let us denote by $\mathcal{O}_{\rm c}$ the cell cytoplasm, and by $\mathcal{O}_{\rm m}^{\varepsilon}$ the cell membrane surrounding $\mathcal{O}_{\rm c}$, whose thickness is constant and denoted by $\varepsilon$. Assuming, without loss of generality, that the domain $\mathcal{O}_{\rm c}$ is independent of $\varepsilon$, the extracellular domain is then $\varepsilon$–dependent. We denote it by $\mathcal{O}_{\rm e}^{\varepsilon}$, in a such way that (see Figure A.1) :

$$\mathcal{O} = \mathcal{O}_{\rm c} \cup \overline{\mathcal{O}_{\rm m}^{\varepsilon}} \cup \mathcal{O}_{\rm e}^{\varepsilon}.$$

The boundary of the cytoplasm is the smooth surface denoted by $\Gamma$ while $\Gamma^{\varepsilon}$ is the cell boundary, *i.e.* $\Gamma^{\varepsilon}$ is the boundary of $\overline{\mathcal{O}_{\rm c}} \cup \mathcal{O}_{\rm m}^{\varepsilon}$.

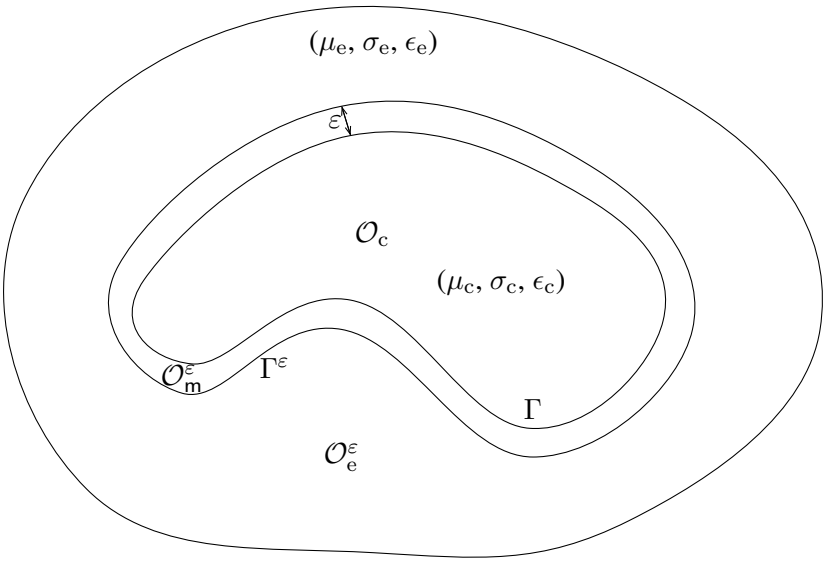


Figure A.1: A cross-section of the domain $\mathcal{O}$ and its subdomains $\mathcal{O}_{\rm c}$, $\mathcal{O}_{\rm m}^{\varepsilon}$, $\mathcal{O}_{\rm e}$

The electromagnetic properties of $\mathcal{O}$ are given by the following piecewise-constant functions $\underline{\mu}$, $\underline{\epsilon}$, and $\underline{\sigma}$ corresponding to the respective magnetic permeability, electrical permittivity, and conductivity of $\mathcal{O}$:

$$\underline{\mu} = \begin{cases} \mu_{\rm c}, & \text{in } \mathcal{O}_{\rm c}, \\ \mu_{\rm m}, & \text{in } \mathcal{O}_{\rm m}^{\varepsilon}, \\ \mu_{\rm e}, & \text{in } \mathcal{O}_{\rm e}^{\varepsilon}, \end{cases} \qquad \underline{\epsilon} = \begin{cases} \epsilon_{\rm c}, & \text{in } \mathcal{O}_{\rm c}, \\ \epsilon_{\rm m}, & \text{in } \mathcal{O}_{\rm m}^{\varepsilon}, \\ \epsilon_{\rm e}, & \text{in } \mathcal{O}_{\rm e}^{\varepsilon}, \end{cases} \qquad \underline{\sigma} = \begin{cases} \sigma_{\rm c}, & \text{in } \mathcal{O}_{\rm c}, \\ \sigma_{\rm m}, & \text{in } \mathcal{O}_{\rm m}^{\varepsilon}, \\ \sigma_{\rm e}, & \text{in } \mathcal{O}_{\rm e}^{\varepsilon}, \end{cases} .$$

Let us denote by $\mathbf{J}$ the time-harmonic current source and let $\omega$ be the frequency. For the sake of simplicity, we assume that $\mathbf{J}$ is smooth , supported in $\mathcal{O}_{\rm e}^{\varepsilon}$ and that it vanishes in a neighborhood of the cell membrane. Maxwell's equations link the electric field $\mathbf{E}$ and the magnetic field $\mathbf{H}$, through Faraday's and Ampère's laws in $\mathcal{O}$ :

$$\operatorname{curl} \mathbf{E}^{\varepsilon} - i\omega\underline{\mu}\mathbf{H}^{\varepsilon} = 0 \quad \text{and} \quad \operatorname{curl} \mathbf{H}^{\varepsilon} + (i\omega\underline{\epsilon} - \underline{\sigma})\,\mathbf{E}^{\varepsilon} = \mathbf{J} \quad \text{in} \quad \mathcal{O}\,.$$

We complement this problem with a Silver-Müller boundary condition set on $\partial\mathcal{O}$. Denoting by $\underline{\kappa}$ the complex wave number given by

$$\forall x \in \mathcal{O}, \quad \underline{\kappa}^2(x) = \omega^2 \underline{\mu}(x) \left( \underline{\epsilon}(x) + i\frac{\underline{\sigma}(x)}{\omega} \right), \quad \operatorname{Im}(\underline{\kappa}(x)) > 0,$$

Maxwell's system of first order partial differential equations can be reduced to the following second-order equation

$$\operatorname{curl}\operatorname{curl}\mathbf{E}^\varepsilon - \underline{\kappa}^2\mathbf{E}^\varepsilon = i\omega\underline{\mu}\mathbf{J} \quad \text{in} \quad \mathcal{O}_\mathrm{c}\cup\mathcal{O}_\mathsf{m}^\varepsilon\cup\mathcal{O}_\mathrm{e}^\varepsilon\,, \tag{A.1a}$$

with the following transmission conditions across $\Gamma$ and $\Gamma^\varepsilon$

$$\mathbf{E}_\mathrm{e}^\varepsilon\times\mathbf{n}|_{\Gamma^\varepsilon} = \mathbf{E}_\mathrm{m}^\varepsilon\times\mathbf{n}|_{\Gamma^\varepsilon}, \quad \frac{1}{\mu_\mathrm{e}}\operatorname{curl}\mathbf{E}_\mathrm{e}^\varepsilon\times\mathbf{n}|_{\Gamma^\varepsilon} = \frac{1}{\mu_\mathrm{m}}\operatorname{curl}\mathbf{E}_\mathrm{m}^\varepsilon\times\mathbf{n}|_{\Gamma^\varepsilon}, \tag{A.1b}$$

$$\mathbf{E}_\mathrm{c}^\varepsilon\times\mathbf{n}|_{\Gamma} = \mathbf{E}_\mathrm{m}^\varepsilon\times\mathbf{n}|_{\Gamma}, \quad \frac{1}{\mu_\mathrm{c}}\operatorname{curl}\mathbf{E}_\mathrm{c}^\varepsilon\times\mathbf{n}|_{\Gamma} = \frac{1}{\mu_\mathrm{m}}\operatorname{curl}\mathbf{E}_\mathrm{m}^\varepsilon\times\mathbf{n}|_{\Gamma}, \tag{A.1c}$$

where $\mathbf{E}_\mathrm{e}^\varepsilon$, $\mathbf{E}_\mathrm{m}^\varepsilon$, $\mathbf{E}_\mathrm{c}^\varepsilon$ denote the respective restrictions of $\mathbf{E}^\varepsilon$ to the domains $\mathcal{O}_\mathrm{e}^\varepsilon$, $\mathcal{O}_\mathsf{m}^\varepsilon$ and $\mathcal{O}_\mathrm{c}$. The boundary condition is given as

$$\operatorname{curl}\mathbf{E}^\varepsilon\times\mathbf{n} - i\kappa_\mathrm{e}\,\mathbf{n}\times\mathbf{E}^\varepsilon\times\mathbf{n} = 0 \quad \text{on} \quad \partial\mathcal{O}. \tag{A.1d}$$

### A.2.2 The mid-frequency case

**Two first orders of the asymptotic expansion**

The first term $\mathbf{E}^0$ of the expansion satisfies the problem without the layer:

$$\operatorname{curl}\operatorname{curl}\mathbf{E}^0 - \kappa_\mathrm{e}^2\mathbf{E}^0 = i\omega\mu_\mathrm{e}\mathbf{J}\,, \text{ in } \mathcal{O}_\mathrm{e}, \tag{A.2a}$$

$$\operatorname{curl}\operatorname{curl}\mathbf{E}^0 - \kappa_\mathrm{c}^2\mathbf{E}^0 = 0\,, \text{ in } \mathcal{O}_\mathrm{c}, \tag{A.2b}$$

with the transmission conditions:

$$\left[\mathbf{E}^0\times\mathbf{n}\right]_\Gamma = 0, \quad \frac{1}{\mu_\mathrm{e}}\operatorname{curl}\mathbf{E}^0\times\mathbf{n}|_{\Gamma^+} = \frac{1}{\mu_\mathrm{c}}\operatorname{curl}\mathbf{E}^0\times\mathbf{n}|_{\Gamma^-}, \tag{A.2c}$$

and the Silver-Müller condition

$$\operatorname{curl}\mathbf{E}^0\times\mathbf{n} - i\kappa_\mathrm{e}\,\mathbf{n}\times\mathbf{E}^0\times\mathbf{n} = 0 \quad \text{on} \quad \partial\mathcal{O}. \tag{A.2d}$$

$\mathbf{E}^1$ satisfies

$$\operatorname{curl}\operatorname{curl}\mathbf{E}^1 - \kappa^2\mathbf{E}^1 = 0\,, \text{ in } \mathcal{O}_\mathrm{c}\cup\mathcal{O}_\mathrm{e}, \tag{A.3a}$$

$$\operatorname{curl}\mathbf{E}^1\times\mathbf{n} - i\kappa_\mathrm{e}\,\mathbf{n}\times\mathbf{E}^1\times\mathbf{n} = 0 \quad \text{on} \quad \partial\mathcal{O}, \tag{A.3b}$$

with the following transmission conditions on $\Gamma$

$$\mathbf{n}\times\mathbf{E}^1|_{\Gamma^+}\times\mathbf{n} = \mathbf{n}\times\mathbf{E}^1|_{\Gamma^-}\times\mathbf{n} + \mathsf{T}(\mathbf{E}^0)\,, \tag{A.3c}$$

$$\frac{1}{\mu_\mathrm{e}}\left(\operatorname{curl}\mathbf{E}^1\times\mathbf{n}\right)|_{\Gamma^+} = \frac{1}{\mu_\mathrm{c}}\left(\operatorname{curl}\mathbf{E}^1\times\mathbf{n}\right)|_{\Gamma^-} + \mathsf{S}(\mathbf{E}^0)\,. \tag{A.3d}$$

Here $\mathsf{T}$ and $\mathsf{S}$ are surface operators defined on $\Gamma$:

$$\mathsf{T}(\mathbf{E}) = \left(\frac{\mu_\mathrm{m}}{\kappa_\mathrm{m}^2} - \frac{\mu_\mathrm{e}}{\kappa_\mathrm{e}^2}\right)\mathbf{n}\times\mathbf{curl}_\Gamma\operatorname{curl}_\Gamma(\frac{1}{\mu_\mathrm{c}}\operatorname{curl}\mathbf{E})_\mathsf{T}|_{\Gamma^-} + (\mu_\mathrm{m}-\mu_\mathrm{e})\frac{1}{\mu_\mathrm{c}}\left(\operatorname{curl}\mathbf{E}\times\mathbf{n}\right)|_{\Gamma^-}, \tag{A.4}$$

$$\mathsf{S}(\mathbf{E}) = -\left(\frac{\kappa_\mathrm{m}^2}{\mu_\mathrm{m}} - \frac{\kappa_\mathrm{e}^2}{\mu_\mathrm{e}}\right)\left(\mathbf{n}\times\mathbf{E}\times\mathbf{n}\right)|_{\Gamma^+} + \left(\frac{1}{\mu_\mathrm{m}} - \frac{1}{\mu_\mathrm{e}}\right)\mathbf{curl}_\Gamma\operatorname{curl}_\Gamma\left(\mathbf{n}\times\mathbf{E}\times\mathbf{n}\right)|_{\Gamma^+}\,, \tag{A.5}$$

and $\mathbf{curl}_\Gamma$ is the tangential rotational operator and $\operatorname{curl}_\Gamma$ is the surface rotational operator.

### A.2.3 The low-frequency case

For low frequencies, the ratio $|\kappa_{\rm m}/\kappa_{\rm e}|^2$ is of order $\varepsilon$. It is convenient to introduce the complex $\widetilde{\kappa}_{\rm m}$ such as

$$\kappa_{\rm m}^2 = \varepsilon \widetilde{\kappa}_{\rm m}^2,$$

where $\widetilde{\kappa}_{\rm m}$ is such that its imaginary and real parts have the same sign as these of $\kappa_{\rm m}$. We derived an asymptotic expansion [54]

$$\begin{aligned}
&\mathbf{E}^\varepsilon \approx \mathbf{E}^0, \qquad \text{in} \quad \mathcal{O}_{\rm c} \cup \mathcal{O}_{\rm e} \\
&\mathbf{E}^\varepsilon \approx \varepsilon^{-1} \mathbf{E}_{\rm m}^{-1}\left(\mathbf{x}_{\mathsf{T}}, \frac{x_3}{\varepsilon}\right) + \mathbf{E}_{\rm m}^0\left(\mathbf{x}_{\mathsf{T}}, \frac{x_3}{\varepsilon}\right), \qquad \text{for almost any} \quad (\mathbf{x}_{\mathsf{T}}, x_3) \in \Gamma \times (0, \varepsilon)\,.
\end{aligned}$$

Unlike the mid-frequency case, this expansion starts at the order $\varepsilon^{-1}$ in the thin layer. It has been found that at low frequency, the membrane influence appears at the zeroth order term, meaning that the membrane influence should not be neglected, namely the limit field $\mathbf{E}^0$ satisfies the problem

$$\operatorname{curl}\operatorname{curl}\mathbf{E}^0 - \kappa_{\rm e}^2 \mathbf{E}^0 = i\omega\mu_{\rm e}\mathbf{J}, \quad \text{in } \mathcal{O}_{\rm e}, \tag{A.6a}$$

$$\operatorname{curl}\operatorname{curl}\mathbf{E}^0 - \kappa_{\rm c}^2 \mathbf{E}^0 = 0, \quad \text{in } \mathcal{O}_{\rm c}, \tag{A.6b}$$

$$\operatorname{curl}\mathbf{E}^0 \times \mathbf{n} - i\kappa_{\rm e}\mathbf{n} \times \mathbf{E}^0 \times \mathbf{n} = 0, \quad \text{on } \partial\mathcal{O}, \tag{A.6c}$$

with the following transmission conditions set on $\Gamma$

$$\frac{1}{\mu_{\rm e}} \operatorname{curl}\mathbf{E}^0|_{\Gamma^+} \times \mathbf{n} = \frac{1}{\mu_{\rm c}} \operatorname{curl}\mathbf{E}^0|_{\Gamma^-} \times \mathbf{n}, \tag{A.6d}$$

$$\left[\mathbf{n} \times \mathbf{E}^0\right]_\Gamma = -\frac{\mu_{\rm m}}{\widetilde{\kappa}_{\rm m}^2} \mathbf{curl}_\Gamma \operatorname{curl}_\Gamma \left(\frac{1}{\mu_{\rm c}} \operatorname{curl}\mathbf{E}^0|_{\Gamma^-}\right)_{\mathsf{T}}. \tag{A.6e}$$

### A.2.4 GITC and Chun models

In the above sections A.2.2–A.2.3, we have chosen to write the condition on the boundary $\Gamma$ of the inner domain $\mathcal{O}_{\rm c}$ but this is an arbitrary convention. Sometimes it might be interesting to place the fictitious surface on which the transmission conditions hold between the boundary of the inner domain and the surface $\Gamma^\varepsilon$. Actually, for any $\beta \in [0,1]$ we can define the family of surfaces that are *parallel* to $\Gamma$ by

$$\Gamma_\beta = \{\mathbf{x}_{\mathsf{T}} + \beta\varepsilon\mathbf{n}(\mathbf{x}_{\mathsf{T}}), \quad \mathbf{x}_{\mathsf{T}} \in \Gamma\}\,.$$

In addition, in the definition of $\mathbf{S}$ and $\mathbf{T}$, the surface $\Gamma^-$ is involved but here again it is a convention, and a weighted average between $\Gamma^+$ and $\Gamma^-$ could have been chosen. In order to study numerically the influence of such conventions on the convergence rate, for any $\alpha \in [0,1]$, and for any vector field $\mathbf{v}$ defined in a neighborhood of $\Gamma_\beta$, let $\langle \mathbf{v}|_{\Gamma_\beta}\rangle_\alpha$ be defined by

$$\langle \mathbf{v}|_{\Gamma_\beta}\rangle_\alpha = \alpha\, \mathbf{v}|_{\Gamma^+_{2\beta}} + (1-\alpha)\, \mathbf{v}|_{\Gamma^-}.$$

### GITC model

Setting $\mathcal{O}_{\mathrm{e}}^{\beta} = \{\mathbf{x} \in \mathcal{O}_{\mathrm{e}} \mid \mathrm{dist}(\mathbf{x}, \Gamma) > 2\beta\varepsilon\}$ the field $\mathbf{E}_{[1]}^{\varepsilon}$ which approximates $\mathbf{E}^{\varepsilon}$ (at the order 2) is obtained by solving the problem :

$$\mathrm{curl}\,\mathrm{curl}\,\mathbf{E}_{[1]}^{\varepsilon} - \kappa_{\mathrm{e}}^2\mathbf{E}_{[1]}^{\varepsilon} = i\omega\mu_{\mathrm{e}}\mathbf{J}\ ,\ \text{in}\ \mathcal{O}_{\mathrm{e}}^{\beta}\ , \tag{A.7a}$$

$$\mathrm{curl}\,\mathrm{curl}\,\mathbf{E}_{[1]}^{\varepsilon} - \kappa_{\mathrm{c}}^2\mathbf{E}_{[1]}^{\varepsilon} = 0\ ,\ \text{in}\ \mathcal{O}_{\mathrm{c}}, \tag{A.7b}$$

$$\mathrm{curl}\,\mathbf{E}_{[1]}^{\varepsilon} \times \mathbf{n} - i\kappa_{\mathrm{e}}\,\mathbf{n} \times \mathbf{E}_{[1]}^{\varepsilon} \times \mathbf{n} = 0 \quad \text{on} \quad \partial\mathcal{O}, \tag{A.7c}$$

with the following transmission conditions, called generalized impedance transmission conditions (GITC) of order 2:

$$\left[\mathbf{n} \times \mathbf{E}_{[1]}^{\varepsilon}\right]_{\beta} = \varepsilon\left(-A_{\beta}\ \mathbf{curl}_{\Gamma_{\beta}}\,\mathrm{curl}_{\Gamma_{\beta}}\,\lambda\ +\ B_{\beta}\lambda\right) \tag{A.7d}$$

$$\left[\frac{\mathbf{n}}{\mu} \times \mathrm{curl}\,\mathbf{E}_{[1]}^{\varepsilon}\right]_{\beta} = \varepsilon\left(-C_{\beta}\ \mathbf{curl}_{\Gamma_{\beta}}\,\mathrm{curl}_{\Gamma_{\beta}}\left\langle(\mathbf{E}_{[1]}^{\varepsilon})_{\mathsf{T}}\right\rangle_{1-\alpha} +\ D_{\beta}\left\langle(\mathbf{E}_{[1]}^{\varepsilon})_{\mathsf{T}}\right\rangle_{1-\alpha}\right), \tag{A.7e}$$

(here $[\mathbf{v}]_{\beta} := \mathbf{v}|_{\Gamma_{2\beta}} - \mathbf{v}|_{\Gamma}$) with the additional unknown $\lambda$ defined as

$$\lambda = \left\langle \frac{1}{\mu}(\mathrm{curl}\,\mathbf{E}_{[1]}^{\varepsilon}|_{\Gamma_{\beta}})_{\mathsf{T}}\right\rangle_{\alpha},$$

and where constants $A_{\beta}, B_{\beta}, C_{\beta}, D_{\beta}$ are defined in (A.8)

$$A_{\beta} = \frac{\mu_{\mathrm{m}}}{\kappa_{\mathrm{m}}^2} - \beta\frac{\mu_{\mathrm{c}}}{\kappa_{\mathrm{c}}^2} - (1-\beta)\frac{\mu_{\mathrm{e}}}{\kappa_{\mathrm{e}}^2}, \qquad B_{\beta} = \mu_{\mathrm{m}} - \beta\mu_{\mathrm{c}} - (1-\beta)\mu_{\mathrm{e}}, \tag{A.8a}$$

$$C_{\beta} = \frac{1}{\mu_{\mathrm{m}}} - \frac{\beta}{\mu_{\mathrm{c}}} - \frac{1-\beta}{\mu_{\mathrm{e}}}, \qquad D_{\beta} = \frac{\kappa_{\mathrm{m}}^2}{\mu_{\mathrm{m}}} - \beta\frac{\kappa_{\mathrm{c}}^2}{\mu_{\mathrm{c}}} - (1-\beta)\frac{\kappa_{\mathrm{e}}^2}{\mu_{\mathrm{e}}}. \tag{A.8b}$$

### Link with the low-frequency case : Resistive model

From low to mid frequency, the GITC (A.7) provides an approximation of $\mathbf{E}^{\varepsilon}$. The order of approximation should be $O(\varepsilon)$ at low frequency (*i.e.* for $|\kappa_{\mathrm{m}}/\kappa_{\mathrm{e}}|^2 = O(\varepsilon)$ ) and $O(\varepsilon^2)$ at mid frequency, where $|\kappa_{\mathrm{m}}/\kappa_{\mathrm{e}}| \sim 1$. Note that in this case, (A.6) also falls into the above framework (A.7) by changing $A_{\beta}$, $B_{\beta}$, $C_{\beta}$ and $D_{\beta}$ into

$$A_{\beta}^{R} = \frac{1}{\varepsilon}\frac{\mu_{\mathrm{m}}}{\widetilde{\kappa}_{\mathrm{m}}^2}, \qquad B_{\beta}^{R} = C_{\beta}^{R} = D_{\beta}^{R} = 0.$$

### Chun model

Chun *et al.* have derived in [32] transmission conditions when the two boundaries $\Gamma, \Gamma^{\varepsilon}$ are not reduced to a single boundary. In this approach, the membrane is not meshed, and transmission conditions are set between $\Gamma$ and $\Gamma^{\varepsilon}$. When curvature terms are removed, the second/third order transmission conditions obtained are similar to the GITC

$$\mathbf{n} \times \mathbf{E}_{[1]}^{\varepsilon}|_{\Gamma^{\varepsilon}} - \mathbf{n} \times \mathbf{E}_{[1]}^{\varepsilon}|_{\Gamma} = \varepsilon\left(-A\ \mathbf{curl}_{\Gamma}\,\mathrm{curl}_{\Gamma}\,\lambda\ +\ B\lambda\right) \tag{A.9a}$$

$$\begin{aligned}\frac{\mathbf{n}}{\mu_{\mathrm{e}}} \times \mathrm{curl}\,\mathbf{E}_{[1]}^{\varepsilon}|_{\Gamma^{\varepsilon}} - \frac{\mathbf{n}}{\mu_{\mathrm{c}}} \times \mathrm{curl}\,\mathbf{E}_{[1]}^{\varepsilon}|_{\Gamma} = \varepsilon\Bigg(&-C\ \mathbf{curl}_{\Gamma}\,\mathrm{curl}_{\Gamma}\left\langle(\mathbf{E}_{[1]}^{\varepsilon})_{\mathsf{T}}\right\rangle_{1-\alpha} \\ &+\ D\left\langle(\mathbf{E}_{[1]}^{\varepsilon})_{\mathsf{T}}\right\rangle_{1-\alpha}\Bigg)\end{aligned} \tag{A.9b}$$

(the unknown $\lambda$ is defined now as $\lambda = \left\langle \frac{1}{\mu}(\mathrm{curl}\,\mathbf{E}^{\varepsilon}_{[1]}|_{\Gamma})_{\mathsf{T}} \right\rangle_{\alpha}$) where the constants are given by

$$A = \frac{\mu_{\mathrm{m}}}{\kappa_{\mathrm{m}}^2}, \quad B = \mu_{\mathrm{m}}, \quad C = \frac{1}{\mu_{\mathrm{m}}}, \quad D = \frac{\kappa_{\mathrm{m}}^2}{\mu_{\mathrm{m}}}. \tag{A.10a}$$

Fourth/fifth order transmission conditions are also derived in Chun *et al.*, involving higher-order operator. We have chosen to not consider these higher-order transmission in order to keep a comparison with only second/third order conditions.

## A.3 Numerical Simulations

### A.3.1 Numerical method and models

Weak formulations are discretized with five order curved hexahedral edge elements of the first kind [33]. The geometry is meshed with hexahedral elements. The following models are compared :

- **Symmetric model** (Problem (A.7) with $\beta = 0.5$) : this is the model obtained by Delourme *et al.* [46]. In this model, the membrane is replaced by the boundary $\Gamma_{1/2}$, which is the median boundary between $\Gamma$ and $\Gamma^{\varepsilon}$.
- **GITC model** (Problem (A.7) with $\beta = 0$) : this model is similar to the previous one, but the membrane is replaced by the boundary $\Gamma$ instead of $\Gamma_{1/2}$.
- **Resistive model** (Problem (A.6)) : this model is similar to a GITC model where coefficients $A_\beta, B_\beta, C_\beta, D_\beta$ are simplified, assuming that the frequency is small.
- $\mathbf{E}^0 + \varepsilon\mathbf{E}^1$ **model** (solving problems (A.2) and (A.3)) : this is the model proposed in [55], where $\mathbf{E}^0$ is computed, then $\mathbf{E}^1$ is computed with a right-hand-side depending on $\mathbf{E}^0$. Once $\mathbf{E}^0$ and $\mathbf{E}^1$ computed, the approximated solution is given as $\mathbf{E}^0 + \varepsilon\mathbf{E}^1$.
- **Chun model** (using conditions (A.9) with $\alpha = 0.5$) : this is the model obtained by Chun *et al.* [32]. In this model, the membrane is not meshed, and the two boundaries $\Gamma$, $\Gamma^{\varepsilon}$ are distinct.

Note that, as it can be seen, all the models are giving similar transmissions conditions (only expression of coefficients $A_\beta, B_\beta, C_\beta, D_\beta$ differ with respect to each position of the membrane): all these models can be seen as different way to derive the asymptotic expansion of the electromagnetic field solution to (A.1).

### A.3.2 Validation

The models are validated for the scattering of a sphere with the following parameters

$$\begin{aligned} \epsilon_m &= 3.5, \quad \mu_{\mathrm{m}} = 2.0, \quad \sigma_m = 0.05 \\ \epsilon_c &= 2.0, \quad \mu_{\mathrm{c}} = 1.5, \quad \sigma_c = 0.02 \\ \epsilon_{\mathrm{e}} &= 1.0, \quad \mu_{\mathrm{e}} = 1.0, \quad \sigma_e = 0.0 \end{aligned}$$

An objective was to see if choosing $\alpha = 0$ or $\alpha = 1$ is better than $\alpha = 0.5$. The source is imposed via a Silver-Müller condition ($\mathbf{J} = 0$). As it can be observed in Fig. A.2, the choice $\alpha = 0.5$ gives more accurate results than the other tested values of $\alpha$ for this model case. The GITC model and symmetric model both provide a convergence in $O(\varepsilon^2)$, the symmetric model being more

accurate than GITC for this case. Chun's model provides a convergence in $O(\varepsilon^3)$, and is the most accurate. Expected rates of convergence are numerically observed on this simple case, therefore these models are correctly implemented. We think that the symmetric model is more accurate than GITC model, because when

$$\epsilon_e = \epsilon_c, \quad \mu_e = \mu_c, \quad \sigma_e = \sigma_c,$$

the symmetric model provides a convergence in $O(\varepsilon^3)$. Since chosen values are not that far from satisfying those equalities, the symmetric model is more accurate.

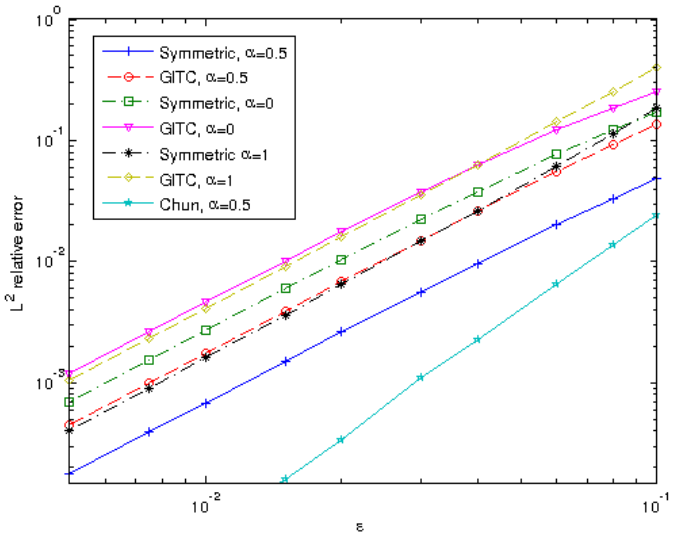


Figure A.2: Relative $L^2$ error versus thickness $\varepsilon$ for the symmetric model and GITC for different values of $\alpha$

### A.3.3 Electric parameters of biological cell

In this section, $\alpha$ will be taken equal to $0.5$ since this value gave the best results in the validation case. We study here the case of a biological cell, assumed to be a sphere whose radius is equal to $10$ $\mu$m with the following parameters

$$\begin{aligned} \epsilon_m &= 10.0, \quad \mu_{\mathrm{m}} = 1.0, \quad \sigma_m = 5.0e-7 \\ \epsilon_c &= 80.0, \quad \mu_{\mathrm{c}} = 1.0, \quad \sigma_c = 1.0 \\ \epsilon_{\mathrm{e}} &= 80.0, \quad \mu_{\mathrm{e}} = 1.0, \quad \sigma_e = 0.5 \end{aligned}$$

These parameters are close to the real parameters measured in biological cells. $\mu$ is identically equal to $1$, as a result $B_\beta$ and $C_\beta$ are equal to $0$ for all models except Chun's model. The conductivity of the membrane $\sigma_m$ is small compared to $\sigma_e, \sigma_c$. This fact also induces two regimes: a low-frequency regime where

$$\omega^2\epsilon_m + i\sigma_m\omega \text{ is much smaller than } \omega^2\epsilon_e + i\sigma_e\omega$$

and a high-frequency regime where these quantities are approximatively of the same order. The source is here a Gaussian distribution. The outer boundary is a sphere of radius $20$ $\mu$m. The radius of the membrane is taken equal to $10$ $\mu$m, the thickness of the membrane is taken equal to $0.01\mu$m.

To illustrate the difference between the two regimes (low-frequency and high-frequency), the exact solution is displayed along the axis Oz for two frequencies : 10 Mhz, 100 Mhz in Figure A.3. For a frequency equal to 100 Mhz, the solution is almost continuous, whereas for a frequency equal to 10 Mhz, the solution presents an important discontinuity through the membrane. This illustration shows that there are two asymptotic regimes with respect to $\varepsilon$, a high-frequency regime, which is the continuous solution (the term $\mathbf{E}^0$ (A.2) is dominant), and a low-frequency regime, which is computed by the resistive model (A.6). This last asymptotic is indeed discontinuous throughout the interface $\Gamma$. The symmetric model provides a solution that fits perfectly to the exact solution.

In Figure A.4, the different models are compared versus the frequency and the following regimes are observed:

- High-frequency regime (frequency above $10^{12}$Hz) : the $L^2$ error increases with the frequency because the wavelength decreases whereas the membrane thickness is constant. The error obtained with the $\mathbf{E}^0 + \varepsilon\mathbf{E}^1$ model and the resistive model are close, the resistive model being less accurate. The error obtained with the GITC model, symmetric and Chun's model is similar, the two last models being more accurate. The symmetric and Chun's model give the same error, because the error is here dominated by the numerical error (due to the discretization) and not by the model error.

- Mid-frequency regime (frequency between $10^8$Hz and $10^{12}$Hz) : the $L^2$ error of all the models, except the $\mathbf{E}^0 + \varepsilon\mathbf{E}^1$ model, is dominated by the numerical error. As a result, all the models are giving the same relative $L^2$ error, approximately $2 \cdot 10^{-4}$. This level can be decreased if the mesh is refined. In this regime, the $\mathbf{E}^0 + \varepsilon\mathbf{E}^1$ model gives an error which increases with the frequency, the error goes beyond 100 %. This behaviour can be seen as a locking phenomenon for the $\mathbf{E}^0 + \varepsilon\mathbf{E}^1$ model, since the constant of convergence is worsening when the frequency is decreasing, whereas the other models seem robust for small frequencies. In this regime, there is no particular advantage to use a model over another one (except the $\mathbf{E}^0 + \varepsilon\mathbf{E}^1$ model of course).

- Low-frequency regime (frequency below $10^8$Hz) : the $L^2$ error of all the models increases when the frequency decreases. This phenomenon stems from the fact that the numerical method is not robust for small frequencies. The finite element matrix also tends to a singular matrix. The numerical method is rather appropriate for mid-frequency cases than for low-frequency cases. It can be observed that Chun's model is more sensitive to this problem than other models.

In Figure A.5, the models are compared versus the thickness for a high-frequency case ($f = 5 \cdot 10^{12} Hz$. For this case, the symmetric model, Chun's model, $\mathbf{E}^0 + \varepsilon\mathbf{E}^1$ and GITC seem to produce a convergence in $O(\varepsilon^2)$, whereas the resistive model converges in $O(\varepsilon)$. The model $\mathbf{E}^0 + \varepsilon\mathbf{E}^1$ is also clearly less accurate than GITC.

## A.4 Conclusion and perspectives

To avoid the meshing of the thin membrane, five approximations of the electromagnetic field have been used, we have detailed the drawbacks and advantages of each model:

- **Symmetric model** (Problem (A.7) with $\beta = 0.5$). This model is accurate for all frequencies. However, the position of the median interface $\Gamma_{1/2}$ must be known, the position of this interface depends on $\varepsilon$, therefore a different mesh is needed for each value of $\varepsilon$.

- **GITC model** (Problem (A.7) with $\beta = 0$). This model is accurate for all frequencies, but less accurate than symmetric model or Chun's model. If the boundary of the cytoplasm $\Gamma$ is known, the transmission conditions are directly posed on this interface. There is no need to construct the boundary $\Gamma^\varepsilon$, therefore the same mesh can be used for different values of $\varepsilon$.

- **Resistive model** (Problem (A.6) ($\beta = 0$)). This model is accurate for the low-frequency case, but is inaccurate for high frequency. This model is the most simple to consider since $B_\beta = C_\beta = D_\beta = 0$.

- $\mathbf{E}^0 + \varepsilon\mathbf{E}^1$ **model** (solving problems (A.2) and (A.3)). This model provides a poor accuracy, with a locking phenomenon for the low-frequency case. In our opinion, this model should be avoided. However, it may be interesting if one wants to study the influence of the membrane thickness on the electric field by changing the value of $\varepsilon$ for mid-frequencies. Actually, the coefficients $\mathbf{E}^0$ and $\mathbf{E}^1$ do not depend on $\varepsilon$ and they have to be computed only once: the change of $\varepsilon$ appearing in the sum $\mathbf{E}_1^\varepsilon = \mathbf{E}^0 + \varepsilon\mathbf{E}^1$, whereas for other models, a change in the value of $\varepsilon$ makes it necessary to compute the electric field again.

- **Chun model** (using conditions (A.9) with $\alpha = 0.5$). This model is accurate for all frequencies. A first drawback is the necessity to mesh two distinct boundaries $\Gamma$ and $\Gamma^\varepsilon$. This last boundary depends on $\varepsilon$, therefore a different mesh is needed for each value of $\varepsilon$. Another drawback over other models is that the finite element matrix is non-symmetric (except for planar interfaces) due to the two separated boundaries.

The coefficients $A, B, C, D$ in Chun's model are always positive contrary to other models for which the positivity depends on the coefficients $\epsilon, \mu$ in the cytoplasm and the exterior. As a result, Chun's model is stable in the time-domain (as proved in [32]) whereas other models are generally not stable. In [46], a proposed solution to ensure positive coefficients for the symmetric model consists of separating the interface into two distinct boundaries with a distance equal to $\alpha\varepsilon$, and the coefficients are consequently modified and become positive for $\alpha$ large enough, giving stable transmission conditions in time-domain. In our opinion, time-domain simulations should prefer Chun's model, since it is always stable and accurate as well. Thus, a comparison of these approximations in time-domain should be the object of a future work.

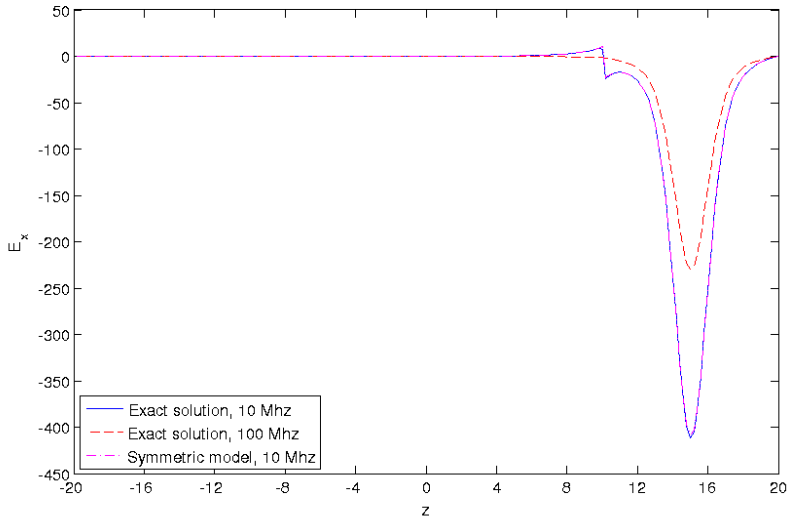


Figure A.3: Exact solution for the biological cell for a frequency equal to 10 and 100 Mhz, and solution obtained with the symmetric model. Real part of $E_x$.

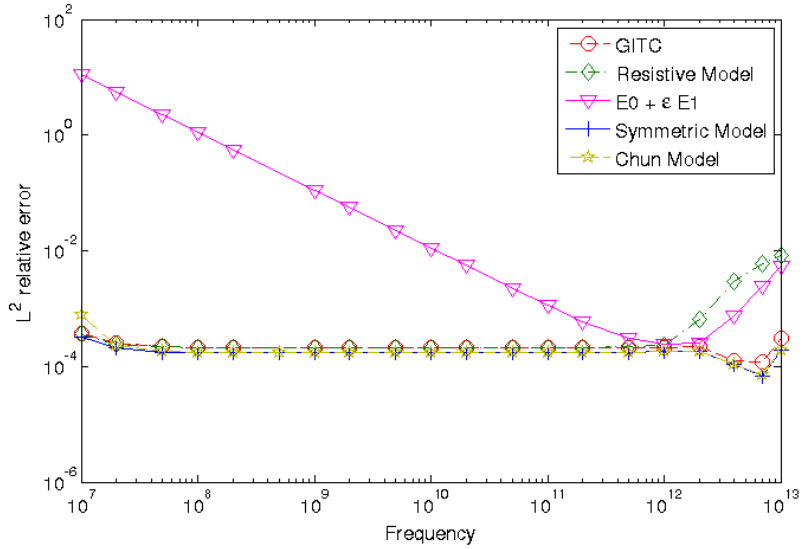


Figure A.4: Relative $L^2$ error of the different models versus the frequency (in Hz).

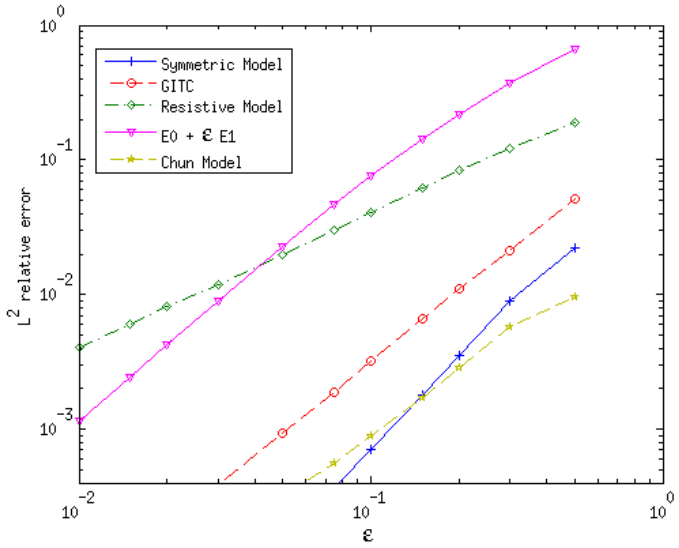


Figure A.5: Relative $L^2$ error of the different models versus the thickness (in $\mu m$). Frequency equal to 5 THz.

# Appendix B

# Asymptotic study for Stokes-Brinkman model with jump embedded transmission conditions

## B.1 Introduction

In [7] we address the problem of fluid flow modeling in complex media which combine porous regions and fluid regions with free flow. This issue holds for instance in the study of aquifer media made up of a porous media containing cracks and conduits (see [29]) and also the passive control of the flow around an obstacle covered by a porous thin layer (see [20]).

In this work the free flow satisfies the linear Stokes equation. In the porous media, one considers two models, the Brinkman and the Darcy models. There are several interface conditions in the literature. In the case of the Stokes-Brinkman coupling, the simpler interface condition is the continuity of the velocity and the normal stress. More accurate models are given by Ochoa-Tapia & Whitaker transmission conditions, by Beavers & Joseph conditions or Beaver, Joseph & Saffman conditions (see [29]). In this work, we deal with the more general jump embedded transmission conditions described in [6]. This condition links the jumps and the averages of both the velocity and the shear stress on the interface. A small parameter appears in this system, in particular the equivalent viscosity in the porous part is small, so that when this parameter tends to zero, we expect that the flow in the porous part will be described by the Darcy law. Our interest lies in the asymptotic study justifying the obtention of the limit model. In particular we describe the boundary layer due to the jump conditions appearing in the porous medium.

## B.2 The mathematical model

Let us describe the Stokes-Brinkman model with jump embedded transmission conditions. The problem is set in the domain $\Omega \subset \mathbb{R}^3$ made of a fluid region $\Omega_+$ and a porous subdomain $\Omega_-$. We assume that the domains $\Omega_-$ and $\Omega_+$ are Lipschitz and bounded, and that $\Omega_- \subset \overline{\Omega_-} \subset \Omega$. We denote $\Sigma = \partial\Omega_-$ so that we have $\Omega = \Omega_- \cup \Sigma \cup \Omega_+$ (see Figure B.2). We denote by $\mathbf{n}$ the outward unit normal at $\partial\Omega_-$. On the fluid region $\Omega_+$, the velocity $\mathsf{v}_\varepsilon^+$ and the pressure $\mathsf{p}_\varepsilon^+$ satisfy the Stokes equations. In the porous region $\Omega_-$, the velocity $\mathsf{v}_\varepsilon^-$ and the pressure $\mathsf{p}_\varepsilon^-$ satisfy a Brinkman model. We couple these models by transmission conditions at the common interface $\Sigma$ which link the jumps of the velocity and the normal stress vector with the averages of these quantities on $\Sigma$.

We denote by $\boldsymbol{\sigma}^+(\mathsf{v}_\varepsilon^+, \mathsf{p}_\varepsilon^+)$ (resp. $\boldsymbol{\sigma}^-(\mathsf{v}_\varepsilon^-, \mathsf{p}_\varepsilon^-)$) the stress tensor in the fluid (resp. in the

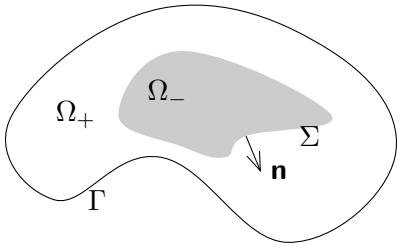


Figure 1 – The domain $\Omega$ and the subdomains $\Omega_-$, $\Omega_+$

porous) medium :

$$\boldsymbol{\sigma}^+(\mathsf{v}_\varepsilon^+, \mathsf{p}_\varepsilon^+) = 2\mu \mathbf{d}(\mathsf{v}_\varepsilon^+) - \mathsf{p}_\varepsilon^+ \mathbb{I}, \quad \boldsymbol{\sigma}^-(\mathsf{v}_\varepsilon^-, \mathsf{p}_\varepsilon^-) = 2\varepsilon \mathbf{d}(\mathsf{v}_\varepsilon^-) - \mathsf{p}_\varepsilon^- \mathbb{I},$$

with

- $\mathbf{d}(v) = \dfrac{1}{2}\Big(\nabla v + \nabla^\perp v\Big)$, that is $(\mathbf{d}(v))_{ij} = \dfrac{1}{2}\left(\mathbf{d}v^j x_i + \mathbf{d}v^i x_j\right)$,
- $\mu$ is the viscosity of the fluid and $\varepsilon$ is the effective viscosity in the porous medium.

The problem writes

$$\begin{cases} -\nabla \cdot \boldsymbol{\sigma}^-(\mathsf{v}_\varepsilon^-, \mathsf{p}_\varepsilon^-) + \kappa \mathsf{v}_\varepsilon^- = \mathsf{g}^- & \text{in} \quad \Omega_- \\ -\nabla \cdot \boldsymbol{\sigma}^+(\mathsf{v}_\varepsilon^+, \mathsf{p}_\varepsilon^+) = \mathsf{g}^+ & \text{in} \quad \Omega_+ \\ \nabla \cdot \mathsf{v}_\varepsilon^- = 0 & \text{in} \quad \Omega_- \\ \nabla \cdot \mathsf{v}_\varepsilon^+ = 0 & \text{in} \quad \Omega_+ \\ \boldsymbol{\sigma}^+(\mathsf{v}_\varepsilon^+, \mathsf{p}_\varepsilon^+) \cdot \mathbf{n} = \boldsymbol{\sigma}^-(\mathsf{v}_\varepsilon^-, \mathsf{p}_\varepsilon^-) \cdot \mathbf{n} + \boldsymbol{M}\{\mathsf{v}_\varepsilon\} + l & \text{on} \quad \Sigma \\ \{\boldsymbol{\sigma}(\mathsf{v}_\varepsilon, \mathsf{p}_\varepsilon) \cdot \mathbf{n}\} = \boldsymbol{S}(\mathsf{v}_\varepsilon^+ - v_\varepsilon^-) + \mathsf{h} & \text{on} \quad \Sigma \\ \mathsf{v}_\varepsilon = 0 & \text{on} \quad \Gamma \end{cases} \tag{B.1}$$

where $\kappa > 0$ is fixed positive constant and :

- The matrix $\boldsymbol{M}$ is zero on $\mathbf{n}^\perp$ and satisfies $\boldsymbol{M}\xi = \beta(\xi \cdot \mathbf{n})\mathbf{n}$ with $\beta > 0$.
- The matrix $\boldsymbol{S}$ satisfies $\boldsymbol{S}_{|\mathbf{n}^\perp} = \alpha \mathbb{I}_{|\mathbf{n}^\perp}$ and $\boldsymbol{S}(\mathbf{n}) = \dfrac{1}{\varepsilon}\mathbf{n}$:

$$\boldsymbol{S}(\xi) = \frac{1}{\varepsilon}(\mathbf{n} \cdot \xi)\mathbf{n} + \alpha(\xi - (\mathbf{n} \cdot \xi)\mathbf{n}), \quad \text{with} \quad \alpha > 0\,.$$

Note that using the divergence free conditions, we can replace the first equations in (B.1) by

$$-\varepsilon \Delta \mathsf{v}_\varepsilon^- + \nabla \mathsf{p}_\varepsilon^- + \kappa \mathsf{v}_\varepsilon^- = \mathsf{g}^- \quad \text{in} \quad \Omega_-$$

$$-\mu \Delta \mathsf{v}_\varepsilon^+ + \nabla \mathsf{p}_\varepsilon^+ = \mathsf{g}^+ \quad \text{in} \quad \Omega_+$$

## B.3 Statement of the main results

### B.3.1 Uniform estimates

Let us describe the associated variational formulation which is used to prove existence of weak solutions for (B.1). We introduce a weak formulation of the problem (B.1) for $\mathsf{v} = (\mathsf{v}^+, \mathsf{v}^-)$ in the space

$$V = \{\mathsf{u} \in \mathbf{L}^2(\Omega) \,|\, \mathsf{u}^\pm := \mathsf{u}_{|\Omega_\pm} \in \mathbf{H}^1(\Omega_\pm) \ \mathrm{div}\, \mathsf{u}^\pm = 0 \quad \text{in} \quad \Omega_\pm, \quad \mathsf{u}^+ = 0 \quad \text{on} \quad \Gamma\}\,,$$

endowed with the piecewise $\mathrm{H}^1$ norm. Such a variational formulation writes : Find $\mathsf{v} = (\mathsf{v}^-, \mathsf{v}^+) \in V$ such that

$$\forall \mathsf{u} \in V, \quad a_\varepsilon(\mathsf{v}, \mathsf{u}) = b(\mathsf{u}), \tag{B.2}$$

where

$$a_\varepsilon(\mathsf{v}, \mathsf{u}) := 2\varepsilon \int_{\Omega_-} \mathbf{d}(\mathsf{v}^-) : \mathbf{d}(\mathsf{u}^-)\, \mathrm{d}\mathbf{x} + \int_{\Omega_-} \kappa \mathsf{v}^- \cdot \mathsf{u}^-\, \mathrm{d}\mathbf{x} + 2\mu \int_{\Omega_+} \mathbf{d}(\mathsf{v}^+) : \mathbf{d}(\mathsf{u}^+)\, \mathrm{d}\mathbf{x}$$
$$+ < \beta\{\mathsf{v}\cdot\mathbf{n}\}, \{\mathsf{u}\cdot\mathbf{n}\} >_{-1/2,\Sigma} + < \alpha[\mathsf{v}_\tau], [\mathsf{u}_\tau] >_{-1/2,\Sigma} + \varepsilon^{-1} < [\mathsf{v}\cdot\mathbf{n}], [\mathsf{u}\cdot\mathbf{n}] >_{-1/2,\Sigma},$$

with $<,>_{-1/2,\Sigma}$ being a duality pairing between $\mathrm{H}^{-1/2}(\Sigma)^3$ and $\mathrm{H}^{1/2}(\Sigma)^3$, $[\mathsf{v}] = \mathsf{v}^+ - \mathsf{v}^-$ denoting the jump of $\mathsf{v}$ across $\Sigma$, and

$$b(\mathsf{u}) = \int_\Omega \mathsf{g}\cdot\mathsf{u}\, \mathrm{d}\mathbf{x} + < \mathsf{h}, [\mathsf{u}] >_{-1/2,\Sigma} + < l, \{\mathsf{u}\} >_{-1/2,\Sigma},$$

compare with [5, Th 1.1], [6, Th 2.1]. The duality pairing $<,>_{-1/2,\Sigma}$ between $\mathrm{H}^{-1/2}(\Sigma)^3$ and $\mathrm{H}^{1/2}(\Sigma)^3$ coincides with the duality pairing in $\mathrm{L}^2(\Sigma)^3$.

For $\varepsilon > 0$, one proves the existence and uniqueness of weak solution for (B.1) and we obtain uniform estimates of the solutions with respect to the parameter $\varepsilon$, [7].

**Theorem B.1** *Let $\mathsf{g}^\pm \in \mathbf{L}^2(\Omega_\pm)^3$ and $\mathsf{h}, l \in \mathrm{H}^{-\frac{1}{2}}(\Sigma)^3$. Then, the problem (B.2) has a unique solution $\mathsf{v} = \mathsf{v}_\varepsilon \in V$ for all $\varepsilon > 0$. Moreover, for $\varepsilon > 0$ small enough, the following uniform estimate holds :*

$$\varepsilon\|\mathbf{d}(\mathsf{v}^-)\|^2_{0,\Omega_-} + \frac{\kappa}{4}\|\mathsf{v}^-\|^2_{0,\Omega_-} + \frac{\mu C^2}{3}\|\mathsf{v}^+\|^2_{1,\Omega_+} + \frac{1}{4\varepsilon}\|[\mathsf{v}\cdot\mathbf{n}]\|^2_{0,\Sigma} + \frac{\alpha}{4}\|[\mathsf{v}]\|^2_{0,\Sigma} + \frac{\beta}{4}\|\{\mathsf{v}\cdot\mathbf{n}\}\|^2_{0,\Sigma}$$
$$\leqslant c\left(\|\mathsf{g}\|^2_{0,\Omega} + \|\mathsf{h}\|^2_{-\frac{1}{2},\Sigma} + \|l\|^2_{-\frac{1}{2},\Sigma}\right), \tag{B.3}$$

*with a constant $c = c(\mu, \kappa, \alpha, \beta)$.*

### B.3.2 A Wentzel-Kramers-Brillouin expansion

The asymptotic limit of the Stokes-Brinkman model towards the Stokes-Darcy one with Beavers-Joseph interface conditions is studied in [6, 29] in the case of a flat interface when the viscosity $\tilde{\mu}$ in the porous region is very small $\tilde{\mu} = \varepsilon \ll 1$ and when the jump of the normal velocities is penalized. We address in this work the problem of the convergence of the model (B.1) when the parameter $\varepsilon$ tends to zero and in the case of a smooth interface $\Sigma$. When $\varepsilon$ tends to zero,

we formally converge to the following Stokes Darcy problem with Beavers & Joseph interface conditions

$$\begin{cases} \nabla \mathsf{p}_0^- + \kappa \mathsf{v}_0^- = \mathsf{g}^- & \text{in} \quad \Omega_- \\ -\nabla \cdot \boldsymbol{\sigma}(\mathsf{v}_0^+, \mathsf{p}_0^+) = \mathsf{g}^+ & \text{in} \quad \Omega_+ \\ \nabla \cdot \mathsf{v}_0^- = 0 & \text{in} \quad \Omega_- \\ \nabla \cdot \mathsf{v}_0^+ = 0 & \text{in} \quad \Omega_+ \\ \boldsymbol{\sigma}(\mathsf{v}_0^+, \mathsf{p}_0^+) \cdot \mathbf{n} = -\mathsf{p}_0^- \mathbf{n} + \dfrac{\beta}{2} \left( (\mathsf{v}_0^+ + \mathsf{v}_0^-) \cdot \mathbf{n} \right) \mathbf{n} + \mathsf{l} & \text{on} \quad \Sigma \\ (\mathsf{v}_0^+ - \mathsf{v}_0^-) \cdot \mathbf{n} = 0 & \text{on} \quad \Sigma \\ \mathsf{v}_0^+ = 0 & \text{on} \quad \Gamma \,. \end{cases} \tag{B.4}$$

This problem is incompatible with the limit (as $\varepsilon$ tends to zero) of the tangential part of the interface condition $\{\boldsymbol{\sigma}(\mathsf{v}_\varepsilon, \mathsf{p}_\varepsilon) \cdot \mathbf{n}\} = \boldsymbol{S}(\mathsf{v}_\varepsilon^+ - v_\varepsilon^-) + \mathsf{h}$ on $\Sigma$ so that it appears a boundary layer inside the porous medium. We describe this boundary layer by an asymptotic expansion at any order with a WKB method. We exhibit series expansions in powers of $\sqrt{\varepsilon}$ for the flow $\mathsf{v}_\varepsilon$, and the pressure $\mathsf{p}_\varepsilon$ which are solutions of the transmission problem. In the fluid part,

$$\mathsf{v}_\varepsilon^+(x) \approx \sum_{j \geqslant 0} \varepsilon^{\frac{j}{2}} \mathrm{v}_j^+(x) \,, \quad \mathsf{p}_\varepsilon^+(x) \approx \sum_{j \geqslant 0} \varepsilon^{\frac{j}{2}} \mathrm{p}_j^+(x) \,. \tag{B.5}$$

In the porous part, we denote by $d : \Omega_- \to \mathbb{R}^+$ the euclidean distance to $\Sigma$, $d(x) = \mathrm{dist}(x, \Sigma)$. We describe the velocity and the pressure on the following way:

$$\mathsf{v}_\varepsilon^-(x) \approx \sum_{j \geqslant 0} \varepsilon^{\frac{j}{2}} \mathsf{v}_j^-(x, \frac{d(x)}{\sqrt{\varepsilon}}) \,, \quad \text{with} \quad \mathsf{v}_j^-(x, \mathsf{z}) = \mathrm{v}_j^-(x) + \widetilde{\mathrm{v}}_j^-(x, \mathsf{z}) \,, \tag{B.6}$$

$$\mathsf{p}_\varepsilon^-(x) \approx \sum_{j \geqslant 0} \varepsilon^{\frac{j}{2}} \mathsf{p}_j^-(x, \frac{d(x)}{\sqrt{\varepsilon}}) \,, \quad \text{with} \quad \mathsf{p}_j^-(x, \mathsf{z}) = \mathrm{p}_j^-(x) + \mathfrak{p}_j(x, \mathsf{z}) \,. \tag{B.7}$$

The terms $\widetilde{\mathrm{v}}_j^-$ and $\mathfrak{p}_j$ are boundary layer terms and defined on $\Sigma \times \mathbb{R}^+$. They are required to tend to $0$ (such as their derivatives) when $\mathsf{z} \to \infty$.

This expansion is justified rigorously by proving error estimates, [7, Th 7.1] :

**Theorem B.2** *Let* $\mathrm{k} \geq 5$. *We assume that the data in* (B.1) *satisfy hypothesis*

$$\mathsf{g}^- \in \mathbf{H}^{\mathrm{k}}(\Omega_-), \quad \mathsf{g}^+ \in \mathbf{H}^{\mathrm{k}-1}(\Omega_+), \quad \mathsf{l} \in \mathbf{H}^{\mathrm{k}-\frac{1}{2}}(\Sigma) \quad \textit{and} \quad \mathsf{h} \in \mathbf{H}^{\mathrm{k}-\frac{1}{2}}(\Sigma).$$

*We fix* $k = \mathrm{k} - 2$. *Let* $\mathrm{v}_j^+$, $\mathrm{v}_j^-$, $\widetilde{\mathrm{v}}_j^-$, $\mathrm{p}_j^+$, $\mathrm{p}_j^-$ *and* $\mathfrak{p}_j$,$j \in \{0, \ldots, \mathrm{k}-1\}$ *given by [7, Prop. 5.2].We define* $(\mathsf{r}_{k,\varepsilon}^\pm, \mathsf{q}_{k,\varepsilon}^\pm)$ *by removing to the solution* $(\mathsf{v}_\varepsilon, \mathsf{p}_\varepsilon)$ *of* (B.1) *the truncated expansion up to the*

*order* $\varepsilon^{\frac{k}{2}}$ *:*

$$\mathsf{r}^+_{k,\varepsilon}(x) = v^+_\varepsilon(x) - \sum_{j=0}^{k} \varepsilon^{\frac{j}{2}} \mathrm{v}^+_j(x)\,, \tag{B.8}$$

$$\mathsf{r}^-_{k,\varepsilon}(x) = v^-_\varepsilon(x) - \sum_{j=0}^{k} \varepsilon^{\frac{j}{2}} \left( \mathrm{v}^-_j(x) + \mathfrak{v}_j(x, \frac{d(x)}{\sqrt{\varepsilon}}) \right), \tag{B.9}$$

$$\mathsf{q}^+_{k,\varepsilon}(x) = \mathsf{p}^+_\varepsilon(x) - \sum_{j=0}^{k} \varepsilon^{\frac{j}{2}} \mathsf{p}^+_j(x)\,, \tag{B.10}$$

$$\mathsf{q}^-_{k,\varepsilon}(x) = \mathsf{p}^-_\varepsilon(x) - \sum_{j=0}^{k} \varepsilon^{\frac{j}{2}} \left( \mathrm{p}^-_j(x) + \mathfrak{p}_j(x, \frac{d(x)}{\sqrt{\varepsilon}}) \right). \tag{B.11}$$

*We have the following estimate :*

$$\varepsilon \|\nabla \mathsf{r}^-_{k,\varepsilon}\|^2_{0,\Omega_-} + \frac{\kappa}{4} \|\mathsf{r}^-_{k,\varepsilon}\|^2_{0,\Omega_-} + \frac{\mu C^2}{3} \|\mathsf{r}^+_{k,\varepsilon}\|^2_{1,\Omega_+} \leqslant C \varepsilon^{\frac{k-2}{2}}.$$

An immediate corollary of our asymptotic expansion is the following convergence theorem:

**Theorem B.3** *We assume that the data in* (B.1) *satisfy:*

$$\mathsf{g}^- \in \mathbf{H}^5(\Omega_-), \quad \mathsf{g}^+ \in \mathbf{H}^4(\Omega_+), \quad \mathsf{l} \in \mathbf{H}^{\frac{9}{2}}(\Sigma) \quad \textit{and} \quad \mathsf{h} \in \mathbf{H}^{\frac{9}{2}}(\Sigma).$$

*Then, the solution* $\mathsf{v}_\varepsilon$ *for* (B.1) *given by Theorem B.1 satisfies:*

$$\mathsf{v}^+_\varepsilon(x) = \mathsf{v}^+_0(x) + \mathsf{r}^+_\varepsilon(x) \qquad \textit{for } x \in \Omega_+$$

$$\mathsf{v}^-_\varepsilon(x) = \mathsf{v}^-_0(x) + \widetilde{\mathrm{v}}^-_0(x, \tfrac{d(x)}{\sqrt{\varepsilon}}) + \mathsf{r}^-_\varepsilon(x) \qquad \textit{for } x \in \Omega_-$$

*where*

- $\mathsf{v}_0$ *is the solution of* (B.4)*,*
- $\widetilde{\mathrm{v}}^-_0$ *is a boundary layer term of the form* $\widetilde{\mathrm{v}}^-_0(x, \mathsf{z}) = \mathsf{w}_0(x) \exp(-\sqrt{\kappa}\mathsf{z})$*,*
- $d(x)$ *is the euclidean distance to* $\Sigma$*,*
- $\mathsf{r}_\varepsilon$ *is a remainder terms.*

*This remainder term satisfies the following estimate:*

$$\varepsilon \|\mathbf{d}(\mathsf{r}^-_\varepsilon)\|^2_{0,\Omega_-} + \frac{\kappa}{4} \|\mathsf{r}^-_\varepsilon\|^2_{0,\Omega_-} + \frac{\mu C^2}{3} \|\mathsf{r}^+_\varepsilon\|^2_{1,\Omega_+} \leqslant C \varepsilon^{\frac{1}{2}}.$$

The concept of WKB expansion is rather classical in the modeling of problems arising in fluid mechanics. For instance in [26, 24, 25] the authors derive WKB expansions with boundary layer terms or thin layer asymptotics to describe penalization methods in the context of viscous incompressible flow.

One difficulty to validate the WKB expansion lies in the proof of existence and regularity results for one part of the asymptotics which appear in this expansion at any order and which solve Darcy-Stokes problems with non-standard transmission conditions [7, Prop 6.4].

**Proposition B.4** *Let $k \geq 1$. We assume that $g^+ \in \mathbf{H}^{k-1}(\Omega_+)$, $g^- \in \mathbf{H}^k(\Omega_-)$, and $l \in H^{k-\frac{1}{2}}(\Sigma)$. Then the solution of the problem* (B.12)

$$\begin{cases} \kappa \mathrm{v}^- + \nabla \mathrm{p}^- = g^- & \text{in} \quad \Omega_- \\ \nabla \cdot \mathrm{v}^- = 0 & \text{in} \quad \Omega_- \\ -\nabla \cdot \boldsymbol{\sigma}^+(\mathrm{v}^+, \mathrm{p}^+) = g^+ & \text{in} \quad \Omega_+ \\ \nabla \cdot \mathrm{v}^+ = 0 & \text{in} \quad \Omega_+ \\ \boldsymbol{\sigma}^+(\mathrm{v}^+, \mathrm{p}^+) \cdot \mathbf{n} = l - \mathrm{p}^- \mathbf{n} + \frac{\beta}{2}((\mathrm{v}^+ + \mathrm{v}^-) \cdot \mathbf{n})\mathbf{n} & \text{on} \quad \Sigma \\ (\mathrm{v}^+ - \mathrm{v}^-) \cdot \mathbf{n} = 0 & \text{on} \quad \Sigma \\ \mathrm{v}^+ = 0 & \text{on} \quad \Gamma \end{cases} \tag{B.12}$$

*satisfies* $\mathrm{v}^+ \in \mathbf{H}^{k+1}(\Omega_+)$, $\mathrm{v}^- \in \mathbf{H}^k(\Omega_-)$, $\mathrm{p}^+ \in \mathrm{H}^k(\Omega_+)$ *and* $\mathrm{p}^- \in \mathrm{H}^{k+1}(\Omega_-)$.

It is possible to tackle these problems by carefully introducing a Dirichlet–to–Neumann operator which lead us to prove well-posedness results and elliptic regularity results simply for the Stokes operator with mixed boundary conditions.

## B.4 Perspectives

A next issue to tackle is the case where the inertial forces are not neglected which leads to solve Navier-Stokes equations in the fluid region. A preliminary work has to be concerned with the modeling of non-linear interface conditions between the fluid and porous regions.

# Appendix C

# Spectral methods and polynomial solutions for singular integral equations

## C.1 Introduction

Two-dimensional boundary-value problems involving a Neumann-type boundary condition on a thin plate or crack can often be reduced to one-dimensional hypersingular integral equations. Examples are potential flow past a rigid plate, acoustic scattering by a hard strip, water-wave interaction with thin impermeable barriers [119], and stress fields around cracks [103]; for many additional references, see [108] and [104, §6.7.1]. Collocation methods and Galerkin methods have been used by many authors to solve these equations, and they are known to be very effective. Convergence results are also available; see, for example, [70, 61] and [71, §7.9].

In [65], some of these results are generalized to *two-dimensional* hypersingular integral equations. Thus, rather than integrating over a finite interval, we now integrate over a circular disc. Such equations arise, for example, in the scattering of acoustic waves by a hard disc. We develop a spectral method, using Fourier expansions in the azimuthal direction and Jacobi polynomials in the radial direction. The method is proved to be convergent. Then, Tranter's method is discussed. This method was devised in the 1950s to solve certain pairs of dual integral equations. It is shown that this method is also convergent because it leads to the same algebraic system as the spectral method. Both methods have been used in the literature to generate numerical results for a variety of physical problems involving discs. For the spectral method, see [92, 64, 157, 66] and [17, §5.2]. For Tranter's method, see [156, 43, 143] and [49, p. 251]. We illustrate the convergence of the spectral method with numerical results for an axisymmetric problem. In order to have a concrete example, we have given a study of acoustic scattering by a thin sound-hard screen.

Several works deal with the airfoil equation over an interval and its generalizations, see e.g. [112, 149, 150, 152]. In its original form, this equation can be written as

$$\frac{1}{\pi}\int_{-1}^{1}\frac{f(t)}{x-t}\mathrm{d}t = g(x)\,, \quad x\in(-1,1)\,, \tag{C.1}$$

and it models the flow over an infinitely thin airfoil without viscosity and in the bidimensional case [19]. Here $f$ is the local circulation density and it can be shown to be equal to the difference in induced velocity over the upper and lower side of the airfoil. The right-hand side $g$ is given by the product of $2\pi$, the onset velocity and the slope of airfoil which in case of a flat plate is nothing but the product of $2\pi$, the onset velocity and the angle of incidence. The case when $g$ is an odd function includes for instance an airfoil with zero angle of incidence and parabolic camber distribution. Applications in elasticity and surface wave scattering are also described by

this equation [100].

In [63], we consider the airfoil equation over close disjoint intervals (C.17). Approximate solutions are derived. Quasi-polynomial solutions for the approximate models are found. As an application, a spectral method is developed to solve a generalized airfoil equation set on close disjoint intervals.

## C.2 Hypersingular integral equations over a disc

Let $x$ and $y$ be Cartesian coordinates. Let $r$ and $\theta$ be polar coordinates, so that $x = r\cos\theta$ and $y = r\sin\theta$. The unit disc is

$$D = \{(r,\theta) : 0 \le r < 1, \ \ -\pi < \theta \le \pi\}.$$

Then, we consider the following hypersingular integral equation

$$\frac{1}{4\pi} \, \text{⨍}\!\!\!\!\!\!-_D \frac{w(\rho)}{R^3} \, u(\rho,\varphi) \, dA + \int_D K(\rho,\varphi;r,\theta) \, u(\rho,\varphi) \, w(\rho) \, dA = f(r,\theta), \tag{C.2}$$

for $(r,\theta) \in D$, where $dA = \rho \, d\rho \, d\varphi$. Here, $u$ is to be found, $f$ is known, $K(\rho,\varphi;r,\theta)$ is a known weakly-singular kernel, and,

$$w(\rho) = \sqrt{1-\rho^2}. \tag{C.3}$$

Also, $R$ is the distance between two points, $(r,\theta)$ and $(\rho,\varphi)$, on the disc,

$$R = \sqrt{r^2 + \rho^2 - 2r\rho\cos(\theta-\varphi)}.$$

### C.2.1 The spectral method

We look for approximate solutions of (C.2), $u_N \in V_N$ where the space $V_N$ is defined as

$$V_N = \text{span}\{\Psi_m^{n\sigma}, \quad m = 0,1,\ldots,N_1, \ n = 0,1,\ldots,N_2, \ \sigma = \text{e},\text{o}\},$$

and $N$ is the dimension of $V_N$. Here, we define functions $\Psi_m^{n\sigma}$ over the unit disc $D$ by

$$\Psi_m^{n\sigma}(r,\theta) = A_m^n \frac{\Phi_m^n(r)}{w(r)} E_n^\sigma(\theta). \tag{C.4}$$

In the radial direction, we expand using orthogonal polynomials :

$$\Phi_m^n(\rho) = c_m \rho^n w(\rho) \, P_m^{(n,1/2)}(1-2\rho^2), \quad \text{with} \quad c_m = \frac{m!}{\Gamma(m+\frac{3}{2})}. \tag{C.5}$$

Here $P_n^{(\alpha,\beta)}$ is a Jacobi polynomial [116, §18.3]. In the azimuthal direction, we expand using orthogonal functions $E_m^\sigma(\theta)$ as follows: $E_0^{\text{e}} = 1$, $E_0^{\text{o}} = 0$, $E_m^{\text{e}}(\theta) = \sqrt{2}\cos m\theta$, $E_m^{\text{o}}(\theta) = \sqrt{2}\sin m\theta$, $m = 0,1,2,\ldots$

Then $u_N$ can be expressed as a linear combination of functions $\Psi_m^{n\sigma}$. For brevity, we write

$$u_N = \sum_{m,n,\sigma}^{N} a_m^{n\sigma} \Psi_m^{n\sigma} \equiv \sum_{m=0}^{N_1} \sum_{n=0}^{N_2} \sum_{\sigma=\text{e},\text{o}} a_m^{n\sigma} \Psi_m^{n\sigma}. \tag{C.6}$$

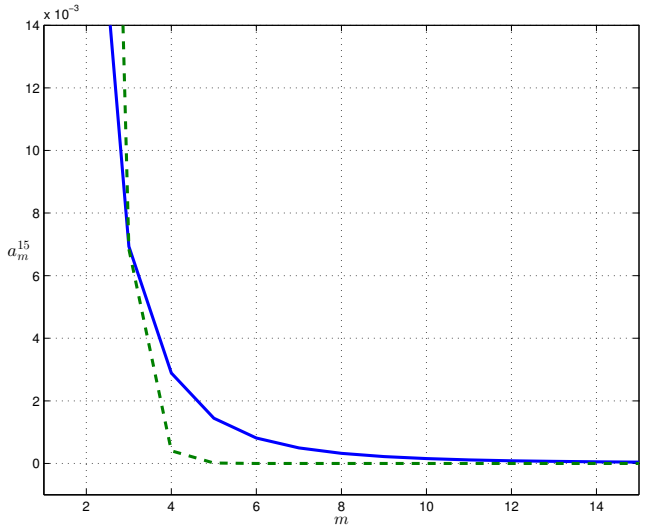


Figure C.1: The coefficients $a_m^{15}$ for the case $f(r) = r$, $Q(r) = J_4(2r)$ (solid line) and for $f = J_0$, $Q(r) = J_2(4r)$ (dashed line).

Then, the spectral method for solving (C.2) consists of solving equation (C.7)

$$\mathcal{C}_l^k a_l^{k\nu} + \sum_{m,n,\sigma}^{N} \langle K\Psi_m^{n\sigma}, \Psi_l^{k\nu}\rangle a_m^{n\sigma} = \langle f, \Psi_l^{k\nu}\rangle, \qquad \begin{matrix} l = 0, 1, \ldots, N_1, \\ k = 0, 1, \ldots, N_2, \\ \nu = \mathrm{e}, \mathrm{o}, \end{matrix} \tag{C.7}$$

where $\mathcal{C}_m^n = -1/(c_m c_n)$. We show that this method converges in mean [65].

### C.2.2 A numerical example

The spectral method can be readily implemented. For a specific example, we apply it to a simple but non-trivial axisymmetric problem, with a symmetric separable kernel. Thus

$$K(\rho, \varphi; r, \theta) = Q(\rho)Q(r) \quad \text{and} \quad f(r, \theta) = f_0(r)$$

for some functions $Q$ and $f_0$. Then, there is just one non-trivial system to solve,

$$\mathcal{C}_l^0 a_l^N + (2\pi)^2 A_l^0 \sum_{m=0}^{N} I_{ml}^0 A_m^0 a_m^N = \langle f, \Psi_l^{0\mathrm{e}}\rangle, \quad l = 0, 1, \ldots, N, \tag{C.8}$$

where $N = N_1$ and we have written $a_m^N \equiv a_m^{0\mathrm{e}}$ to emphasize the dependence on $N$.

An analytical solution and convergence results are given for the case of $Q = J_0$ and $f = J_0$, in [65]. We solved numerically (C.8) for different choices of $f$ (the right-hand side) and $Q$ (the function determining the kernel $K$), it is seen that each sequence $(a_m^N)_m$ (for $N = 5, 10, 30$) decays to zero very rapidly and the stability and fast convergence of the spectral method are apparent. The same characteristics are observed for other choices of $f$ and $Q$. For instance, for $f(r) = Q(r) = J_0(4r)$. In Figure C.1, we can see, graphically, the decay of $a_m^{15}$ for other cases involving Bessel functions.

### C.2.3 Connection with Tranter's method

Boundary value problems that lead to the hypersingular integral equation (C.2) can often be treated by reduction to a pair of dual integral equations for an auxiliary function $B$. These equa-

tions have the form

$$\frac{1}{4\pi^2}\iint \kappa(1+h(\kappa))B\,e^{-i(\xi x+\eta y)}\,d\xi\,d\eta = g(x,y), \qquad (x,y)\in D, \tag{C.9}$$

$$\iint B\,e^{-i(\xi x+\eta y)}\,d\xi\,d\eta = 0, \qquad (x,y)\in D', \tag{C.10}$$

where $D$ is the unit disc in the $xy$-plane and $D'$ is the rest of that plane. The double integrals are over the whole $\xi\eta$-plane, $\kappa=\sqrt{\xi^2+\eta^2}$ and $h(\kappa)$ is a given function satisfying $h(\kappa)\to 0$ as $\kappa\to\infty$.

Expand $B$ and $g$ in Fourier series,

$$B(\xi,\eta) = 2\pi\sum_{n,\sigma} i^n\,B_n^\sigma(\kappa)E_n^\sigma(\beta), \quad g(x,y)=\sum_{n,\sigma} g_n^\sigma(r)E_n^\sigma(\theta),$$

where we have introduced polar coordinates, defined by

$$x=r\cos\theta, \quad y=r\sin\theta, \quad \xi=\kappa\cos\beta, \quad \eta=\kappa\sin\beta. \tag{C.11}$$

The result is

$$\int_0^\infty B_n^\sigma(\kappa)J_n(\kappa r)(1+h(\kappa))\kappa^2\,d\kappa = g_n^\sigma(r), \qquad 0\le r<1, \tag{C.12}$$

$$\int_0^\infty B_n^\sigma(\kappa)J_n(\kappa r)\kappa\,d\kappa = 0, \qquad r>1, \tag{C.13}$$

with separate pairs of dual integral equations for each pair, $n$ and $\sigma$. In connection with Tranter's method [148], write

$$B_n^\sigma(\kappa) = \kappa^{-3/2}\sum_{m=0}^\infty \alpha_m^{n\sigma}J_{n+2m+\mu}(\kappa), \tag{C.14}$$

we find that the coefficients $\alpha_m^{n\sigma}$ solve the system

$$\frac{\alpha_l^{n\sigma}}{2n+4l+3}+\frac{2}{\pi}\sum_{m=0}^\infty \alpha_m^{n\sigma}\int_0^\infty h(\kappa)j_{n+2m+1}(\kappa)j_{n+2l+1}(\kappa)\,d\kappa = \frac{1}{\sqrt{2}}\int_0^1 \Phi_l^n(r)g_n^\sigma(r)\,dr.$$

We have shown that the spectral method lead to the same system when the kernel $K(\rho,\varphi;r,\theta)$ is an even function of $\varphi-\theta$. We deduce that truncated forms of Tranter's method are convergent.

### C.2.4 An example: acoustic scattering by a hard screen

Consider a flat, sound-hard screen, $\Omega$, in the plane $z=0$. There is an incident field, $u_{\rm in}$, and the problem is to compute the scattered field, $u$. Thus, we seek a bounded solution of $(\nabla^2+k^2)u=0$, satisfying the Sommerfeld radiation condition at infinity and the boundary condition

$$\frac{\partial u}{\partial z} = g_{\rm in} \quad \text{on both sides of } \Omega, \tag{C.15}$$

where $g_{\rm in}(x,y) = -\partial u_{\rm in}/\partial z$ evaluated at $z=0$. It can be shown that the solution must be an odd function of $z$, so the problem can be reduced to one in the half-space $z>0$.

Let

$$v(x,y) = u(x,y,0+) - u(x,y,0-);$$

this gives the discontinuity in $u$ across the plane $z = 0$. Using Fourier transforms we derive the hypersingular integral equation

$$\frac{1}{4\pi} \not\int_\Omega \frac{v}{R^3}\, dA' + \int_\Omega \mathcal{K}(x-x', y-y') v(x', y')\, dA' = g_{\text{in}}(x, y), \quad (x, y) \in \Omega$$

where

$$\mathcal{K}(x-x', y-y') = \frac{1}{4\pi} \int_0^\infty \kappa(\kappa - \gamma) J_0(\kappa R)\, d\kappa, \quad \gamma = (\kappa^2 - k^2)^{1/2}. \tag{C.16}$$

## C.3 The airfoil equation on near disjoint intervals

In [63], we consider the airfoil equation with a Cauchy type of singularity and set in close disjoint intervals (C.17); that is, in two intervals with a small aperture of size $2\varepsilon > 0$ :

$$\frac{1}{\pi} \int_{-1}^{-\varepsilon} \frac{f_\varepsilon(t)}{x-t} \mathrm{d}t + \frac{1}{\pi} \int_{\varepsilon}^{1} \frac{f_\varepsilon(t)}{x-t} \mathrm{d}t = -\psi(x)\,, \quad x \in G_\varepsilon = (-1, -\varepsilon) \cup (\varepsilon, 1)\,. \tag{C.17}$$

We assume that $\psi$ is Hölder continuous on $G_\varepsilon$. Tricomi [149] derived analytical solutions for the airfoil equation set in two disjoint intervals. Dutta and Banerjea [57] presented this solution in a slightly different form and have used it to deduce a solution of the associated hypersingular integral equation.

### C.3.1 Approximate models and polynomial solutions

The limit of $f_\varepsilon$ as $\varepsilon$ tends to zero has been identified. Under a condition of domination the null-circulation solution of the airfoil equation (C.17) satisfies the pointwise convergence result when $\varepsilon \to 0$ :

$$f_\varepsilon(x) \longrightarrow f_0(x) \quad \text{for all} \quad x \in G_\varepsilon\,. \tag{C.18}$$

Here, the function $f_0$ is defined as

$$f_0(x) = \frac{1}{\pi x \sqrt{1-x^2}} \Psi_0(x) \quad \text{for all} \quad x \in G_0 = (-1, 1) \setminus \{0\}\,, \tag{C.19}$$

and $\Psi_0$ is defined as a Cauchy type singular integral

$$\Psi_0(x) = \int_{-1}^{1} \frac{\sqrt{1-t^2}}{x-t} t\psi(t)\, \mathrm{d}t\,. \tag{C.20}$$

The formal limit $f_0$ and the solution of the airfoil equation (C.1) (with $g = -\psi$) are compared :

$$f(x) = f_0(x) + \frac{1}{x}\frac{1}{\pi} \int_{-1}^{1} \sqrt{\frac{1-t^2}{1-x^2}} \psi(t)\, \mathrm{d}t \quad \text{for all} \quad x \in G_0\,. \tag{C.21}$$

Hence, $f$ coincides with $f_0$ when $\psi$ is an odd function or for an infinite set of Chebyshev polynomials (see e.g. [102]). Then the first two terms of an expansion in power series of $\varepsilon$ are obtained for particular analytical solutions $f_\varepsilon$ when $\psi = T_n$ is a Chebyshev polynomial of the first kind :

$$f_\varepsilon \approx f_0 + \varepsilon^2 f_2 \quad \text{when} \quad \varepsilon \to 0\,, \tag{C.22}$$

and convergence results in weighted Sobolev spaces are proved. We illustrate numerically convergence results of $f_\varepsilon$ towards $f_0$ in $\mathcal{O}(\varepsilon^2)$, Figure C.2.

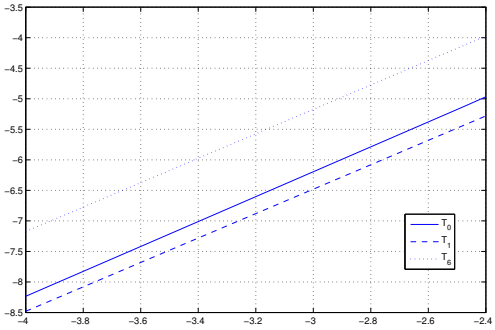


Figure C.2: $\log \|f_\varepsilon - f_0\|_{\mathrm{L}^2_{w_0}}$ plotted against $\log \varepsilon$; $\psi \in \{T_0, T_1, T_6\}$ and $w_0(x) := |x|^{11/2}\sqrt{1-x^2}$

Polynomial solutions for the Cauchy type singular integral (C.19) are found

$$\frac{1}{\pi x\sqrt{1-x^2}} \int_{-1}^{1} \frac{\sqrt{1-t^2}}{x-t} t\psi(t)\,\mathrm{d}t = f_0(x) \quad \text{for all} \quad x \in (-1,1)\setminus\{0\}\,. \tag{C.23}$$

Setting ($U_n$ are Chebyshev polynomials of the second kinds)

$$\psi(x) = x^{-1}U_n(x) \tag{C.24}$$

for all $x \in (-1,1)$ (and $x \neq 0$ when $n$ is even) in (C.23), there holds

$$f_0(x) = \frac{1}{x\sqrt{1-x^2}} T_{n+1}(x). \tag{C.25}$$

### C.3.2 A spectral method for a generalized airfoil equation in close disjoint intervals

Given the results represented above a spectral method for the generalized equation in close disjoint intervals is proposed

$$\frac{1}{\pi}\int_{G_\varepsilon} \left\{\frac{1}{x-t} + K(x,t)\right\} f_\varepsilon(t)\, w(t)\mathrm{d}t = h(x)\,, \quad x \in G_\varepsilon, \tag{C.26}$$

where $K$ is a known regular kernel and $w(t) = \frac{1}{t\sqrt{1-t^2}}$. Expand the solution $f_\varepsilon$ as

$$f_\varepsilon = \sum_{n=0}^{N} a_n T_{n+1}. \tag{C.27}$$

Substituting in (C.26) and using polynomial solutions

$$\sum_{n=0}^{N} a_n[-x^{-1}U_n(x) + \mathcal{K}T_{n+1}(x)] = \psi(x), \tag{C.28}$$

where $\mathcal{K}$ is the integral operator given by

$$\mathcal{K}g(x) = \frac{1}{\pi}\int_{G_\varepsilon} K(x,t)g(t)\, w(t)\mathrm{d}t.$$

Equation (C.28) can be solved by a Galerkin or collocation method.

## C.4 Conclusion and perspectives

We have shown that two apparently different numerical methods are convergent. The first is a spectral method for solving two-dimensional hypersingular integral equations over a disc. The unknown function is expanded in a tensor-product manner, with trigonometric functions of the angular variable and orthogonal polynomials in the radial variable. The Hilbert-space arguments used by Golberg are generalized and a convergence theorem is proved by using tensor-product techniques. Our results are proved in weighted $L^2$ spaces. It may be possible to obtain results in other spaces, but we have not pursued this. For some results in this direction, see [120]. There is also work by Stephan and his collaborators on Galerkin boundary element methods for hypersingular integral equations over open flat domains; see, for example, [78].

The second method, Tranter's method, is older and arises when the underlying boundary value problem is reduced to dual integral equations instead of a hypersingular integral equation. In this method, a different unknown function is expanded in a series of Bessel functions of various orders (a Neumann series). Although the two methods appear to be unrelated, they are not: they both lead to the same linear algebraic system.

The observed convergence accords with our theoretical analysis. It would be useful to estimate the rate of convergence, but we have not done that yet. Extensions to systems of integral equations may also be feasible; certainly, there are relevant numerical results in the literature obtained using variants of the spectral method [92, 17] and of Tranter's method [44, 43, 143, 145]. Again, numerical convergence has been observed but the algorithms have not been analysed.

# Summary

We develop asymptotic methods to solve problems arising in the context of acoustic, elastic or electromagnetic wave propagation phenomena and which involve small parameters (boundary layer problems, thin-layer problems, problems with small defects). Such phenomena are eventually described with multi-scale expansions and asymptotic models. Reduced models have been implemented in Finite Element codes in order to analyse numerically their properties. Several works are presented in a first part which is divided into two chapters. The first chapter is devoted to thin-layer transmission problems in acoustic and elastic media. This work enters into the scope of the HPC GA project (High Performance Computing for Geophysics Applications). The second chapter concerns transmission problems of electromagnetic waves across thin layers with high conductivities. This part is complemented with an asymptotic study on the accuracy of different approximations of the electromagnetic field for thin-layer transmission problems, Appendix A. In the context of fluid flow modeling in complex media combining porous and fluid regions with free flow and a high contrast of viscosities, we develop a WKB expansion to solve a singular perturbation problem, Appendix B.

Corner and edge singularities on interfaces may increase the level of difficulty in the analysis of elliptic problems in comparison with smooth interfaces. We develop asymptotic technics to determine corner and edge asymptotics in elliptic systems for several applications in electromagnetism and in elasticity. Eddy current problems have been addressed in the presence of a corner singularity on an interface (dielectric/conductor) and crack problems have been addressed in the context of elasticity. The asymptotic analysis of such a problem relies on the determination of a (Kondrat'ev type) singular expansion which is a series of asymptotics defined in a vicinity of a corner or edge singularity. This expansion generalizes the Taylor one which holds in smooth domains. The notion of asymptotics involve two ingredients which are the singular coefficients and the singular functions (also called the *singularities*). The singularities are associated with singular exponents and may be determined with the Mellin analysis. The singular coefficients may be extracted with numerical methods such as the quasi dual function method (QDFM) which requires the knowledge of dual singularities. Several works related to these problems are presented in a second part which is divided into two chapters. Chapter 3 is mainly devoted to the determination of corner asymptotics of the magnetic potential in the eddy-current model. The first terms of a multi-scale expansion of the magnetic potential are also introduced to tackle the magneto-harmonic problem as the skin depth goes to zero. As an application, a modified (Leontovich) impedance boundary condition close to a corner singularity has been proposed. Chapter 4 is devoted to the notion of edge asymptotics for the Laplace operator. We make the focus on the extraction of edge flux intensity factors (EFIFs) associated with the integer eigenvalues for the Laplace operator over a 3-D domain with a straight crack. The dual singularities are determined and the QDFM has been extended for the extraction of EFIFs.

Finally, spectral methods and polynomial solutions have been developed to solve hypersingular integral equations over a disc and the airfoil equation (with a Cauchy type of singularity) over close disjoint intervals, Appendix C.

# Bibliography


[1] T. Abboud and H. Ammari. Diffraction at a curved grating: TM and TE cases, homogenization. *J. Math. Anal. Appl.*, 202(3):995–1026, 1996.

[2] H. Ammari, E. Beretta, E. Francini, H. Kang, and M. Lim. Reconstruction of small interface changes of an inclusion from modal measurements ii: The elastic case. *Journal de Mathmatiques Pures et Appliques*, 94(3):322 – 339, 2010.

[3] H. Ammari, E. Bretin, J. Garnier, H. Kang, H. Lee, and A. Wahab. *Mathematical Methods in Elasticity Imaging*. Princeton University Press, 2015.

[4] H. Ammari and J.C. Nédélec. Time-harmonic electromagnetic fields in thin chiral curved layers. *SIAM Journal on Mathematical Analysis*, 29(2):395–423, 1998.

[5] P. Angot. A fictitious domain model for the Stokes/Brinkman problem with jump embedded boundary conditions. *C. R. Math. Acad. Sci. Paris*, 348(11-12):697–702, 2010.

[6] P. Angot. On the well-posed coupling between free fluid and porous viscous flows. *Appl. Math. Lett.*, 24(6):803–810, 2011.

[7] P. Angot, G. Carbou, and V. Péron. Asymptotic study for stokes–brinkman model with jump embedded transmission conditions. *Asymptotic Analysis*, 96(3-4):223–249, 2016.

[8] X. Antoine, H. Barucq, and L. Vernhet. High-frequency asymptotic analysis of a dissipative transmission problem resulting in generalized impedance boundary conditions. *Asymptot. Anal.*, 26(3-4):257–283, 2001.

[9] H. Barucq, R. Djellouli, and E. Estecahandy. Efficient DG-like formulation equipped with curved boundary edges for solving elasto-acoustic scattering problems. *International Journal for Numerical Methods in Engineering*, 98(10):747–780, 2014.

[10] H. Barucq, R. Djellouli, and E. Estecahandy. On the existence and the uniqueness of the solution of a fluid–structure interaction scattering problem. *Journal of Mathematical Analysis and applications*, 412(2):571–588, 2014.

[11] H. Barucq, A. Erdozain, and V. Péron. Impedance Transmission Conditions for the Electric Potential across a Highly Conductive Casing. Research Report RR-8998, Inria Bordeaux Sud-Ouest, December 2016.

[12] H. Barucq, T. Frelet-Chaumont, J. Diaz, and V. Péron. Upscaling for the Laplace problem using a discontinuous Galerkin method. *Journal of Computational and Applied Mathematics*, 240:192–203, 2013.

[13] H. Bateman. *The Mathematical Analysis of Electrical and Optical Wave-Motion on the basis of Maxwell's Equations*. Cambridge University Press, 1915.

[14] A. Bendali and K. Lemrabet. The effect of a thin coating on the scattering of a time-harmonic wave for the Helmholtz equation. *SIAM J. Appl. Math.*, 56(6):1664–1693, 1996.

[15] O. Biro, K. Preis, K.R. Richter, R. Heller, P. Komarek, and W. Maurer. FEM calculation of eddy current losses and forces in thin conducting sheets of test facilities for fusion reactor components. *IEEE Trans. Magn.*, 28(2):1509–1512, 1992.

[16] M. Bonnet, A. Burel, M. Duruflé, and P. Joly. Effective transmission conditions for thin-layer transmission problems in elastodynamics. The case of a planar layer model. *ESAIM: Mathematical Modelling and Numerical Analysis*, 50:43–75, 2016.

[17] A. Bostrom. Review of hypersingular integral equation method for crack scattering and application to modeling of ultrasonic nondestructive evaluation. *Applied Mechanics Reviews*, 56(4):383–406, 2003.

[18] D. Braess. *Finite Elements: Theory, Fast Solvers, and Applications in Solid Mechanics*. Cambridge University Press, 3th edition, 2007.

[19] J. P. Breslin and P. Andersen. *Hydrodynamics of ship propellers*, volume 3 of *Cambridge Ocean Technology Series*. Cambridge University Press, 1994.

[20] C.-H. Bruneau and I. Mortazavi. Contrôle passif d'écoulements incompressibles autour d'obstacles à l'aide de milieux poreux. *Comptes Rendus de l'Académie des Sciences-Series IIB-Mechanics*, 329(7):517–521, 2001.

[21] F. Buret, M. Dauge, P. Dular, L. Krähenbühl, V. Péron, R. Perrussel, C. Poignard, and D. Voyer. Eddy currents and corner singularities. *IEEE Trans. on Mag.*, 48(2):679–682, 2012.

[22] G. Caloz, M. Dauge, E. Faou, and V. Péron. On the influence of the geometry on skin effect in electromagnetism. *Computer Methods in Applied Mechanics and Engineering*, 200(9-12):1053–1068, 2011.

[23] G. Caloz, M. Dauge, and V. Péron. Uniform estimates for transmission problems with high contrast in heat conduction and electromagnetism. *Journal of Mathematical Analysis and Applications*, 370(2):555–572, 2010.

[24] G. Carbou. Penalization method for viscous incompressible flow around a porous thin layer. *Nonlinear Anal. Real World Appl.*, 5(5):815–855, 2004.

[25] G. Carbou. Brinkmann model and double penalization method for the flow around a porous thin layer. *J. Math. Fluid Mech.*, 10(1):126–158, 2008.

[26] G. Carbou and P. Fabrie. Boundary layer for a penalization method for viscous incompressible flow. *Adv. Differential Equations*, 8(12):1453–1480, 2003.

[27] M. Castro, J. Diaz, and V. Péron. Equivalent absorbing boundary conditions for heterogeneous acoustic media. *TEMA (São Carlos)*, 15(3):301–310, 2014.

[28] J. Chabassier, M. Duruflé, and V. Péron. Equivalent boundary conditions for acoustic media with exponential densities. Application to the atmosphere in helioseismology. Research Report RR-8954, Inria Bordeaux Sud-Ouest ; Université de Pau et des Pays de l'Adour ; Université de Bordeaux, September 2016.

[29] N. Chen, M. Gunzburger, and X. Wang. Asymptotic analysis of the differences between the Stokes-Darcy system with different interface conditions and the Stokes-Brinkman system. *J. Math. Anal. Appl.*, 368(2):658–676, 2010.

[30] Z. S. Chen, G. Hofstetter, and H. A. Mang. A Galerkin-type BE-FE formulation for elasto-acoustic coupling. *Computer methods in applied mechanics and engineering*, 152(1):147–155, 1998.

[31] E. Christodoulou, C. Elliotis, C. Xenophontos, and G. C. Georgiou. The singular function boundary integral method for 3-D Laplacian problems with a boundary straight edge singularity. *Appl. Math. and Comp.*, 219:1073–1081, 2012.

[32] S. Chun, H. Haddar, and J. S. Hesthaven. High-order accurate thin layer approximations for time-domain electromagnetics, Part II: transmission layers. *J. Comput. Appl. Math.*, 234(8):2587–2608, 2010.

[33] G. Cohen and M. Duruflé. Non spurious spectral-like element methods for Maxwell's equations. *J. Comput. Math*, 25:282–304, 2007.

[34] M. Costabel and M. Dauge. Construction of corner singularities for Agmon-Douglis-Nirenberg elliptic systems. *Math. Nachr.*, 162:209–237, 1993.

[35] M. Costabel, M. Dauge, and R. Duduchava. Asymptotics without logarithmic terms for crack problems. *Communication in PDEs*, 28(5–6):869–926, 2003.

[36] M. Costabel, M. Dauge, and S. Nicaise. Corner Singularities and Analytic Regularity for Linear Elliptic Systems. Part I: Smooth domains. 211 pages v2: Improvement of layout.

[37] M. Costabel, M. Dauge, and Z. Yosibash. A quasidual function method for extracting edge stress intensity functions. *SIAM Jour. Math. Anal.*, 35(5):1177–1202, 2004.

[38] B. Cotterell and J. R. Rice. On a slightly curved or kinked crack. *Int. Jour. Fracture*, 16:155–169, 1980.

[39] M. Dauge. *Elliptic Boundary Value Problems in Corner Domains – Smoothness and Asymptotics of Solutions*. Lecture Notes in Mathematics, Vol. 1341. Springer-Verlag, Berlin, 1988.

[40] M. Dauge, P. Dular, L. Krähenbühl, V. Péron, R. Perrussel, and C. Poignard. Corner asymptotics of the magnetic potential in the eddy-current model. *Mathematical Methods in the Applied Sciences*, 37(13):1924–1955, 2014.

[41] M. Dauge, E. Faou, and V. Péron. Comportement asymptotique à haute conductivité de l'épaisseur de peau en électromagnétisme. *C. R. Acad. Sci. Paris Sér. I Math.*, 348(7-8):385–390, 2010.

[42] M. Dauge, S. Nicaise, M. Bourlard, and J. M.-S. Lubuma. Coefficients des singularités pour des problèmes aux limites elliptiques sur un domaine à points coniques. II. Quelques opérateurs particuliers. *RAIRO Modél. Math. Anal. Numér.*, 24(3):343–367, 1990.

[43] A. M. J. Davis and R. J. Nagem. Effect of viscosity on acoustic diffraction by a circular disk. *The Journal of the Acoustical Society of America*, 115(6):2738–2748, 2004.

[44] A.M.J. Davis and S.G.L. Smith. Tangential oscillations of a circular disk in a viscous stratified fluid. *Journal of Fluid Mechanics*, 656:342–359, 2010.

[45] E.M. Deeley. Surface impedance near edges and corners in three-dimensional media. *IEEE Trans. on Mag.*, 26(2):712–714, 1990.

[46] B. Delourme, H. Haddar, and P. Joly. On the Well-Posedness , Stability And Accuracy Of An Asymptotic Model For Thin Periodic Interfaces In Electromagnetic Scattering Problems. *Mathematical Models and Methods in Applied Sciences*, 2013.

[47] J. Diaz and V. Péron. Equivalent Conditions for Elasto-Acoustics. In *Waves 2013: The 11th International Conference on Mathematical and Numerical Aspects of Waves*, pages 345–346, Gammarth, Tunisie, June 2013.

[48] J. Diaz and V. Péron. Equivalent Robin boundary conditions for acoustic and elastic media. *Math. Models Methods Appl. Sci.*, 26(8):1531–1566, 2016.

[49] D. G. Duffy. *Mixed boundary value problems*. CRC Press, 2008.

[50] P. Dular, V. Péron, L. Krähenbühl, and C. Geuzaine. Progressive eddy current modeling via a finite element subproblem method. *International Journal of Applied Electromagnetics and Mechanics*, 46(2):341–348, 2014.

[51] P. Dular, V. Péron, L. Krähenbühl, and C. Geuzaine. Subproblem finite-element refinement of inductors from wire to static and dynamic volume models. *IEEE Transactions on Magnetics*, 51(3):1–4, 2015.

[52] P. Dular, V. Péron, R. Perrussel, L. Krähenbühl, and C. Geuzaine. Perfect Conductor and Impedance Boundary Condition Corrections via a Finite Element Subproblem Method. *IEEE Transactions on Magnetics*, 50(2):7000504, February 2014.

[53] M. Durán and J.-C. Nédélec. Un problème spectral issu d'un couplage élasto-acoustique. *M2AN Math. Model. Numer. Anal.*, 34(4):835–857, 2000.

[54] M. Duruflé, V. Péron, and C. Poignard. Thin Layer Models for Electromagnetism. In *Waves 2011: The 10th International Conference on Mathematical and Numerical Aspects of Waves*, pages 687–690, Vancouver, Canada, July 2011.

[55] M. Duruflé, V. Péron, and C. Poignard. Time-harmonic Maxwell equations in biological cells—the differential form formalism to treat the thin layer. *Confluentes Math.*, 3(2):325–357, 2011.

[56] M. Duruflé, V. Péron, and C. Poignard. Thin layer models for electromagnetism. *Commun. Comput. Phys.*, 16(1):213–238, 2014.

[57] B. Dutta and S. Banerjea. Solution of a hypersingular integral equation in two disjoint intervals. *Appl. Math. Lett.*, 22(8):1281–1285, 2009.

[58] A. El Kacimi and O. Laghrouche. Numerical modelling of elastic wave scattering in frequency domain by the partition of unity finite element method. *International journal for numerical methods in engineering*, 77(12):1646–1669, 2009.

[59] B. Engquist and J.C. Nédélec. Effective boundary condition for acoustic and electromagnetic scattering in thin layers. *Technical Report of CMAP*, 278, 1993.

[60] A. Erdozain. *Fast inversion of 3D Borehole Resistivity Measurements using Model Reduction Techniques based on 1D Semi-Analytical Solutions*. PhD thesis, Université de Pau et des Pays de l'Adour, Universidad del Pas Vasco - Euskal Herriko Unibertsitatea, 2016.

[61] V. J. Ervin and E. P. Stephan. Collocation with Chebyshev polynomials for a hypersingular integral equation on an interval. *Journal of computational and applied mathematics*, 43(1-2):221–229, 1992.

[62] Elodie Estecahandy. *Contribution to the mathematical analysis and to the numerical solution of an inverse elasto-acoustic scattering problem*. PhD thesis, Université de Pau et des Pays de l'Adour, 2013.

[63] L. Farina, M. Ferreira, and V. Péron. The airfoil equation on near disjoint intervals: Approximate models and polynomial solutions. *Journal of Computational and Applied Mathematics*, 298:97–104, 2016.

[64] L. Farina and P. A. Martin. Scattering of water waves by a submerged disc using a hypersingular integral equation. *Applied ocean research*, 20(3):121–134, 1998.

[65] L. Farina, P. A. Martin, and V. Péron. Hypersingular integral equations over a disc: convergence of a spectral method and connection with Tranter's method. *J. Comput. Appl. Math.*, 269:118–131, 2014.

[66] L. Farina and J. S. Ziebell. Solutions of hypersingular integral equations over circular domains by a spectral method. *Applications of Mathematics 2013*, pages 52–66, 2013.

[67] M. Fischer and L. Gaul. Fast BEM–FEM mortar coupling for acoustic–structure interaction. *International Journal for Numerical Methods in Engineering*, 62(12):1677–1690, 2005.

[68] L. Gaul, D. Brunner, and M. Junge. Simulation of elastic scattering with a coupled FMBE-FE approach. In *Recent Advances in Boundary Element Methods*, pages 131–145. Springer, 2009.

[69] C. Geuzaine, P. Dular, and W. Legros. Dual formulations for the modeling of thin electromagnetic shells using edge elements. *IEEE Trans. Magn.*, 36(4):799–803, 2000.

[70] M. A. Golberg. The convergence of several algorithms for solving integral equations with finite-part integrals. *J. Integral Equations*, 5(4):329–340, 1983.

[71] M. A. Golberg, C.-S. Chen, and J. A. Fromme. Discrete projection methods for integral equations. *APPLIED MECHANICS REVIEWS*, 50:B75–B75, 1997.

[72] P. Grisvard. *Boundary Value Problems in Non-Smooth Domains*. Pitman, London, 1985.

[73] H. Haddar, P. Joly, and H.-M. Nguyen. Generalized impedance boundary conditions for scattering problems from strongly absorbing obstacles: the case of Maxwell's equations. *Math. Models Methods Appl. Sci.*, 18(10):1787–1827, 2008.

[74] T. Hagstrom, M. L. De Castro, D. Givoli, and D. Tzemach. Local high-order absorbing boundary conditions for time-dependent waves in guides. *Journal of Computational Acoustics*, 15(01):1–22, 2007.

[75] T. Hagstrom and T. Warburton. A new auxiliary variable formulation of high-order local radiation boundary conditions: corner compatibility conditions and extensions to first-order systems. *Wave motion*, 39(4):327 – 338, Apr 2004.

[76] T. Hargé. Valeurs propres d'un corps élastique. *C. R. Acad. Sci. Paris Sér. I Math.*, 311(13):857–859, 1990.

[77] R. J. Hartranft and G. C. Sih. The use of eigenfunction expansions in the general solution of three-dimensional crack problems. *Jour. Math. Mech.*, 19(2):123–138, 1967.

[78] N. Heuer, M. E. Mellado, and E. P. Stephan. A $p$-adaptive algorithm for the BEM with the hypersingular operator on the plane screen. *Internat. J. Numer. Methods Engrg.*, 53(1):85–104, 2002. $p$ and $hp$ finite element methods: mathematics and engineering practice (St. Louis, MO, 2000).

[79] R. Hiptmair. Symmetric coupling for eddy current problems. *SIAM J. Numer. Anal.*, 40(1):41–65, 2002.

[80] T. Huttunen, J. P. Kaipio, and P. Monk. An ultra-weak method for acoustic fluid-solid interaction. *J. Comput. Appl. Math.*, 213(1):166–185, 2008.

[81] H. Igarashi, A. Kost, and T. Honma. Impedance boundary condition for vector potentials on thin layers and its application to integral equations. *Eur. Phys. J. AP*, 1:103–109, 1998.

[82] J.-M. Jin, J. L. Volakis, C.L. Yu, and A.C. Woo. Modeling of resistive sheets in finite element solutions. *IEEE Trans. Antennas and Propagation*, 40(6):727–731, 1992.

[83] D. S. Jones. Low-frequency scattering by a body in lubricated contact. *Quart. J. Mech. Appl. Math.*, 36(1):111–138, 1983.

[84] M. Käser and M. Dumbser. A highly accurate discontinuous Galerkin method for complex interfaces between solids and moving fluids. *Geophysics*, 73(3):T23–T35, 2008.

[85] E.F. Knott and T.B.A. Senior. Non-specular radar cross section study. Technical Report 011764-1-T, Univ. Michigan. Radiation Lab., Ann Arbor, MI, USA, Jan 1974.

[86] D. Komatitsch, C. Barnes, and J. Tromp. Wave propagation near a fluid-solid interface: A spectral-element approach. *Geophysics*, 65(2):623–631, 2000.

[87] V. A. Kondratev. Boundary value problems for elliptic equations in domains with conical or angular points. *Trudy Moskov. Mat. Obšč.*, 16:209–292, 1967.

[88] V. A. Kondratev and O. A. Oleinik. Boundary-value problems for partial differential equations in non-smooth domains. *Russian Math. Surveys*, 38:1–86, 1983.

[89] V. A. Kozlov, V. G. Maz'ya, and J. Rossmann. *Elliptic boundary value problems in domains with point singularities*. Mathematical Surveys and Monographs, 52. American Mathematical Society, Providence, RI, 1997.

[90] L. Krähenbühl, F. Buret, R. Perrussel, D. Voyer, P. Dular, V. Péron, and C. Poignard. Numerical treatment of rounded and sharp corners in the modeling of 2D electrostatic fields. *Journal of microwaves, optoelectronics and electromagnetic applications*, 10(1):66–81, 2011.

[91] L. Krähenbühl and D. Muller. Thin layers in electrical engineering. Example of shell models in analysing eddy-currents by boundary and finite element methods. *IEEE Trans.Mag.*, 29(2):1450–1455, 1993.

[92] S. Krenk and H. Schmidt. Elastic wave scattering by a circular crack. *Philosophical Transactions of the Royal Society of London A: Mathematical, Physical and Engineering Sciences*, 308(1502):167–198, 1982.

[93] O. D. Lafitte. Diffraction in the high frequency regime by a thin layer of dielectric material. I. The equivalent impedance boundary condition. *SIAM J. Appl. Math.*, 59(3):1028–1052 (electronic), 1999.

[94] O. D. Lafitte and G. Lebeau. Équations de Maxwell et opérateur d'impédance sur le bord d'un obstacle convexe absorbant. *C. R. Acad. Sci. Paris Sér. I Math.*, 316(11):1177–1182, 1993.

[95] S. G. Larsson and A. J. Carlsson. Influence of non-singular stress terms and specimen geometry on small-scale yielding at crack tips in elastic-plastic materials. *Journal of the Mechanics and Physics of Solids*, 21(4):263–277, 1973.

[96] D. Leguillon and S. Murer. Crack deflection in a biaxial stress state. *Int. Jour. Fracture*, 150:75–90, 2008.

[97] M. A. Leontovich. Approximate boundary conditions for the electromagnetic field on the surface of a good conductor. In *Investigations on radiowave propagation*, volume 2, pages 5–12. Printing House of the USSR Academy of Sciences, Moscow, 1948.

[98] T. Levi-Civita. La teoria elettrodinamica di Hertz di fronte ai fenomeni di induzione. *Rend. Lincei (5)*, 11(2):75–81, 1902. (in Italian).

[99] C. J. Luke and P. A. Martin. Fluid-solid interaction: acoustic scattering by a smooth elastic obstacle. *SIAM J. Appl. Math.*, 55(4):904–922, 1995.

[100] B. N. Mandal and A. Chakrabarti. *Applied singular integral equations*. Science Publishers, 2011.

[101] A Márquez, S Meddahi, and V Selgas. A new BEM–FEM coupling strategy for two-dimensional fluid–solid interaction problems. *Journal of Computational Physics*, 199(1):205–220, 2004.

[102] P. A. Martin. Exact solution of a simple hypersingular integral equation. *J. Integral Equations Appl.*, 4(2):197–204, 1992.

[103] P. A. Martin. Perturbed cracks in two dimensions: an integral-equation approach. *International Journal of Fracture*, 104(3):315–325, 2000.

[104] P. A. Martin. *Multiple scattering: interaction of time-harmonic waves with N obstacles*, volume 107. Cambridge University Press, 2006.

[105] I.D. Mayergoyz and G. Bedrosian. On calculation of 3-D eddy currents in conducting and magnetic shells. *IEEE Transactions on Magnetics*, 31(3):1319–1324, 1995.

[106] V. G. Maz'ya and B. A. Plamenevskii. On the coefficients in the asymptotic of solutions of the elliptic boundary problem in domains with conical points. *Amer. Math. Soc. Trans. (2)*, 123:57–88, 1984.

[107] J. McWhirter. Computation of three-dimensional eddy currents in thin conductors. *IEEE Trans. Magn.*, 18(2):456–460, 1982.

[108] G. Monegato. Definitions, properties and applications of finite-part integrals. *Journal of Computational and Applied Mathematics*, 229(2):425–439, 2009.

[109] P. Monk and V. Selgas. An inverse fluid-solid interaction problem. *Inverse Probl. Imaging*, 3(2):173–198, 2009.

[110] M.-A. Moussaoui. Sur l'approximation des solutions du problème de Dirichlet dans un ouvert avec coins. In *Singularities and constructive methods for their treatment (Oberwolfach, 1983)*, volume 1121 of *Lecture Notes in Math.*, pages 199–206. Springer, Berlin, 1985.

[111] S. Muñoz, J. L. Sebastián, M. Sancho, and J. M. Miranda. Transmembrane voltage induced on altered erythrocyte shapes exposed to RF fields. *Bioelectromagnetics*, 25(1):631–633 (electronic), 2004.

[112] N. I. Muskhelishvili. *Singular integral equations. Boundary problems of function theory and their application to mathematical physics*. P. Noordhoff N. V., Groningen, 1953. Translation by J. R. M. Radok.

[113] T. Nakata, N. Takahashi, K. Fujiwara, and Y. Shiraki. 3D magnetic field analysis using special elements. *IEEE Trans. Magn.*, 26(5):2379–2381, 1990.

[114] D. Natroshvili, A.-M. Sändig, and W. L. Wendland. Fluid-structure interaction problems. In *Mathematical aspects of boundary element methods (Palaiseau, 1998)*, volume 414 of *Chapman & Hall/CRC Res. Notes Math.*, pages 252–262. Chapman & Hall/CRC, Boca Raton, FL, 2000.

[115] S. Nicaise. *Polygonal interface problems*. Methoden und Verfahren der Mathematischen Physik, 39. Verlag Peter D. Lang, Frankfurt-am-Main, 1993.

[116] NIST. Digital library of mathematical functions.

[117] B. Nkemzi and M. Jung. Flux intensity functions for the Laplacian at polyhedral edges. *Int. Jour. Fracture*, 175:167–185, 2012.

[118] N. Omer, Z. Yosibash, M. Costabel, and M. Dauge. Edge flux intensity functions in polyhedral domains and their extraction by a quasidual function method. *Int. Jour. Fracture*, 129:97–130, 2004.

[119] N. F. Parsons and P. A. Martin. Trapping of water waves by submerged plates using hypersingular integral equations. *Journal of Fluid Mechanics*, 284:359–375, 1995.

[120] F. Penzel. On the solution of integral equations on the circular disk by use of orthogonal polynomials. In *Factorization, singular operators and related problems (Funchal, 2002)*, pages 205–217. Kluwer Acad. Publ., Dordrecht, 2003.

[121] V. Péron. *Modélisation mathématique de phénomènes électromagnétiques dans des matériaux à fort contraste*. PhD thesis, Université Rennes 1, France, 2009. http://tel.archives-ouvertes.fr/tel-00421736/fr/.

[122] V. Péron. Equivalent Boundary Conditions for an Elasto-Acoustic Problem set in a Domain with a Thin Layer. Rapport de recherche RR-8163, INRIA, June 2013.

[123] V. Péron. Equivalent boundary conditions for an elasto-acoustic problem set in a domain with a thin layer. *ESAIM: Mathematical Modelling and Numerical Analysis*, 48(5):1431–1449, 2014.

[124] V. Péron. Impedance transmission conditions for eddy current problems. document de travail, April 2017.

[125] V. Péron, K. Schmidt, and M. Duruflé. Equivalent transmission conditions for the time-harmonic maxwell equations in 3d for a medium with a highly conductive thin sheet. *SIAM Journal on Applied Mathematics*, 76(3):1031–1052, 2016.

[126] R. Perrussel, C. Poignard, V. Péron, R. Sabariego, P. Dular, and L. Krähenbühl. Asymptotic expansion for the magnetic potential in the eddy-current problem. In *10th International Symposium on Electric and Magnetic Fields (EMF 2016)*, Lyon, France, April 2016.

[127] J. Poltz and K. Romanowski. Solution of quasi-stationary field problems by means of magnetic scalar potential. *IEEE Trans. Magn.*, 19(6):2425–2428, 1983.

[128] J. R. Rice. Limitations to the small scale yielding approximation for crack tip plasticity. *Journal of the Mechanics and Physics of Solids*, 22(1):17–26, 1974.

[129] J.O.A. Robertsson. A numerical free-surface condition for elastic/viscoelastic finite-difference modeling in the presence of topography. *Geophysics*, 61(6):1921–1934, 1996.

[130] D. Rodger and N. Atkinson. Finite element method for 3D eddy current flow in thin conducting sheets. *IEE Proceedings A*, 135(6):369–374, 1988.

[131] S. M. Rytov. Calcul du skin effect par la méthode des perturbations. *Journal of Physics*, 11(3):233–242, 1940.

[132] K. Schmidt and A. Chernov. A unified analysis of transmission conditions for thin conducting sheets in the time-harmonic eddy current model. *SIAM J. Appl. Math.*, 73(6):1980–2003, 2013.

[133] K. Schmidt and A. Chernov. Robust transmission conditions of high order for thin conducting sheets in two dimensions. *IEEE Trans. Magn.*, 50(2):41–44, 2014.

[134] K. Schmidt and R. Hiptmair. Asymptotic boundary element methods for thin conducting sheets. *Discrete Contin. Dyn. Syst. Ser. S*, 8(3):619–647, 2015.

[135] K. Schmidt, O. Sterz, and R. Hiptmair. Estimating the Eddy-Current modeling error. *IEEE Trans. on Mag.*, 44(6):686–689, 2008.

[136] S. Schneider. FE/FMBE coupling to model fluid-structure interaction. *Int. J. Numer. Meth. Engng.*, 76(13):2137–2156, 2008.

[137] J. L. Sebastián, S. Muñoz, M. Sancho, and J. M. Miranda. Analysis of the influence of the cell geometry and cell proximity effects on the electric field distribution from direct rf exposure. *Phys. Med. Biol.*, 46:213–225 (electronic), 2001.

[138] T. Senior. Approximate boundary conditions. *IEEE Trans. Antennas and Propagation*, 29(5):826–829, 1981.

[139] T. B. A. Senior, J. L. Volakis, and Institution of Electrical Engineers. *Approximate Boundary Conditions in Electromagnetics*. IEE Electromagnetic Waves Series. Inst of Engineering & Technology, 1995.

[140] S. Shannon, V. Péron, and Z. Yosibash. Singular asymptotic solution along an elliptical edge for the Laplace equation in 3-D. *Engineering Fracture Mechanics*, 134:174–181, 2015.

[141] S. Shannon, V. Péron, and Z. Yosibash. The Laplace equation in 3D domains with cracks: dual singularities with log terms and extraction of corresponding edge flux intensity functions. *Mathematical Methods in the Applied Sciences*, 39(17):4951–4963, 2016.

[142] S. Shannon, Z. Yosibash, M. Dauge, and M. Costabel. Extracting generalized edge flux intensity functions with the quasidual function method along circular 3-d edges. *International Journal of Fracture*, 181(1):25–50, 2013.

[143] J. D. Sherwood. Resistance coefficients for stokes flow around a disk with a navier slip condition. *Physics of Fluids*, 24(9):093103, 2012.

[144] B. A. Szabó and Z. Yosibash. Numerical analysis of singularities in two dimensions. II. Computation of generalized flux/stress intensity factors. *Internat. J. Numer. Methods Engrg.*, 39(3):409–434, 1996.

[145] J. P. Tanzosh and H. A. Stone. Transverse motion of a disk through a rotating viscous fluid. *Journal of Fluid Mechanics*, 301:295–324, 1995.

[146] J. Teissié, M. Golzio, and M.P. Rols. Mechanisms of cell membrane electropermeabilization: A minireview of our present (lack of?) knownledge. *Biochimica et Biophysica Acta*, 1724:270–280, 2005.

[147] O. V. Tozoni and I. D. Mayergoyz. *Analysis of three-dimensional electromagnetic fields*. Technika, Kiev, 1974. in russian.

[148] C. J. Tranter. A further note on dual integral equations and an application to the diffraction of electromagnetic waves. 1954.

[149] F. G. Tricomi. *Integral equations*. Pure and Applied Mathematics. Vol. V. Interscience Publishers, Inc., New York, 1957.

[150] E. O. Tuck. Application and solution of Cauchy singular integral equations. In *Application and numerical solution of integral equations (Proc. Sem., Australian Nat. Univ., Canberra, 1978)*, volume 6 of *Monographs Textbooks Mech. Solids Fluids: Mech. Anal.*, pages 21–49. Sijthoff & Noordhoff, Alphen aan den Rijn, 1980.

[151] T. von Petersdorff and E. P. Stephan. Decompositions in edge and corner singularities for the solution of the Dirichlet problem of the Laplacian in a polyhedron. *Math. Nachr.*, 149:71–103, 1990.

[152] W. L. Wendland. On applications and the convergence of boundary integral methods. In *Treatment of integral equations by numerical methods (Durham, 1982)*, pages 463–476. Academic Press, London, 1982.

[153] Z. Yosibash, N. Omer, M. Costabel, and M. Dauge. Edge stress intensity functions in polyhedral domains and their extraction by a quasidual function method. *Int. Jour. Fracture*, 136:37 – 73, 2005.

[154] Z. Yosibash, S. Shannon, M. Dauge, and M. Costabel. Circular edge singularities for the Laplace equation and the elasticity system in 3-D domains. *Int. Jour. Fracture*, 168:31–52, 2011.

[155] S. Yuferev, L. Proekt, and N. Ida. Surface impedance boundary conditions near corner and edges: Rigorous consideration. *IEEE Trans. on Mag.*, 37(5):3465–3468, 2001.

[156] W. Zhang and H. A. Stone. Oscillatory motions of circular disks and nearly spherical particles in viscous flows. *Journal of Fluid Mechanics*, 367:329–358, 1998.

[157] J. S. Ziebell and L. Farina. Water wave radiation by a submerged rough disc. *Wave Motion*, 49(1):34–49, 2012.